REDOX ACTIVE TYROSINES IN PHOTOSYSTEM II: ROLE IN PROTON COUPLED ELECTRON TRANSFER REACTIONS

A Thesis
Presented to
The Academic Faculty

by

James M. Keough

In Partial Fulfillment
of the Requirements for the Degree
Doctor of Philosophy in the
School of Chemistry and Biochemistry

Georgia Institute of Technology
May 2013

REDOX ACTIVE TYROSINES IN PHOTOSYSTEM II: ROLE IN PROTON COUPLED ELECTRON TRANSFER REACTIONS

Approved by:

Dr. Bridgette A. Barry, Advisor
School of Chemistry and Biochemistry
Georgia Institute of Technology

Dr. Adegboyega K. Oyelere
School of Chemistry and Biochemistry
Georgia Institute of Technology

Dr. Mostafa El-Sayed
School of Chemistry and Biochemistry
Georgia Institute of Technology

Dr. Ingeborg Schmidt-Krey
School of Biology
Georgia Institute of Technology

Dr. Facundo Fernandez
School of Chemistry and Biochemistry
Georgia Institute of Technology

Date Approved: December 13, 2012

Table of Contents

LIST OF TABLES

APENDIX B

LIST OF FIGURES

CHAPTER 1

CHAPTER 2

CHAPTER 3

CHAPTER 4

Appendix A

APPENDIX B

APPENDIX C

LIST OF SYMBOLS AND ABBREVIATIONS

OEC	Oxygen-evolving complex
PSII	Photosystem II
PSI	Photosystem I
Y_Z	Tyr161-D1
$Y_Z^{\bullet}$	Neutral radical of Tyr161-D1
Y_D	Tyr160-D1
$Y_D^{\bullet}$	Neutral radical of Tyr160-D1
EPR	Electron paramagnetic resonance
ATP	Adenosine triphosphate
ADP	Adenosine diphosphate
NADPH	Nicotinamide adenine dinucleotide phosphate
b_6f	Cytochrome b_6f complex
PQ	Plastoquinone
PQH_2	Plastoquinol
PC	Plastocyanin
P_{700}	Special pair of photosystem I
P_{700}^{+}	Oxidized form of the special pair of photosystem I
Chl *a*	Chlorophyll *a*
Chl	Chlorophyll
P_{680}	Oxidant to tyrosine Z

P_{680}^{+}	Oxidized form of the oxidant to tyrosine Z
PCET	Proton coupled electron transfer
PTET	Proton transfer followed by electron transfer
ETPT	Electron transfer followed by proton transfer
CPET	Concerted proton-electron transfer
KIE	Kinetic isotope effect
D_2O	^2H_2O
S_n	Oxidation state of the oxygen-evolving complex
S_nY_Z	Tyrosine Z in the S_n state (n = 0-4)
$S_nY_Z^{\bullet}$	Neutral radical of tyrosine Z in the S_n state (n = 0-4)
KIE	Kinetic isotope effect (defined as the rate $^2H_2O/^1H_2O$)
pL	-log[lyonium Ion] where lyonium is ^1H, ^2H, or ^3H

SUMMARY

The demand for energy has been a growing concern for modern man. The prophetic paper titled “Photochemistry of the Future” by Giacomo Ciamician written in 1912 clearly states the problems that we still face today; “Modern civilization is the daughter of coal, for this offers to mankind the solar energy in its most concentrated form; that is, in a form in which it has been accumulated in a long series of centuries. Modern man uses it with increasing eagerness and thoughtless prodigality”. We as a people have made much progress since then, but the major problem of finding an energy source that is able to meet our demands remains. The sun is our only viable energy source and plants, algae, and cyanobacteria are the only entities on the planet that know how to harvest solar energy efficiently. Unveiling the secrets of photosynthesis is our best chance at discovering how to exploit the sun for our energy needs. Despite over a century of research there is still much to learn of about photosynthesis. It is agreed that the most important process within photosynthesis is the oxidation of water to molecular oxygen and protons. This process occurs within photosystem II where high potentials are harnessed through proton coupled electron transfer reactions. Proton coupled electron transfer reactions often involve tyrosine residues, because when oxidized, the phenolic side chain deprotonates. Tyrosine Z (Y_Z) is responsible for extracting electrons in a stepwise fashion from the oxygen evolving-complex in order to build enough potential to oxidize water. This process requires that each step Y_Z must deprotonate and reprotonate in order to maintain the high midpoint potential that is necessary to oxidize the oxygen-evolving complex, which makes Y_Z highly involved in proton coupled electron transfer reactions. In this thesis Y_Z has been studied within oxygen-evolving photosystem II

utilizing electron paramagnetic resonance spectroscopy to monitor the tyrosyl radical that is formed upon light excitation. Kinetic analysis of Y_Z has shed light on the factors that are important for PSII to carry out water oxidation at the oxygen-evolving complex. Most notably the strong hydrogen-bonding network and the midpoint potential of Y_Z have been shown to be integral aspects of the water splitting reactions of PSII. By studying Y_Z within oxygen-evolving PSII, conclusions are readily applied to the native system.

CHAPTER 1

INTRODUCTION

1.1 Demand for Energy

Currently our demand for energy is only met through technological advances that have enabled us to exploit resources outside our capabilities and utilize energy more efficiently.(1) Without continued innovation in the energy sector, the planet will not be able to survive the growing demand for clean energy.(1) Some of the most plentiful sources of energy on the planet are water and sunlight. For this reason, it is not a new idea to use water and sunlight to fuel the planet. Jules Verne recognized that coal supplies were exhaustible and that hydrogen derived from the electrolysis of water could be used as fuel when he stated that "water will be the coal of the future" in 1874.(2) Therefore many efforts to create new technologies are based on duplicating or mimicking structural and functional aspects of photosynthesis.(3, 4) Photosynthesis is among the most fundamental energy conversion process known.(5) Oxygenic photosynthetic processes convert light and CO_2 into an estimated 4 to 17 x 10^{11} tons of reduced carbon each year, which is the equivalent to harnessing between 1 x 10^{11} to 5 X 10^{14} kJ of energy.(6, 7) This quantity of energy amounts to about 10% of the energy that is consumed on our planet annually. While this quantity seems low, plants, cyanobacteria and algae are not designed to store energy that benefits humankind. Photovoltaics remain expensive when compared to fossil fuels at 25 times the price on a per kilowatt basis, yet it would only require 0.16% of the global land mass with 10% efficient photovoltaics to

produce 20 TW of energy annually.(4, 8) As long as fossil fuels remain the cheaper option, motivation will be lacking to pay for a cleaner form of energy. For these reasons, we should strive to understand photosynthetic processes in order to create processes that are cheaper and efficient as those found in nature.

1.2 Photosynthesis

Oxygenic photosynthesis is the process used by plants, algae, and cyanobacteria to convert sunlight and carbon dioxide into chemical energy and molecular oxygen.(5, 9) As shown in Figure 1.1, this process occurs in the thylakoid membranes of all photosynthetic organisms to produce adenosine triphosphate (ATP) and nicotinamide adenine dinucleotide phosphate (NADPH).(9) The simplest apparatus is found within prokaryotic cyanobacteria where the plasma membrane forms invaginations that contain the photosynthetic proteins (Figure 1.2B). Plants and algae utilize a more complex setup. The thylakoid membrane is stacked organelles within chloroplasts. The stacked regions of thylakoid membranes are called the grana and the regions that connect the grana are termed the lamellae (Figure 1.2A). Plants accumulate different photosynthetic proteins in each of these areas of the thylakoid membrane, whereas the thylakoid membranes of cyanobacteria are more homogeneous. However different these apparatuses may be the functions remain the same. Within the thylakoid membrane are four membrane-bound enzymes: photosystem II (PSII), cytochrome b_6f complex (b_6f), photosystem I (PSI), and ATP synthase.(10, 11) PSII sequentially absorbs four quanta of light, which in turn oxidizes two molecules of water to yield four protons and one molecule of dioxygen on the lumenal side of the complex. On the stromal side of the complex, within the membrane, two molecules of plastoquinone (PQ) are reduced to two

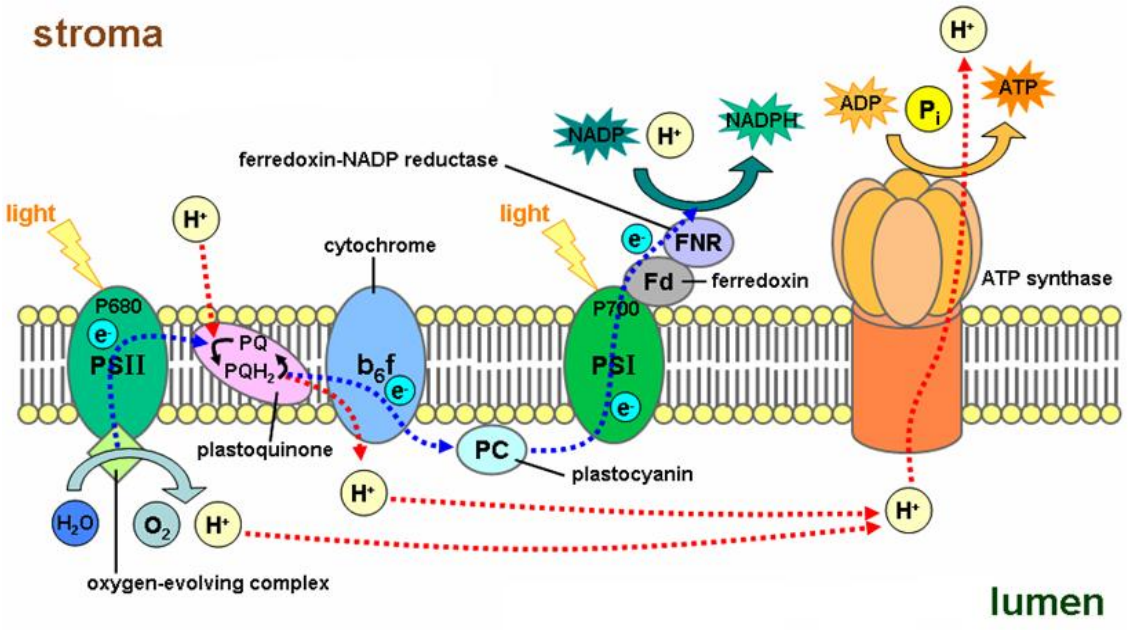

Figure 1.1. Cartoon depiction of a thylakoid membrane containing the photosynthetic proteins. From left to right the membrane-bound proteins are PSII (aqua), b_6f (blue), PSI (green), and ATP synthase (orange). (12)

molecules of plastoquinol (PQH_2).(13, 14) These PQH_2 molecules diffuse to the b_6f complex where plastocyanin (PC) is reduced.(14) The b_6f complex translocates protons and electrons across the membrane. The b_6f complex oxidizes PSII, reduces PSI, and creates a proton gradient.(15) PC then diffuses to a photoexcited PSI where it reduces the special pair of chlorophyll molecules P_{700}^{+} to P_{700}.(13) Upon light excitation, PSI reduces ferredoxin (Fd), which in turn reduces ferredoxin:$NADP^{+}$ reductase (FNR).(13) As a result, two NADPH are produced from two molecules of $NADP^{+}$. NADPH is then utilized as an electron source in the Calvin cycle.(11) The proton gradient established by PSII and b_6f are subsequently used by ATP synthase to produce ATP from ADP and inorganic phosphate.(11, 13)

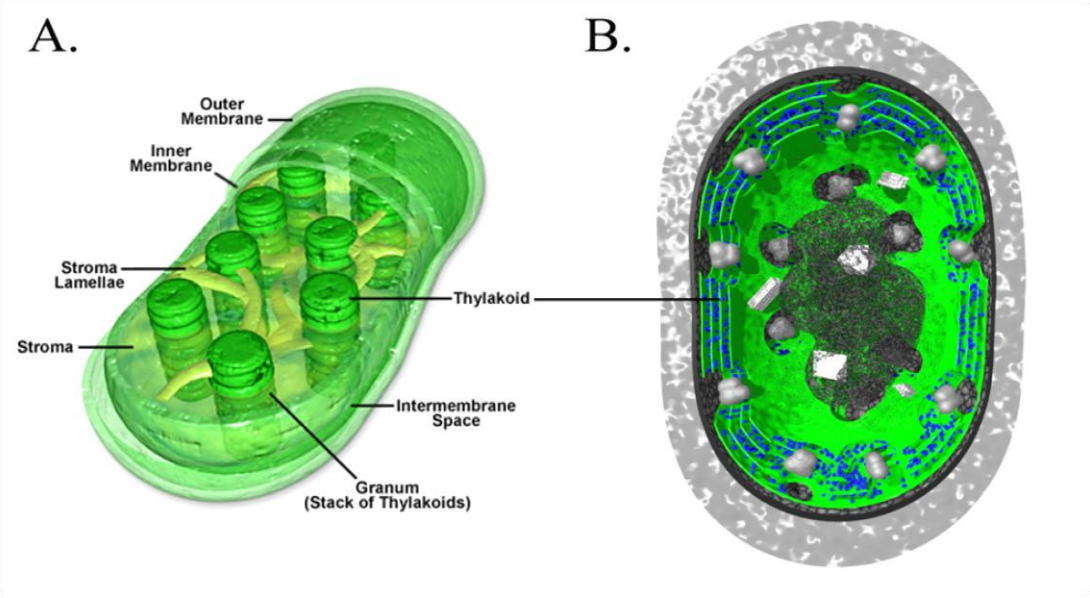

Figure 1.2. Comparison of the organization of the photosynthetic apparatuses within A) higher plants and algae and B) cyanobacteria. The thylakoid membranes exhibit more organization within the chloroplast of higher plants than that of cyanobacteria.(16, 17)

1.3 Photosystem II

At the core of photosynthetic processes is the extraction of electrons and protons from water to form molecular oxygen, which is carried out by PSII. PSII is comprised of over 20 subunits with pseudo-C_2 symmetry.(18-22) The enzyme has 35 chlorophyll *a* (chl *a*) molecules, 12 carotenoid molecules, 25 integral lipids, and 2-3 chloride ions per monomer (Figure 1.3).(21, 22) Catalysis begins within PSII when the primary chlorophyll (chl) donor is excited by light energy.(23, 24) Subsequent electron transfer oxidizes the special pair of chl molecules known as P_{680} to P_{680}^{+}. Within nanoseconds, P_{680}^{+} oxidizes the Tyr161-D1 (Y_Z), which then oxidizes the oxygen-evolving center (OEC).(23-28)

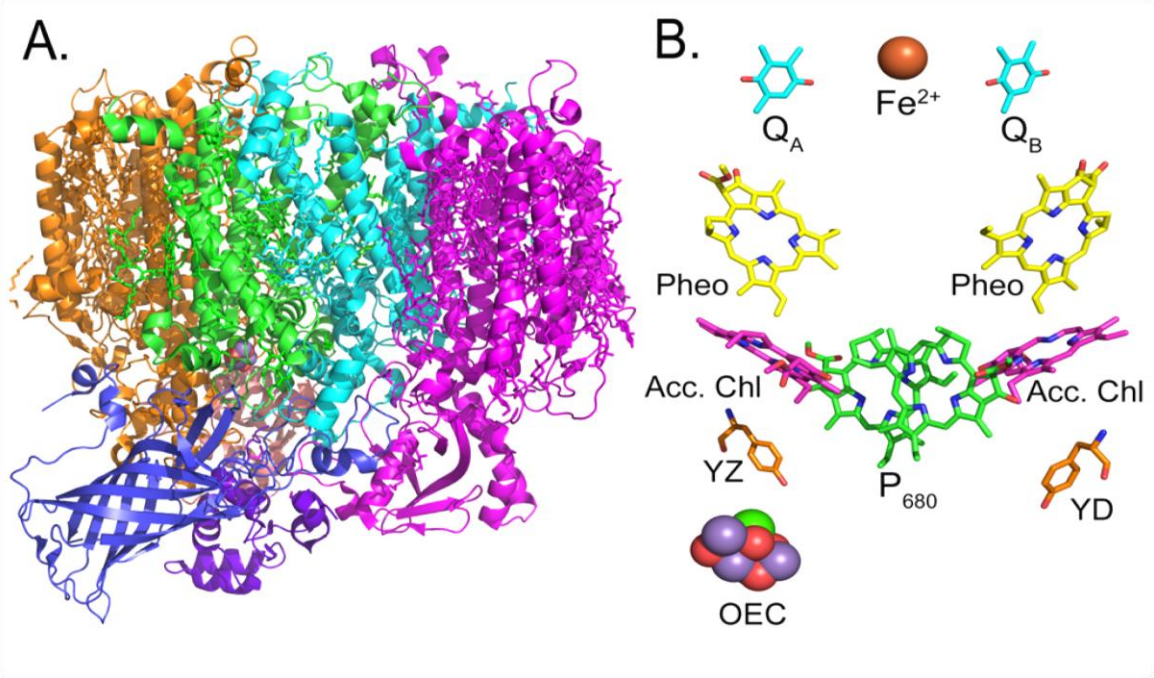

Figure 1.3. A) X-ray crystal structure from *T. elongatus* of PSII at 1.9 Å shown here as a monomer.(22) B) Redox cofactors within PSII from the 1.9 Å structure without the protein matrix.(22)

1.4 Oxygen Evolving Complex

Within PSII, the OEC, a Mn_4CaO_5 cluster (Figure 1.4), stores oxidizing equivalents until two molecules of water are oxidized.(21, 22, 29, 30) Each oxidation step represents the transition of a Mn(III) to Mn(IV) molecule until the final oxidation, wherein a Mn(IV) is oxidized to a very short lived Mn(V) state. At the lowest oxidation state of the cluster it is assumed that the oxidation states are III, III, III, and IV for Mn1, Mn2, Mn3, and Mn4 respectively (Figure 1.4).(31, 32) It can easily be seen that there must be three oxidation steps to transition all Mn(III) ions to Mn(IV) and then one final oxidation to a transient Mn(V) oxidation state followed by catalysis. This four period oscillation is described by the Kok cycle where the OEC cycles through S states entitled S_n, where n is the number of oxidizing equivalents stored (Figure 1.5).(33, 34) The original experiment used to

determine the S states is shown in Figure 1.5A, where oxygen evolution was measured as a function of microsecond xenon lamp flashes. It was shown that the first three flashes

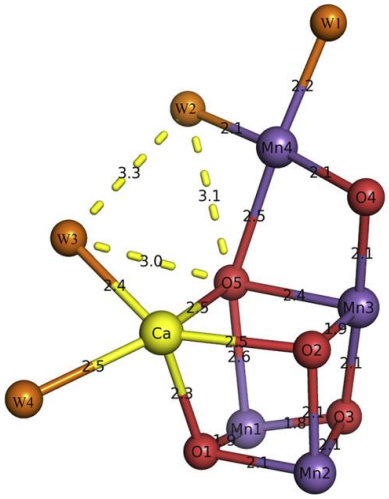

Figure 1.4. Putative structure of the catalytic inorganic Mn_4CaO_5 cluster at 1.9 Å. Spheres are colored orange, yellow, red, and purple representing water, calcium, oxygen, and manganese respectively.(22)

yield oxygen, but that subsequently it required four flashes to evolve oxygen.(33, 35) This result led to the conclusion that the OEC rests in the S_1 state. The S states have interesting temperature dependences.(36-38) Specifically, the $S_1 \rightarrow S_2$ transition has a significantly lower temperature barrier at 135 K than the other transitions. The $S_0 \rightarrow S_1$, $S_2 \rightarrow S_3$, and the $S_3 \rightarrow S_0$ transitions occur at temperatures > 220-225 K , > 230 K, and > 235 K, respectively.(36, 38) This temperature dependence is shown in Figure 1.5B where the half inhibition temperatures are shown in red for each transition.

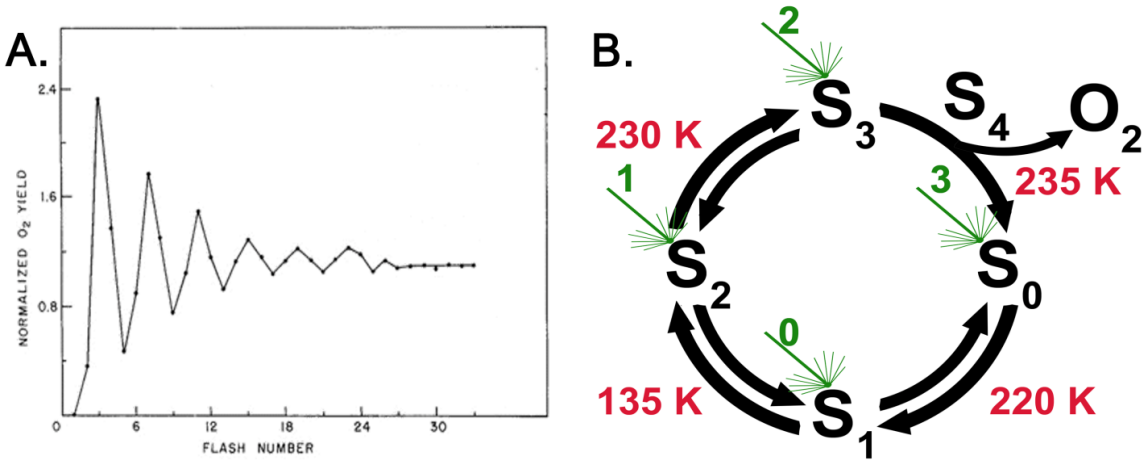

Figure 1.5. A) Plot of oxygen evolution as a function of laser flashes. This was the first experiment demonstrating the period four behavior of water oxidation. B) A depiction of the S-state cycle with the temperature barriers for each transition.(33, 38)

1.5 Tyrosine Z and Tyrosine D

Despite the near C_2 symmetry of the protein complex, there is only one OEC per PSII monomer.(22) Complementary to the D1 subunit is the D2 subunit (shown in green and cyan respectively within Figure 1.3A), which contains few redox-active cofactors but shares many structural similarities to the D1 subunit.(22) Similar to Y_Z in the D1 subunit, the D2 subunit contains a redox-active tyrosine residue, Tyr160-D2 (Y_D), which is also oxidized by P_{680}^+. Y_D is located further from the OEC and has a more stable neutral radical than Y_Z. $Y_D^\bullet$ decays on the order of minutes to hours, whereas $Y_Z^\bullet$ decays on the microseconds to milliseconds time scale.(39) Both Y_Z and Y_D are in hydrogen bond distance to histidine residues, but the orientation differs between the two sites.(21, 22) Y_Z has been shown as an integral component in the water oxidation process. Y_D is important for the function of photosystem II because it has been implicated in the photoassembly of the OEC, and in the decay of the S_2 and S_3 states.(36, 40-42) Y_Z and Y_D are equidistant from P_{680}^+, and $Y_Z^\bullet/Y_Z$ ($\approx$ 930 mV) has a higher midpoint potential

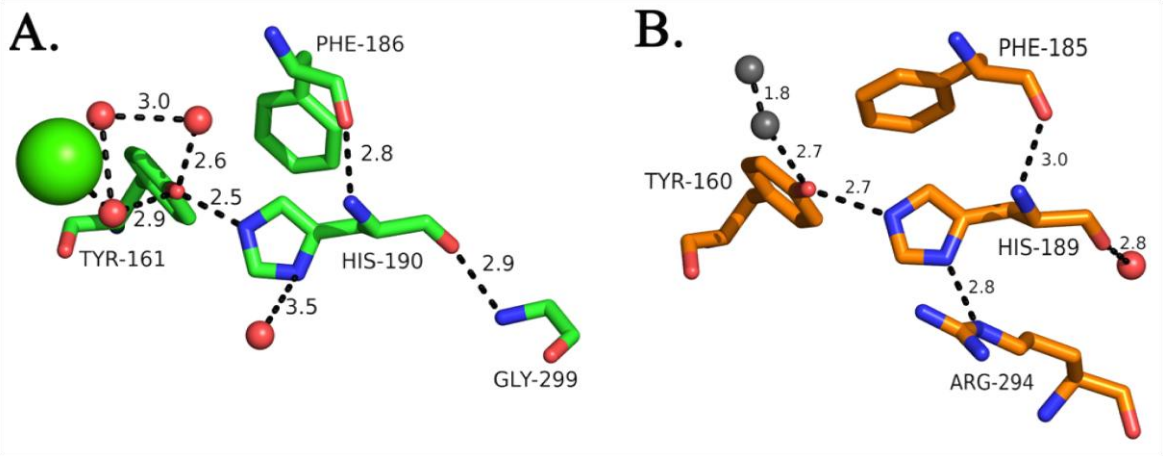

Figure 1.6. A comparison of the local hydrogen-bonding environment for Y_Z (A) and YD (B).(22) Amino acid residues predicted to hydrogen bond with Y_Z and Y_D are shown in green (A) and orange (B), respectively. Assigned, bound water molecules are shown in red (A and B), and the calcium ion is in green (A). An assigned water molecule, which is predicted to have partial occupancy, is shown in gray (B). Predicted hydrogen bonds are depicted with black dashed lines and with distances in Angstroms (The Pymol Molecular Graphics System, Version 1.3, Schrödinger, LLC).

than $Y_D^{\bullet}/Y_D$ (~690 mV).(43-46) Previous studies have shown that $Y_D^{\bullet}$ decay is pL dependent and that the kinetic isotope effect (KIE) increases with pH.(47) A proton inventory was previously constructed for $Y_D^{\bullet}$ recombination showing that there are multiple protons involved in the mechanism.(48) $Y_Z^{\bullet}$ reduction has been shown to be pH independent in both the S_0 and S_2 states with a significant pL independent KIE.(49)

1.6 Proton Coupled Electron Transfer Reactions

Both Y_Z and Y_D are involved in proton coupled electron transfer (PCET) reactions. PCET reactions are of great importance in chemistry and biology.(50, 51) Understanding the nature of these reactions is the key to efficient energy conversion processes. Here we define PCET reactions as the transfer of an electron and a proton regardless of the mechanism. Figure 1.7 demonstrates the possible paths for $Y_Z^{\bullet}$ decay. Three unique PCET mechanisms exist. The top of Figure 1.7 illustrates a proton first

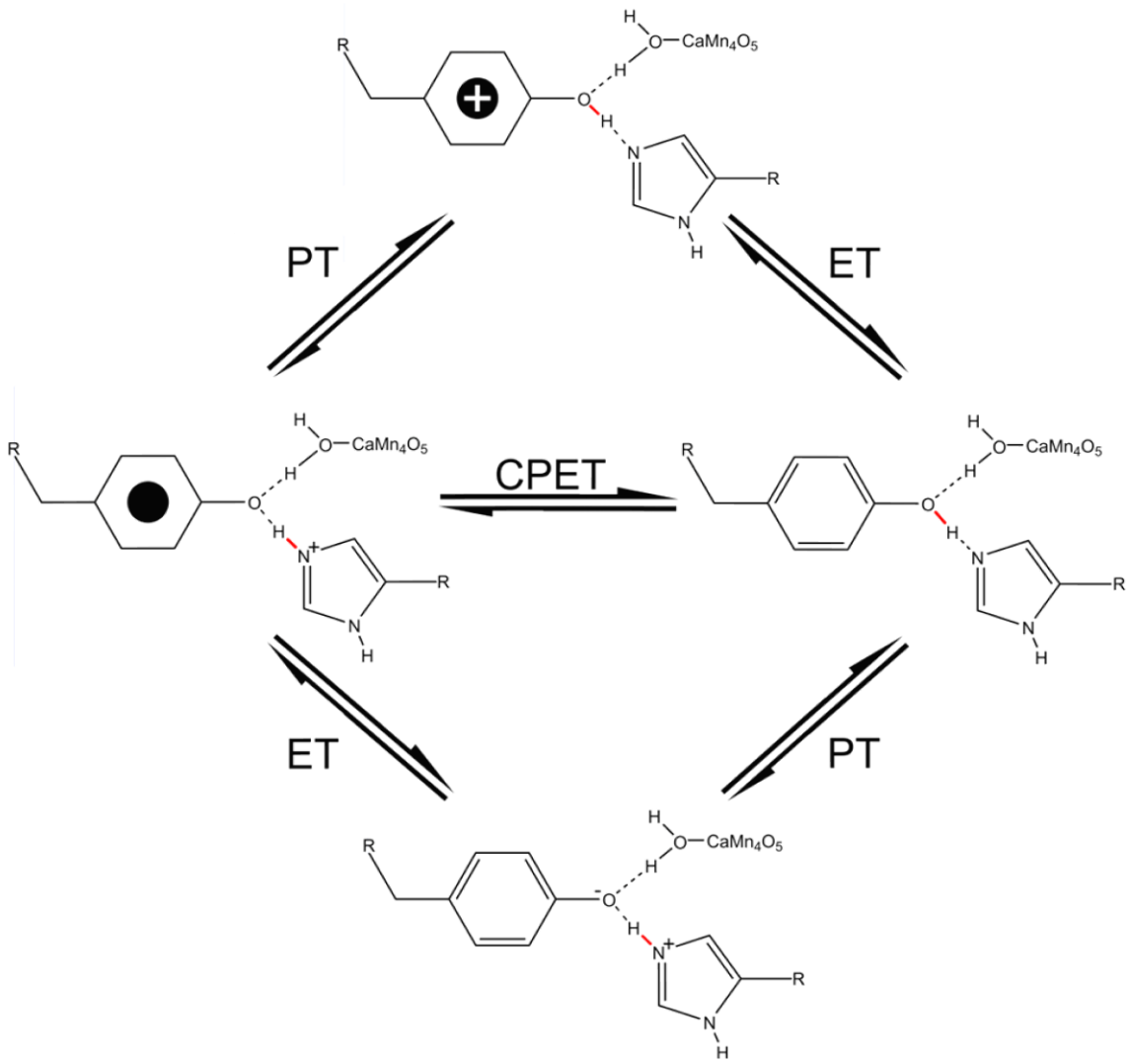

Figure 1.7. Reaction diagram illustrating three possible mechanisms for the decay of the tyrosyl radical with two competing proton donors. (Top) Illustrates a PTET mechanism where a proton is transferred to create a tyrosyl radical cation followed by an electron transfer to form neutral tyrosine. (Bottom) Shows an ETPT mechanism where an electron is transfer to create a tyrosinate followed by a proton transfer to yield tyrosine. (Middle) Shows a CPET mechanism where an electron and a proton are transferred concertedly to skip high energy intermediates and form tyrosine.

pathway, where a proton is initially transferred, generating the cation radical $Y_ZH^{+\bullet}$ followed by an electron transfer to form Y_Z (PTET). The bottom pathway illustrates an electron transfer that creates Y_Z^-, followed by a proton transfer to form Y_Z (ETPT). The middle pathway illustrates the concerted transfer of a proton and an electron in one kinetic step (CPET).

The magnitude of the KIE can be instrumental in determining the type of PCET taking place within a system.(52) For small (<1.3) KIEs the mechanism is expected to be an ETPT, a larger KIE (1.6-81) is exhibited by a CPET mechanism, and PTET will show only a small equilibrium isotope effect (~0.5 ΔpK_a) in D_2O with a pH dependent rate.(53-68)

1.7 Phenol and Tyrosine PCET

PCET reactions involving tyrosine are of great importance to many biological processes including water oxidation,(27) DNA biosynthesis,(69, 70) and oxygen activation.(71-73) For this reason many researchers have turned to biomimetic phenol and tyrosine model compounds to understand these complex processes.(3, 53, 67, 74-77) Most phenol and tyrosine model compounds exhibit CPET mechanisms.(52, 58, 78-81) Intermolecular and intramolecular hydrogen bonds have been shown to facilitate CPET reactions.(52, 58, 59, 76, 78-81) CPET reactions avoid the formation of high-energy intermediates but occur at the expense of higher reorganization energy.(52, 78-80) Hydrogen-bonding facilitates CPET reactions by decreasing the reorganization energy.(76)

1.8 Electron Paramagnetic Resonance Spectroscopy

Electron paramagnetic resonance (EPR) spectroscopy is an invaluable tool for the study of photosynthesis, because the technique allows molecules with unpaired electrons to be studied directly.(82) Every unpaired electron has a magnetic moment that will align itself either parallel or antiparallel to an externally applied magnetic field. The application of an external field causes degenerate electrons to split into distinct energy levels.(82, 83)

Equation 1.1 illustrates the resonance condition for an EPR experiment where ΔE is the energy difference, h is plank's constant, v is the frequency, g is the g-factor, β_e is the Bohr magneton, and B_0 is the external magnetic field.(82) The g-factor is determined by the type of magnetic center that is being studied and is affected by the spin orbit coupling parameters.

Equation 1.1

A free electron has a g-value of g_e = 2.0023**,** whereas a typical value for a chlorophyll-cation radical is g = 2.0025 and a quinone-anion radical is g = 2.0046.(82, 84) The difference is attributed to the quinone having more spin density at the oxygen than the chlorophyll radical. Spin orbit coupling parameters increase with the atomic mass of the nuclei.(82) This effect makes the analysis of a g-factor extremely useful for determining the type of environment surrounding the electrons being studied. Figure 1.8 illustrates how degenerate electrons can be split into discrete energy levels and that these

discrete energy levels can further split by the magnetic field of surrounding nuclei to create hyperfine couplings represented by A_0.

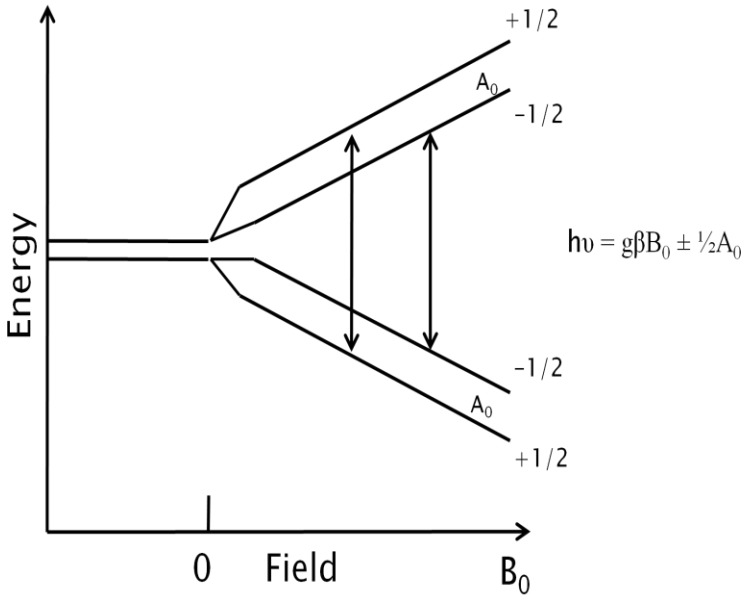

Figure 1.8. Energy diagram illustrating the hyperfine splitting for a degenerate electron within a magnetic field.

In addition to the information that is obtained from the g-value, the lineshape that is formed from the hyperfine couplings of the radical species is also instrumental in determining the environment and the orientation of the radical species.(85-87) The *g*-values for tyrosine radicals are very similar, but their lineshapes differ greatly.(85) The orientation of the β-methylene protons relative to the ring play a significant role in determining the lineshape.(85) This orientation becomes unique to most tyrosyl radicals in various protein systems, because the protein constrains its movement, making EPR analysis of tyrosyl radicals an excellent probe of local structure.

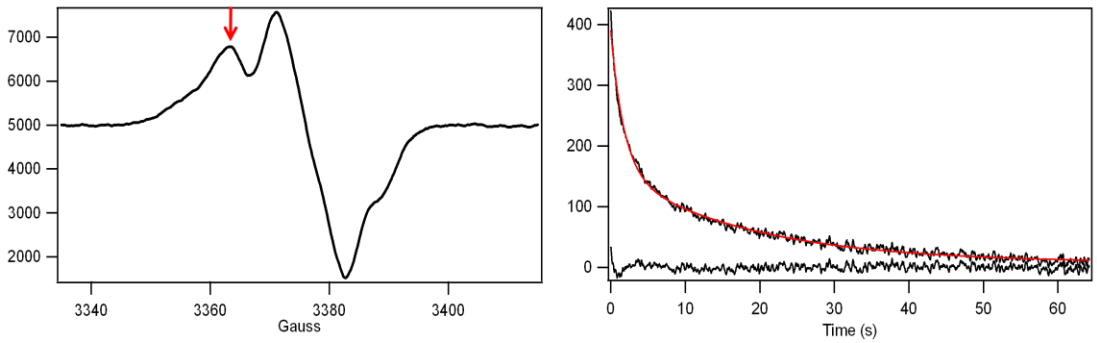

Figure 1.9. Field swept EPR spectrum of $Y_Z^{\bullet}$ in the S_2 state at 190 K and pH 6.5. Red arrow indicates the magnetic field monitored for transient spectra.

Conventional EPR is generally conducted by holding the frequency of the microwave constant while the magnetic field is scanned. This convention is more related to the traditional instrumentation than the theoretical limits of the experiment. When studying the decay kinetics of radicals, the resonant magnetic field can be locked and the radical can be monitored transiently. Figure 1.9 shows (A) field sweep EPR spectrum with a red arrow indicating the magnetic field used for (B) time-resolved EPR transient of $S2Y_Z^{\bullet}$ decay. This technique can lead to the determination of the reaction rates for radicals of interest.

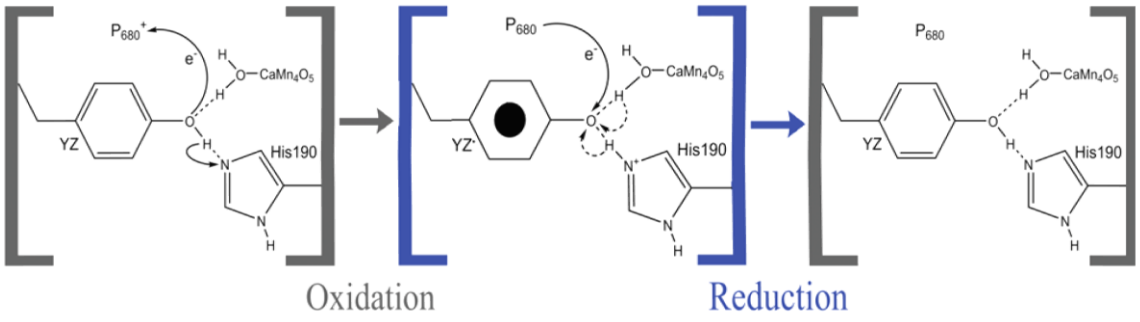

Figure 1.10. Diagram depicting the oxidation and reduction reactions of Y_Z. A two base model for Y_Z PCET reactions in oxygen-evolving preparations of PSII.

1.9 Scope of Thesis

Within this thesis, we test the hypothesis that the oxidation of the OEC modulates the pK_a of proton donors to $Y_Z^{\bullet}$. This hypothesis is tested with EPR spectroscopy in the available S states. We show that we are able to unambiguously monitor tyrosyl radicals within PSII at room temperature and 190 K. In Figure 1.10, we show the oxidation and reduction of Y_Z with hydrogen bond partners His190-D1 and calcium bound water. This work focuses on the reduction reaction highlighted in blue where an electron is transferred from P_{680} to $Y_Z^{\bullet}$ while His190-D1 and calcium bound water compete for proton donation. We determine that the mechanism in both the S_0 and S_2 states is a CPET despite differences in the rate of recombination and KIE.

1.10 References

1. Conti J. J. (2012) Annual Energy Outlook 2012 with projections to 2035. *U.S. Energy and Information Administration.*

2. Verne J. (1874) *Mysterious Island* (Simon and Brown, New York) p 676.

3. Reece S., Nocera, D (2009) Proton-Coupled electron transfer in biology: Results from synergistic studies in natural and model systems. *Annual Review of Biochemistry* 78:673-699.

4. Balzani V., Credi, A., Venturi, M (2008) Photochemical conversion of solar energy. *ChemSusChem* 1:26-58.

5. Arnon D. (1959) Coversion of light into chemical energy in photosynthesis. *Nature* 184:10-21.

6. Field C. B., Behrenfeld M. J., Randerson J. T., & Falkowski P. (1998) Primary Production of the Biosphere: Integrating Terrestrial and Oceanic Components. *Science* 281(5374):237-240.

7. Nealson K. H. & Conrad P. G. (1999) Life: past, present and future. *Philosophical Transactions of the Royal Society of London. Series B: Biological Sciences* 354(1392):1923-1939.

8. Service R. F. (2005) Is it time to shoot for the sun? *Science* 309(5734):548-551.

9. Vermass W. (1998) Revealing the secrets of old sol's sugar factories. *The World and I* 13(3):158-165.

10. Whitmarsh J. G. (1999) *Concepts in Photobiology: Photosynthesis and Photomorphogenesis* (Kluwer Academic Press, Boston) pp 11-51.

11. Voet D. & Voet J. (2004) *Biochemistry 3rd Edition* (Wiley, Hoboken).

12. Taiz L. Z., E. (2002) *Plant Physiology* (Sinauer, New York) 4th Ed.

13. Nelson N. & Yocum C. F. (2006) Structure and function of photosystems I and II. *Annual Review of Plant Biology* 57:521-565.

14. Baniulis D., Yamashita E., Zhang H., Hasan S., & Cramer W. (2008) Structure–Function of the Cytochrome b6f Complex. *Photochemistry and Photobiology* 84(6):1349-1358.

15. Cramer W. A. Z., Huamin; Yan, Jiusheng; Kurisu, Genji; Smith, Janet L. (2006) Transmembrane Traffic in the Cytochrome b_6f Complex. *Annual Review of Biochemitry* 75:769-790.

16. Davidson M. W. (2012) Plant Cell Chloroplast Structure.

17. Fester T. (2010) Cytology of Cyanobacteria.

18. Zouni A., Witt H.-T., Kern J., Fromme P., Krauß N., Saenger W., & Orth P. (2001) Crystal structure of photosystem II from *Synechococcus elongatus* at 3.8 Å resolution. *Nature* 409:739-743.

19. Ferreira K. N., Iverson T. M., Maghlaoui K., Barber J., & Iwata S. (2004) Architecture of the photosynthetic oxygen-evolving center. *Science* 303:1831-1837.

20. Loll B., Kern J., Saenger W., Zouni A., & Biesiadka J. (2005) Towards complete cofactor arrangement in the 3.0 Å resolution structure of photosystem II. *Nature* 438:1040-1044.

21. Guskov A., Kern J., Gabdulkhakov A., Broser M., Zouni A., & Saenger W. (2009) Cyanobacterial photosystem II at 2.9-Å resolution and the role of quinones, lipids, channels and chloride. *Nature structural & molecular biology* 16(3):334-342.

22. Umena Y., Kawakami K., Shen J.-R., & Kamiya N. (2011) Crystal structure of oxygen-evolving photosystem II at a resolution of 1.9 Å. *Nature* 473(7345):55-60.

23. Diner B. A. & Rappaport F. (2002) Structure, dynamics, and energetics of the primary photochemistry of photosystem II of oxygenic photosynthesis. *Annual Review of Plant Biology* 53(1):551-580.

24. Holzwarth A., Müller M., Reus M., Nowaczyk M., Sander J., & Rögner M. (2006) Kinetics and mechanism of electron transfer in intact photosystem II and in the isolated reaction center: pheophytin is the primary electron acceptor. *Proceedings of the National Academy of Sciences* 103(18):6895-6900.

25. Groot M. L., Pawlowicz N. P., Van Wilderen L. J. G. W., Breton J., Van Stokkum I. H. M., & Van Grondelle R. (2005) Initial electron donor and acceptor in isolated photosystem II reaction centers identified with femtosecond mid-IR spectroscopy. *Proceedings of the National Academy of Sciences* 102(37):13087-13092.

26. Ayala I., Kim S., & Barry B. A. (1999) A Difference Fourier transform infrared study of tyrosyl radical Z* decay in photosystem II. *Biophysical Journal* 77(4):2137-2144.

27. Barry B. A. & Babcock G. T. (1987) Tyrosine radicals are involved in the photosynthetic oxygen-evolving system. *Proceedings of the National Academy of Sciences* 84:7099-7103.

28. Boerner R. J. & Barry B. A. (1993) Isotopic labeling and EPR spectroscopy show that a tyrosine residue is the terminal electron donor, Z, in manganese-depleted photosystem II preparations. *The Journal of Biological Chemistry* 268:17151-17154.

29. Babcock G. T. & Sauer K. (1973) Electron paramagnetic resonance Signal II in spinach chloroplasts. *Biochimica et Biophysica Acta* 325:483-503.

30. Babcock G. T. & Sauer K. (1973) Electron paramagnetic resonance signal in spinach chloroplasts II. Alternative spectral forms and inhibitor effects on the kinetics of Signal II in flashing light. *Biochimica et Biophysica Acta* 325:504-519.

31. Grundmeier A. & Dau H. (2012) Structural models of the manganese complex of photosystem II and mechanistic implications. *Biochimica et Biophysica Acta - Bioenergetics* 1817(1):88-105.

32. Siegbahn P. E. M. (2011) Recent theoretical studies of water oxidation in photosystem II. *Journal of Photochemistry and Photobiology B: Biology* 104(1–2):94-99.

33. Kok B., Forbush B., & McGloin M. (1970) Cooperation of charges in photosynthetic O_2 evolution-1. A linear four step mechanism. *Photochemistry and Photobiology* 11(6):457-471.

34. Babcock G. T., Barry B. A., Debus R. J., Hoganson C. W., Atamian M., McIntosh L., Sithole I., & Yocum C. F. (1989) Water oxidation in photosystem II: From radical chemistry to multielectron chemistry. *Biochemistry* 28:9557-9565.

35. Joliot P. & Kok B. (1975) Oxygen evolution in photosynthesis. *Bioenergetics of Photosynthesis*, ed Govindjee (Academic Press, New York), pp 388-412.

36. Ioannidis N. Z., G; Petrouleas, V (2008) The EPR spectrum of tyrosine-Z* and its decay kinetics in O_2-evolving photosystem II. *Biochemistry* 47:6292-6300.

37. Ioannidis N. Z., G; Petrouleas, V (2006) Trapping of the S_2 to S_3 state intermediate of the oxygen-evolving complex of photosystem II. *Biochemistry* 45:6252-6262-6259.

38. Styring S. & Rutherford A. W. (1988) Deactivation kinetics and temperature dependence of the S-state transitions in the oxygen-evolving system of photosystem II measured by EPR spectroscopy. *Biochimica et Biophysica Acta* 933:378-387.

39. Ma C. & Barry B. A. (1996) Electron paramagnetic resonance characterization of tyrosine radical, M^+, in site-directed mutants of photosystem II. *Biophysical Journal* 71:1961-1972.

40. Rutherford A. W., Boussac A., & Faller P. (2004) The stable tyrosyl radical in Photosystem II: why D? *Biochimica et Biophysica Acta - Bioenergetics* 1655(1-3):222-230.

41. Ananyev G. M., Sakiyan I., Diner B. A., & Dismukes G. C. (2002) A functional role for tyrosine-D in assembly of the inorganic core of the water complex of photosystem II and the kinetics of water oxidation. *Biochemistry* 41:974-980.

42. Campbell K. A., Peloquin J. M., Diner B. A., Tang X.-S., Chisholm D. A., & Britt R. D. (1997) The τ-Nitrogen of D2 histidine 189 is the hydrogen bond donor to the tyrosine radical YD□ of photosystem II. *Journal of the American Chemical Society* 119:4787-4788.

43. Boussac A. & Etienne A. L. (1984) Midpoint potential of signal II (slow) in tris-washed photosyste II particles. *Biochimica et Biophysica Acta* 766:576-581.

44. Metz J. G., Nixon P. J., Rögner M., Brudvig G. W., & Diner B. A. (1989) Directed alteration of the D1 polypeptide of photosystem II: evidence that tyrosine-161 is the redox component, Z, connecting the oxygen-evolving complex to the primary electron donor, P_{680}. *Biochemistry* 28:6960-6969.

45. Vass I. & Styring S. (1991) pH-Dependent charge equilibria between tyrosine-D and the S states in photosystem II. Estimation of relative midpoint redox potentials. *Biochemistry* 30(3):830-839.

46. Ishikita H. & Knapp E. W. (2006) Function of redox-active tyrosine in photosystem II. *Biophysical Journal* 90(11):3886-3896.

47. Jenson D. L., Evans A., & Barry B. A. (2007) Proton-coupled electron transfer and tyrosine D of photosystem II. *The Journal of Physical Chemistry B* 111(43):12599-12604.

48. Jenson D. L. & Barry B. A. (2009) Proton-Coupled Electron Transfer in Photosystem II: Proton Inventory of a Redox Active Tyrosine. *Journal of the American Chemical Society* 131(30):10567-10573.

49. Keough J. M., Jenson D. L., Zuniga A. N., & Barry B. A. (2011) Proton Coupled Electron Transfer and Redox-Active Tyrosine Z in the Photosynthetic Oxygen-Evolving Complex. *Journal of the American Chemical Society* 133(29):11084-11087.

50. Vassiliev I. R., Offenbacher A. R., & Barry B. A. (2005) Redox-active tyrosine residues in pentapeptides. *Journal of Physical Chemistry B* 109:23077-23085.

51. Weinberg D. R., Gagliardi C. J., Hull J. F., Murphy C. F., Kent C. A., Westlake B. C., Paul A., Ess D. H., McCafferty D. G., & Meyer T. J. (2012) Proton-Coupled Electron Transfer. *Chemical Reviews* 112(7):4016-4093.

52. Mayer J. M. & Rhile I. J. (2004) Thermodynamics and kinetics of proton-coupled electron transfer: stepwise vs. concerted pathways. *Biochimica et Biophysica Acta - Bioenergetics* 1655:51-58.

53. Rhile I. J., Markle T. F., Nagao H., DiPasquale A. G., Lam O. P., Lockwood M. A., Rotter K., & Mayer J. M. (2006) Concerted Proton Electron Transfer in the Oxidation of Hydrogen-Bonded Phenols. *Journal of the American Chemical Society* 128(18):6075-6088.

54. Sjödin M., Styring S., Åkermark B., Sun L., & Hammarström L. (2002) The mechanism for proton–coupled electron transfer from tyrosine in a model complex and comparisons with YZ oxidation in photosystem II. *Philosophical Transactions of the Royal Society of London. Series B: Biological Sciences* 357(1426):1471-1479.

55. Carra C. I., N; Hammes-Schiffer, S (2003) Proton-coupled electron transfer in a model for tyrosine oxidation in photosystem II. *Journal of the American Chemical Society* 125:10429-10436.

56. Buhks E., Bixon M., & Jortner J. (1981) Deuterium isotope effects on outer sphere electron transfer reactions. *Journal of Physical Chemistry* 85(25):3763-3766.

57. Barry B. A., Chen J., Keough J., Jenson D., Offenbacher A., & Pagba C. (2012) Proton-Coupled Electron Transfer and Redox-Active Tyrosines: Structure and Function of the Tyrosyl Radicals in Ribonucleotide Reductase and Photosystem II. *The Journal of Physical Chemistry Letters* 3(4):543-554.

58. Bonin J. & Robert M. (2011) Photoinduced Proton-Coupled Electron Transfers in Biorelevant Phenolic Systems. *Photochemistry and Photobiology* 87(6):1190-1203.

59. Hammes-Schiffer S. & Soudackov A. V. (2008) Proton-Coupled Electron Transfer in Solution, Proteins, and Electrochemistry. *Journal of Physical Chemistry B* 112(45):14108-14123.

60. Gould I. R. & Farid S. (1988) Specific deuterium isotope effects on the rates of electron transfer within geminate radical-ion pairs. *Journal of the American Chemical Society* 110(23):7883-7885.

61. Hille R. (1991) Electron transfer within xanthine oxidase: a solvent kinetic isotope effect study. *Biochemistry* 30(35):8522-8529.

62. Huynh M. H. V., Meyer T. J., & White P. S. (1999) Proton-Coupled Electron Transfer from Nitrogen. A N−H/N−D Kinetic Isotope Effect of 41.4. *Journal of the American Chemical Society* 121(18):4530-4531.

63. Shafirovich V., Dourandin A., Luneva N. P., & Geacintov N. E. (1999) The Kinetic Deuterium Isotope Effect as a Probe of a Proton Coupled Electron Transfer Mechanism in the Oxidation of Guanine by 2-Aminopurine Radicals. *Journal of Physical Chemistry B* 104(1):137-139.

64. Weatherly S. C., Yang I. V., Armistead P. A., & Thorp H. H. (2002) Proton-Coupled Electron Transfer in Guanine Oxidation: Effects of Isotope, Solvent, and Chemical Modification. *Journal of Physical Chemistry B* 107(1):372-378.

65. Carra C., Iordanova N., & Hammes-Schiffer S. (2003) Proton-coupled electron transfer in a model for tyrosine oxidation in photosystem II. *Journal of the American Chemical Society* 125(34):10429-10436.

66. Lehnert N. & Solomon E. I. (2003) Density-functional investigation on the mechanism of H-atom abstraction by lipoxygenase. *Journal of Biological Inorganic Chemistry* 8(3):294-305.

67. Costentin C., Robert M., & Savéant J.-M. (2006) Carboxylates as Proton-Accepting Groups in Concerted Proton−Electron Transfers. Electrochemistry of the 2,5-Dicarboxylate 1,4-Hydrobenzoquinone/2,5-Dicarboxy 1,4-Benzoquinone Couple. *Journal of the American Chemical Society* 128(27):8726-8727.

68. Hatcher E., Soudackov A. V., & Hammes-Schiffer S. (2006) Proton-Coupled Electron Transfer in Soybean Lipoxygenase: Dynamical Behavior and Temperature Dependence of Kinetic Isotope Effects. *Journal of the American Chemical Society* 129(1):187-196.

69. Offenbacher A. R., Vassiliev I. R., Seyedsayamdost M. R., Stubbe J., & Barry B. A. (2009) Redox-Linked Structural Changes in Ribonucleotide Reductase. *Journal of the American Chemical Society* 131(22):7496-7497.

70. Stubbe J., Nocera D. G., Yee C. S., & Chang M. C. Y. (2003) Radical initiation in the class I ribonucleotide reductase: Long-range proton-coupled electron transfer? *Chemical Reviews* 103(6):2167-2201.

71. Proshlyakov D. A., Pressler M. A., DeMaso C., Leykam J. F., DeWitt D. L., & Babcock G. T. (2000) Oxygen Activation and Reduction in Respiration: Involvement of Redox-Active Tyrosine 244. *Science* 290(5496):1588-1591.

72. Babcock G. T. & Wikstrom M. (1992) Oxygen activation and the conservation of energy in cell respiration. *Nature* 356(6367):301-309.

73. Barry B. A. (2011) Proton coupled electron transfer and redox active tyrosines in Photosystem II. *Journal of Photochemistry and Photobiology B: Biology* 104(1–2):60-71.

74. Costentin C., Robert M., & Savéant J.-M. (2007) Concerted Proton−Electron Transfer Reactions in Water. Are the Driving Force and Rate Constant Depending on pH When Water Acts as Proton Donor or Acceptor? *Journal of the American Chemical Society* 129(18):5870-5879.

75. Sjödin M., Irebo T., Utas J. E., Lind J., Merényi G., Åkermark B., & Hammarström L. (2006) Kinetic Effects of Hydrogen Bonds on Proton-Coupled Electron Transfer from Phenols. *Journal of the American Chemical Society* 128(40):13076-13083.

76. m L. (2008) The Rate Ladder of Proton-Coupled Tyrosine Oxidation in Water: A Systematic Dependence on Hydrogen Bonds and Protonation State. *Journal of the American Chemical Society* 130(29):9194-9195.

77. m L. (2009) The Kinetic Effect of Internal Hydrogen Bonds on Proton-Coupled Electron Transfer from Phenols: A Theoretical Analysis with Modeling of Experimental Data. *Journal of Physical Chemistry B* 113(50):16214-16225.

78. Sjödin M., Styring S., Åkermark B., Sun L., & Hammarström L. (2000) Proton-Coupled Electron Transfer from Tyrosine in a Tyrosine−Ruthenium−tris-Bipyridine Complex: Comparison with TyrosineZ Oxidation in Photosystem II. *Journal of the American Chemical Society* 122(16):3932-3936.

79. Irebo T., Reece S. Y., Sjodin M., Nocera D. G., & Hammarstrom L. (2007) Proton-Coupled Electron Transfer of Tyrosine Oxidation: Buffer Dependence and Parallel Mechanisms. *Journal of the American Chemical Society* 129(50):15462-15464.

80. Bonin J., Costentin C., Louault C., Robert M., Routier M., & Savéant J.-M. (2010) Intrinsic reactivity and driving force dependence in concerted proton–electron transfers to water illustrated by phenol oxidation. *Proceedings of the National Academy of Sciences* 107(8):3367-3372.

81. Zhang M.-T., Irebo T., Johansson m L. (2011) Proton-Coupled Electron Transfer from Tyrosine: A Strong Rate Dependence on Intramolecular Proton Transfer Distance. *Journal of the American Chemical Society* 133(34):13224-13227.

82. Huber M. (2009) Introduction to magnetic resonance methods in photosynthesis. *Photosynthesis Research* 102:305-310.

83. Poole C. P. (1996) *Electron Spin Resonance: A Comprehensive Treatise on Experimental Techniques* (Dover Publications, Mineola, N.Y.).

84. Savitzky A. M., K (2009) High-field EPR. *Photosynthesis Research* 102:311-333.

85. Barry B. A., El-Deeb M. K., Sandusky P. O., & Babcock G. T. (1990) Tyrosine radicals in photosystem II and related model compounds. *The Journal of Biological Chemistry* 265:20139-20143.

86. Bender C. J., Sahlin M., Babcock G. T., Barry B. A., Chandrashekar T. K., Salowe S. P., Stubbe J. A., Lindstrom B., Petersson L., Ehrenberg A., & Sjoberg B.-M. (1989) An ENDOR study of the tyrosyl free radical in ribonucleotide reductase from *Escherichia coli*. *Journal of the American Chemical Society* 111:8076-8083.

87. Dixon W. T. & Murphy D. (1976) Determination of the acidity constants of some phenol radical cations by means of electron spin resonance. *Journal of the Chemical Society London, Faraday Trans. II* 72:1221-1229.

CHAPTER 2

PROTON COUPLED ELECTRON TRANSFER AND REDOX-ACTIVE TYROSINE Z IN THE PHOTOSYNTHETIC OXYGEN-EVOLVING COMPLEX

by

James M. Keough, David L. Jenson, Ashley N. Zuniga, and Bridgette A. Barry*

School of Chemistry and Biochemistry and the Petit Institute for Bioengineering and Bioscience, Georgia Institute of Technology, Atlanta, Georgia 30332

Reprinted with permission from the Journal of the American Chemical Society

Keough J. M., Jenson D. L., Zuniga A. N., & Barry B. A. (2011) Proton Coupled Electron Transfer and Redox-Active Tyrosine Z in the Photosynthetic Oxygen-Evolving Complex. *Journal of the American Chemical Society* 133(29):11084-11087.

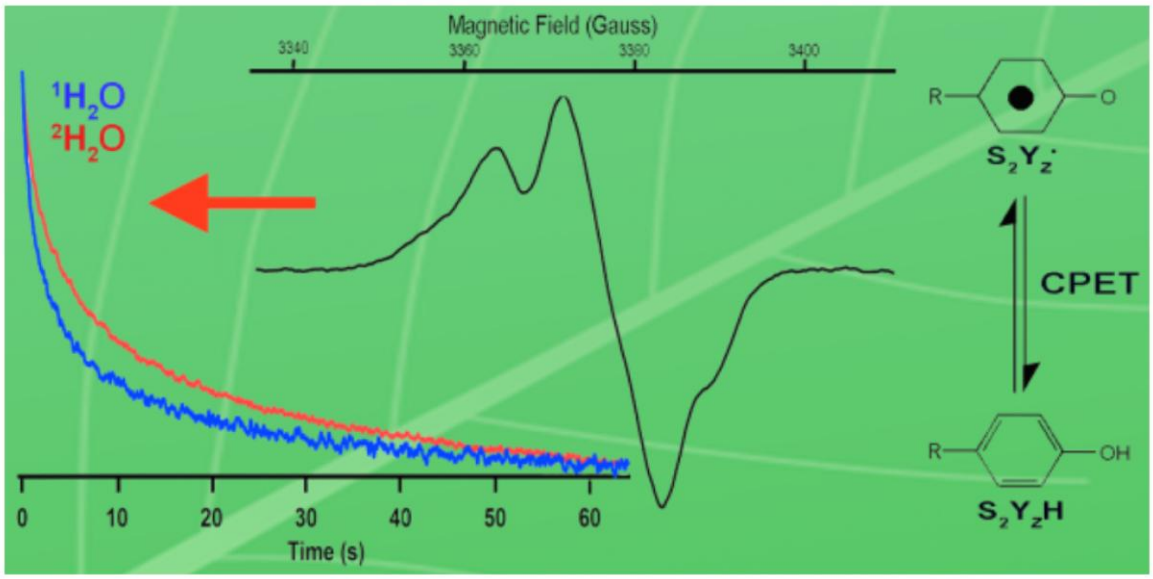

Abstract: Proton coupled electron transfer (PCET) reactions play an essential role in many enzymatic processes. In enzymatic PCET, redox-active tyrosines may be involved as intermediates when the oxidized phenolic side chain deprotonates. Photosystem II (PSII) is an excellent framework for studying PCET reactions, because it contains two redox active tyrosines, Y_D and Y_Z, with different roles in catalysis. One of the redox active tyrosines, Y_Z, is essential for oxygen evolution and is rapidly reduced by the manganese-catalytic site. In this report, we investigate the mechanism of Y_Z PCET in oxygen evolving PSII. To isolate $Y_Z^{\bullet}$ reactions, but retain the manganese-calcium cluster, low temperatures were used to block the oxidation of the metal cluster, high microwave powers were used to saturate the $Y_D^{\bullet}$ EPR signal, and $Y_Z^{\bullet}$ decay kinetics were measured with EPR spectroscopy. Analysis of the pH and solvent isotope dependence was performed. The rate of $Y_Z^{\bullet}$ decay exhibits a significant solvent isotope effect, and the rate of recombination and the solvent isotope effect are pH independent from pH 5.0 to 7.5. These results are consistent with a rate limiting, coupled proton electron transfer (CPET) reaction and are contrasted to results obtained for $Y_D^{\bullet}$ decay kinetics. This effect

may be mediated by an extensive hydrogen bond network around Y_Z. These experiments imply that PCET reactions distinguish the two PSII redox active tyrosines.

2.1 Introduction

In this article, EPR spectroscopy is used to investigate Y_Z PCET reactions in PSII. PSII catalyzes the light driven oxidation of water at a Mn_4CaO_5-containing oxygen-evolving center (OEC). The transmembrane electron transfer pathway involves four chlorophylls (chl), two pheophytin, two plastoquinone, and two redox active tyrosines (Figure 1). Four flashes are required to produce oxygen from water. The OEC cycles among five S_n states, where n refers to the number of oxidizing equivalents stored.(1) PSII contains two redox active tyrosine residues, Y_D and Y_Z (Figure 1),(2, 3) which are located with approximate C_2 symmetry in the reaction center.(4, 5) These tyrosine residues are equidistant from the chlorophyll donor, P_{680}, and are active in PCET reactions, but play different roles in catalysis. Y_Z, Y161 of the D1 polypeptide, is essential for oxygen evolution.(6, 7)_ENREF_6 Y_D, Y160 of the D2 polypeptide, is not essential for catalysis, but may be involved in assembly of the OEC.(6, 8, 9)_ENREF_6 There are other kinetic and energetic differences between the two tyrosines. For example, Y_D forms a more stable radical and is easier to oxidize. As shown in Figure 1, the placement of the OEC and neighboring amino acid side chains distinguishes the two redox active tyrosines. In particular, the OEC calcium ion is located 5 Å from Y_Z, but over 20 Å from Y_D (Figure 2.1). An extensive set of hydrogen bonds, which link the Mn_4-Ca site and Y_Z, is predicted. Hydrogen-bonding distinguishes Y_Z and Y_D.

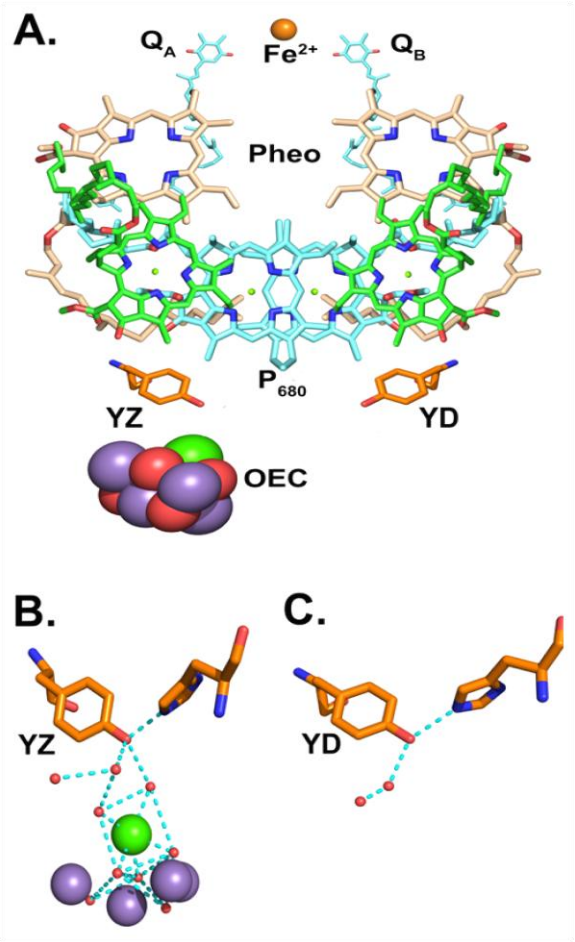

Figure 2.1. (A) Crystal structure of the charge transfer cofactors within PSII at 1.9 Å. (B) Hydrogen-bonding environment surrounding Y_Z. (C) Hydrogen-bonding environment surrounding Y_D. Cyan dashed lines show the predicted hydrogen bonds calculated using the polar contacts function with an edge distance of 3.2 Å and a center distance of 3.6 Å using The Pymol Molecular Graphics System, Version 1.3, Schrödinger, LLC and the 1.9 Å structure (3arc). (5)

Y_Z mediates electron transfer between the primary chlorophyll donor, P_{680}, and the OEC.(10) Photoexcitation of PSII produces a chlorophyll cation radical, P_{680}^{+}, which oxidizes Y_Z on the nanosecond time scale.(10) If Y_D is available to act as an electron donor, i.e. after long dark adaptation, Y_D is also oxidized on the nanosecond time regime by P_{680}^{+}.(11) $Y_Z^{\bullet}$ is reduced by the OEC with a microsecond-millisecond rate, which depends on S state.(12) The S_1 to S_2 transition has a barrier of 100 K, while S_0 to S_1, S_2 to S_3, and the S_3 to S_0 transitions occur at temperatures greater than 225 K.(13)

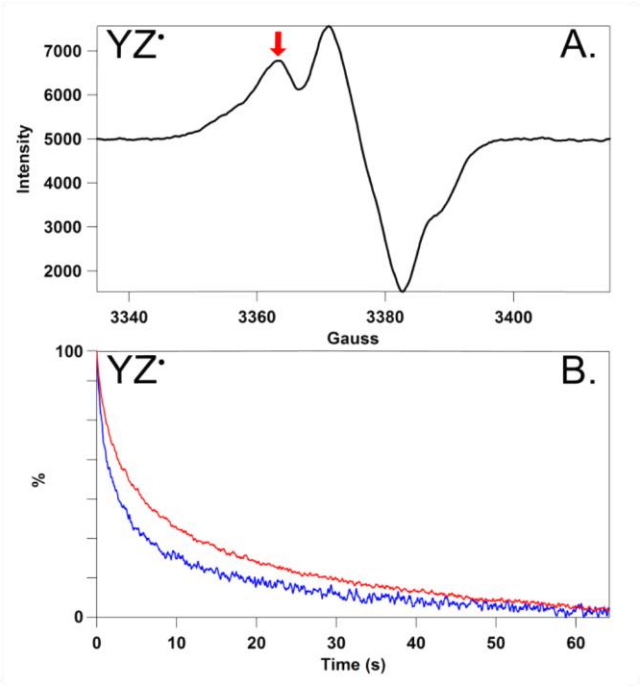

Figure 2.2. (A) Representative EPR spectrum of the $S_2Y_Z^{\bullet}$ state at 190 K and pH 6.5. The spectrum was acquired under red-filtered illumination. The red arrow shows the magnetic field used to monitor kinetics. (B) Representative EPR transients reflecting the decay of $Y_Z^{\bullet}$ at p^1H 6.5 (blue) and p^2H 6.5 (red) at 190K.

Thus, at 190 K, the S_2 to S_3 transition cannot occur. Acceptor side quinone molecules, Q_A and Q_B, act as electron acceptors. At 190 K, PSII is limited to one charge separation; Q_B is not functional.(14) EPR signals from the neutral radicals,(15) $Y_D^{\bullet}$ and $Y_Z^{\bullet}$, can be measured and distinguished by their decay kinetics(16, 17) and by their microwave power dependence in the presence of the OEC.(18)

In many previous studies of Y_Z PCET, the OEC is removed or absent due to biochemical manipulation of PSII. Removal of the OEC slows $Y_Z^{\bullet}$ reduction.(19) However, removal of the OEC may influence Y_Z PCET reactions. By EPR spectroscopy, no change in Y_Z orientation was inferred from study of g tensor orientation.(20) However, changes in the hydrogen-bonding environment around Y_Z (Figure 2.1) may occur due to removal of calcium and manganese.

In this work, $Y_Z^{\bullet}$ PCET was studied in the presence of the OEC. Oxygen-evolving PSII samples were prepared in the S_2 state by illumination at 190 K. A saturating 532 nm flash was then used to generate $S_2Y_Z^{\bullet}Q_A^-$. The S_2 state cannot act as an electron donor at this temperature, and therefore, $Y_Z^{\bullet}$ decays by recombination with Q_A^-. The rate of the $P_{680}^+Q_A^-$ reaction is on the microsecond time scale in plant PSII and is pH and solvent isotope insensitive (see refs (21, 22)). In the absence of the OEC, EPR and optical spectroscopy have reported Y_Z and Q_A^- recombination reactions with an overall time constant of 100-500 msec.(17, 23) In the presence of the OEC, EPR spectroscopy has also reported Y_Z and Q_A^- recombination on the millisecond time scale with rate constants of 9.5 (27%) and 0.8 (73%) s^{-1} (pH 6.5, 190 K).(18)

2.2 Materials and Methods

PSII was isolated from market spinach.(24) The average oxygen evolution rate was 600 μmol O_2/mg chl-hr.(25) The samples were solvent exchanged by repeated centrifugation at 100,000 x g in a ^1H_2O or ^2H_2O (99% Cambridge Isotopes, Andover, MA) buffer containing 0.4 M sucrose, 15 mM NaCl, and 50 mM buffer at each of the following pL values: pL 5.0 (succinate), 5.5 (succinate), 6.0 (2-(N-morpholino)ethanesulfonic acid) (MES), 6.5 (MES), 7.0 (4-(2-hydroxyethyl)-1-piperazineethanesulfonic acid) (HEPES), 7.5 (HEPES). Experiments above pL 7.5 were not possible due to inactivation of the OEC and loss of oxygen evolution at these values. The final concentration was 2 mg/mL, and samples were stored at -70 °C. The pL is reported as the uncorrected meter reading, accounting for the solvent isotope dependence of the glass electrode and the compensating change in the pKa of acids and bases in ^2H_2O.(26)

After a 15 min dark adaptation to trap the S_1 state, samples were homogenized with 500 μM potassium ferricyanide and transferred to the EPR cavity and allowed to equilibrate at 190 K. The 100 mM ferricyanide stock solution was made either in ^1H_2O or ^2H_2O on the same day as the experiment. The ferricyanide was present to oxidize the quinone acceptors after each flash. A field swept spectrum was recorded to select a field position. The 190 K samples were flashed with a 532 nm flash from a Continuum (Santa Clara, CA) Surelite III Nd:YAG laser. The laser intensity was 40 mJ/cm^2, and the beam was expanded with a cylindrical lens. The laser flash generated the $S_2Y_Z^{\bullet}Q_A^-$ and the decay of the $Y_Z^{\bullet}$ EPR signal was monitored. Transient data, associated with $S_2Y_Z^{\bullet}Q_A^-$ decay, were averaged from 3-8 samples, with 15 transients recorded per sample. An offset, averaged from 10 s of data before the laser flash, was subtracted. Flash 1 to 15 yielded similar kinetics. The data from 15 flashes were fit with three exponentials and that fit was used to derive a $t_{½}$ value. This $t_{½}$ value was derived from multiple samples to give an average (mean) and a standard deviation. The EPR analysis was conducted on a Bruker (Billerica, MA) EMX spectrometer equipped with a Bruker ER 4102ST cavity and Bruker ER 4131VT temperature controller. EPR parameters were: magnetic field: 3375 G, microwave frequency: 9.46 GHz, power: 101 mW, modulation amplitude: 5 G, conversion: 20 ms, time constant: 164 ms. High microwave powers were used in order to saturate the $Y_D^{\bullet}$ signal.(18)

Following collection of the transient EPR data, EPR spectra were measured by illuminating the sample within the EPR cavity with red filtered light (600 μmol photons/m^2-s, Dolan Jenner Industries, Boxborough, MA) at 190 K. To show that the expected $Y_Z^{\bullet}$ hyperfine splitting is observed, the microwave power and modulation

amplitude were decreased compared to the conditions used for the EPR transients. Because the microwave power is low, this field swept spectrum also has a contribution from $Y_D^{\bullet}$. The spectra shown are the average of three samples with three spectra obtained for each sample. EPR parameters were: frequency: 9.46 GHz, power: 0.64 mW, and modulation amplitude: 2 G (Figure 2.2) or 5 G (Figure 2.4), conversion time: 41 ms, time constant: 164 ms, sweep time: 21 s.

2.3 Results

A representative field sweep spectrum of $Y_Z^{\bullet}$ in the S_2 state at 190 K is shown in Figure 2.2A. Q_A^- gives rise to a spin coupled signal with an acceptor side Fe^{+2} ion and is not detectable under these conditions.(27) The decay of $Y_Z^{\bullet}$ can be monitored by changes in EPR intensity at fixed magnetic field (Figure 2.2A, arrow). The use of high microwave power saturates the $Y_D^{\bullet}$ signal.(18) As expected, the g value of the $Y_Z^{\bullet}$ radical is 2.004.(15, 28) The $Y_Z^{\bullet}$ spectrum and decay kinetics are similar to previous reports.(18) For example, fits to the p^1H 6.5 data in Figure 2.2B with a biexponential function gave $t_{1/2}$ values of 12.2 s (40%) and 1.2 s (60%), in agreement with the results of ref (18).

In Figure 2.3B, the $Y_Z^{\bullet}$ decay kinetics were monitored, the data were fit, and the overall halftime as a function of p^1H was plotted (black line). The halftimes for $Y_D^{\bullet}$ decay were derived from published rate constants for the majority phase,(26) which are plotted in Figure 2.3A. While the rate of $Y_D^{\bullet}$ decay accelerates at low p^1H (Figure 2.3A), $YZ^{\bullet}$ decay did not show significant pH dependence (Figure 2.3B, black line). Over this pH range, the steady state rate of oxygen evolution was constant, and the content of extrinsic polypeptides, which interact with the OEC, was similar (Figure A.4). Higher pL

values led to activity loss and depletion of the extrinsic polypeptides (Figure A.4 and Figure A.5).

The solvent isotope effect was calculated from the data in Figure 2.3B. Figure 2.3C shows the $Y_Z^{\bullet}$ solvent isotope effect as a function of pL. A significant solvent isotope effect was observed from pL 5 to 7.5 with an average value of ~2. The overall magnitude is consistent with a pH independent, kinetic isotope effect (KIE) on $Y_Z^{\bullet}$ recombination with Q_A^{-}. The observation of a significant solvent isotope effect at all pL values implies that the Y_Z pocket is exposed and readily accessible to water, consistent with recent X-ray crystal structures.(4, 5) Thus, the lack of pH dependence (Figure 2.3C) cannot be attributed to lack of accessibility. By contrast, the decay of $Y_D^{\bullet}$ showed a ~10 fold increase in rate at low pH (Figure 2.3A) and a pH dependent isotope effect, with a maximum value of ~2 at high pL.(26) A proton inventory at high pL was consistent with multiple proton transfer pathways to $Y_D^{\bullet}$, with histidine and water molecules suggested to be the proton donors on two different pathways.(29)

2.4 Discussion

Phenol and tyrosine model compounds have been used to determine the mechanism of PCET reactions. PCET may occur through a concerted pathway, in which the electron and proton are transferred in one kinetic step (CPET). Alternatively, either the electron or proton may be transferred first (ETPT or PTET, respectively). In tyrosine model compounds, a CPET mechanism has been inferred in some studies.(30-33) The magnitude of the KIE and the pH dependence can be used as a first approach to distinguish these mechanisms.

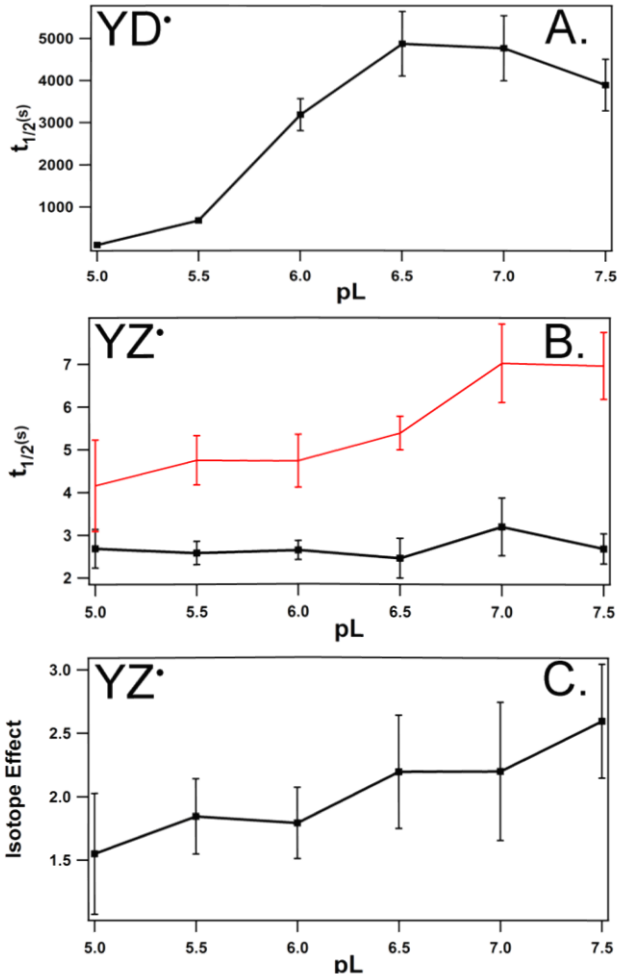

Figure 2.3. (A) pL dependence of $Y_D^{\bullet}$ decay, as assessed by EPR spectroscopy, attributed to $Y_D^{\bullet}Q_A^-$ recombination, and derived from ref.(26) The halftime was derived from the rate constant for the majority phase, corresponding to >85% of the amplitude. (B) pL dependence of $Y_Z^{\bullet}$ recombination in the S_2 state at 190 K. Data were acquired either in ^1H_2O (black) or ^2H_2O (red) buffers. (C) pL dependence of the solvent isotope effect for $Y_Z^{\bullet}$ recombination, derived from the data in (B).

For $Y_D^{\bullet}$ reduction, the pH dependence and the kinetic isotope effect were used to argue that the mechanism is PTET at low pH and CPET at high pH.(29) Unlike $Y_D^{\bullet}$, $Y_Z^{\bullet}$ recombination does not show a stimulated rate at low pH values. The lack of pH dependence and the isotope effect are consistent with a CPET mechanism for $Y_Z^{\bullet}$

reduction throughout this pH range. Our data suggest that PCET mechanism distinguishes Y_D and Y_Z.

The experiments presented here focus on the mechanism of $Y_Z^{\bullet}$ reduction. Previous work has concerned the mechanism of Y_Z oxidation. For OEC depleted preparations, optical studies of P_{680}^{+} reduction were used to argue a CPET mechanism at low pH and a pure ET or a PTET mechanism at high pH.(30, 34) A pKa of ~7.5 was derived from the optical data and attributed to titration of a base near Y_Z.(34) Removal of the OEC may influence PCET reactions. For OEC containing preparations, optical studies of P_{680}^{+} reduction have shown no significant solvent isotope effect on nanosecond components.(35-37) A significant equilibrium isotope effect(38) may explain a difference in KIE on the two reactions. Low fractionation factors can occur if Y_Z is involved in a strong hydrogen bond, in which case deuterium will prefer the solvent.(39)

Model compound studies have shown that intermolecular and intramolecular hydrogen bonds facilitate CPET reactions.(30-33, 40) These reactions avoid the formation of high-energy intermediates, but occur at the expense of high reorganization energies.(30-33) Hydrogen-bonding facilitates reactions by decreasing the reorganization energy (for example, see (41) and references therein). We propose that the extensive hydrogen-bonding network around $Y_Z^{\bullet}$ and the calcium ion facilitates CPET at low pH. This hydrogen-bonding network is shown in the 1.9 Å structure of PSII.(5) In this structure, His190 is located 2.5 Å from Y_Z and several water molecules, bound to calcium, are modeled with one at 2.6 Å (Figure 2.1). The observation that recombination of Y_Z is not accelerated at low pH is of significance with regard to PSII activity, which must be maintained under the acidic conditions of the thylakoid lumen.

ACKNOWLEDGMENT: This work was supported by NIH GM43273 (NIGMS and NEI) to B.A.B.

2.5 References

1. Joliot P. & Kok B. (1975) Oxygen evolution in photosynthesis. *Bioenergetics of Photosynthesis*, ed Govindjee (Academic Press, New York), pp 388-412.

2. Barry B. A. & Babcock G. T. (1987) Tyrosine radicals are involved in the photosynthetic oxygen-evolving system. *Proceedings of the National Academy of Sciences* 84:7099-7103.

3. Boerner R. J., Bixby K. A., Nguyen A. P., Noren G. H., Debus R. J., & Barry B. A. (1993) Removal of stable tyrosine, D^+, affects the structure or redox properties of tyrosine Z in manganese-depleted photosystem II particles from *Synechocystis* 6803. *The Journal of Biological Chemistry* 268:1817-1823.

4. Guskov A., Kern J., Gabdulkhakov A., Broser M., Zouni A., & Saenger W. (2009) Cyanobacterial photosystem II at 2.9-Å resolution and the role of quinones, lipids, channels and chloride. *Nature structural & molecular biology* 16(3):334-342.

5. Umena Y., Kawakami K., Shen J.-R., & Kamiya N. (2011) Crystal structure of oxygen-evolving photosystem II at a resolution of 1.9 Å. *Nature* 473(7345):55-60.

6. Debus R. J., Barry B. A., Babcock G. T., & McIntosh L. (1988) Site-specific mutagenesis identifies a tyrosine radical involved in the photosynthetic oxygen-evolving complex. *Proceedings of the National Academy of Sciences* 85:427-430.

7. Metz J. G., Nixon P. J., Rögner M., Brudvig G. W., & Diner B. A. (1989) Directed alteration of the D1 polypeptide of photosystem II: evidence that tyrosine-161 is the redox component, Z, connecting the oxygen-evolving complex to the primary electron donor, P_{680}. *Biochemistry* 28:6960-6969.

8. Vermaas W. F. J., Rutherford A. W., & Hansson Ö. (1988) Site-directed mutagenesis in photosystem II of the cyanobacterium *Synechocystis sp.* PCC 6803: Donor D is a tyrosine residue in the D2 protein. *Proceedings of the National Academy of Sciences* 85:8477-8481.

9. Ananyev G. M., Sakiyan I., Diner B. A., & Dismukes G. C. (2002) A functional role for tyrosine-D in assembly of the inorganic core of the water complex of photosystem II and the kinetics of water oxidation. *Biochemistry* 41:974-980.

10. Gerken S., Brettel K., Schlodder E., & Witt H. T. (1988) Optical characterization of the immediate donor to Chlorophyll a_{II}^{+} in O_2-evolving photosystem II complexes. *FEBS Letters* 237:69-75.

11. Faller P., Debus R. J., Brettel K., Sugiura M., Rutherford A. W., & Boussac A. (2001) Rapid formation of the stable tyrosyl radical in photosystem II. *Proceedings of the National Academy of Sciences* 98:14368-14373.

12. Babcock G. T., Blankenship R. E., & Sauer K. (1976) Reaction kinetics for positive charge accumulation on the water side of chloroplast Photosystem II. *FEBS Letters* 61:286-289.

13. Styring S. & Rutherford A. W. (1988) Deactivation kinetics and temperature dependence of the S-state transitions in the oxygen-evolving system of photosystem II measured by EPR spectroscopy. *Biochimica et Biophysica Acta* 933:378-387.

14. De Paula J. C., Innes J. B., & Brudvig G. W. (1985) Electron transfer in photosystem II at cryogenic temperatures. *Biochemistry* 24(27):8114-8120.

15. Barry B. A., El-Deeb M. K., Sandusky P. O., & Babcock G. T. (1990) Tyrosine radicals in photosystem II and related model compounds. *The Journal of Biological Chemistry* 265:20139-20143.

16. Kim S. & Barry B. A. (1998) The vibrational spectrum associated with the reduction of tyrosyl radical, D* a comparative biochemical and kinetic study. *Biochemistry* 37:13882-13892.

17. Ayala I., Kim S., & Barry B. A. (1999) A Difference Fourier transform infrared study of tyrosyl radical Z* decay in photosystem II. *Biophysical Journal* 77(4):2137-2144.

18. Ioannidis N. Z., G; Petrouleas, V (2008) The EPR spectrum of tyrosine-Z* and its decay kinetics in O_2-evolving photosystem II. *Biochemistry* 47:6292-6300.

19. Babcock G. T. & Sauer K. (1975) A rapid, light-induced transient in electron paramagnetic resonance Signal II activated upon inhibition of photosynthetic oxygen evolution. *Biochimica et Biophysica Acta* 376:315-328.

20. Matsuoka H., Shen J. R., Kawamori A., Nishiyama K., Ohba Y., & Yamauchi S. (2011) Proton-coupled electron-transfer processes in photosystem II probed by highly resolved g-anisotropy of redox-active tyrosine YZ. *Journal of the American Chemical Society* 133(12):4655-4660.

21. Diner B. A., Force D. A., Randall D. W., & Britt R. D. (1998) Hydrogen bonding, solvent exchange, and coupled proton and electron transfer in the oxidation and reduction of redox-active tyrosine Y_Z in Mn-depleted core complexes of photosystem II. *Biochemistry* 37:17931-17943.

22. Wijn R. d. & Gorkom H. J. v. (2001) Kinetics of electron transfer from Q_A to Q_B in photosystem II. *Biochemistry* 40:11912-11922.

23. Dekker J. P., Gorkom H. J. V., Brok M., & Ouwehand L. (1984) Optical characterization of photosystem II electron donors. *Biochimica et Biophysica Acta* 764:301-309.

24. Berthold D. A., Babcock G. T., & Yocum C. F. (1981) A highly resolved, oxygen-evolving Photosystem II preparation from spinach thylakoid membranes. *FEBS Letters* 134:231-234.

25. Barry B. A. (1995) Tyrosyl radicals in photosystem II. *Methods in Enzymology* 258:303-319.

26. Jenson D. L., Evans A., & Barry B. A. (2007) Proton-coupled electron transfer and tyrosine D of photosystem II. *The Journal of Physical Chemistry B* 111(43):12599-12604.

27. Rutherford A. W. & Zimmerman J. L. (1984) A new EPR signal attributed to the primary plastosemiquinone acceptor in photosystem II. *Biochimica et Biophysica Acta* 767:168-175.

28. Ayala I., Range K., York D., & Barry B. A. (2002) Spectroscopic properties of tyrosyl radicals in dipeptides. *Journal of the American Chemical Society* 124:5496-5505.

29. Jenson D. L. & Barry B. A. (2009) Proton-Coupled Electron Transfer in Photosystem II: Proton Inventory of a Redox Active Tyrosine. *Journal of the American Chemical Society* 131(30):10567-10573.

30. Sjödin M., Styring S., Åkermark B., Sun L., & Hammarström L. (2000) Proton-Coupled Electron Transfer from Tyrosine in a Tyrosine−Ruthenium−tris-Bipyridine Complex: Comparison with TyrosineZ Oxidation in Photosystem II. *Journal of the American Chemical Society* 122(16):3932-3936.

31. Mayer J. M. & Rhile I. J. (2004) Thermodynamics and kinetics of proton-coupled electron transfer: stepwise vs. concerted pathways. *Biochimica et Biophysica Acta - Bioenergetics* 1655:51-58.

32. Irebo T., Reece S. Y., Sjodin M., Nocera D. G., & Hammarstrom L. (2007) Proton-Coupled Electron Transfer of Tyrosine Oxidation: Buffer Dependence and Parallel Mechanisms. *Journal of the American Chemical Society* 129(50):15462-15464.

33. Bonin J., Costentin C., Louault C., Robert M., Routier M., & Savéant J.-M. (2010) Intrinsic reactivity and driving force dependence in concerted proton–electron transfers to water illustrated by phenol oxidation. *Proceedings of the National Academy of Sciences* 107(8):3367-3372.

34. Rappaport F., Boussac A., Force D. A., Peloquin J., Brynda M., Sugiura M., Un S., Britt R. D., & Diner B. A. (2009) Probing the Coupling between Proton and Electron Transfer in Photosystem II Core Complexes Containing a 3-Fluorotyrosine. *Journal of the American Chemical Society* 131(12):4425-4433.

35. Karge M., Irrgang K.-D., & Renger G. (1997) Analysis of the reaction coordinate of photosynthetic water oxidation by kinetic measurements of 355 nm absorption changes at different temperatures in photosystem II preparations suspended in either H_2O or D_2O. *Biochemistry* 36:8904-8913.

36. Haumann M., Bogershausen O., Cherepanov D., Ahlbrink R., & Junge W. (1997) Photosynthetic oxygen evolution: H/D isotope effects and the coupling between electron and proton transfer during redox reactions at the oxidizing side of Photosystem II. *Photosynthesis Research* 51:193-208.

37. Schilstra M. J., Rappaport F., Nugent J. H. A., Barnett C. J., & Klug D. R. (1998) Proton/Hydrogen Transfer Affects the S-State-Dependent Microsecond Phases of P_{680}^+ Reduction during Water Splitting. *Biochemistry* 37(11):3974-3981.

38. Schowen K. B. & Schowen R. L. (1982) Solvent isotope effects of enzyme systems. *Methods in Enzymology* 87:551-606.

39. Cleland W. W. (1992) Low-barrier hydrogen bonds and low fractionation factor bases in enzymatic reactions. *Biochemistry* 31:317-319.

40. Hammes-Schiffer S. & Soudackov A. V. (2008) Proton-Coupled Electron Transfer in Solution, Proteins, and Electrochemistry. *Journal of Physical Chemistry B* 112(45):14108-14123.

41. Irebo m L. (2008) The Rate Ladder of Proton-Coupled Tyrosine Oxidation in Water: A Systematic Dependence on Hydrogen Bonds and Protonation State. *Journal of the American Chemical Society* 130(29):9194-9195.

CHAPTER 3

REDOX CONTROL AND HYDROGEN-BONDING NETWORKS: PROTON COUPLED ELECTRON TRANSFER REACTIONS AND TYROSINE Z IN THE PHOTOSYNTHETIC OXYGEN-EVOLVING COMPLEX

by

James M. Keough, Ashley N. Zuniga, David L. Jenson, and Bridgette A. Barry*

School of Chemistry and Biochemistry and the Petit Institute for Bioengineering and Bioscience, Georgia Institute of Technology, Atlanta, GA 30332

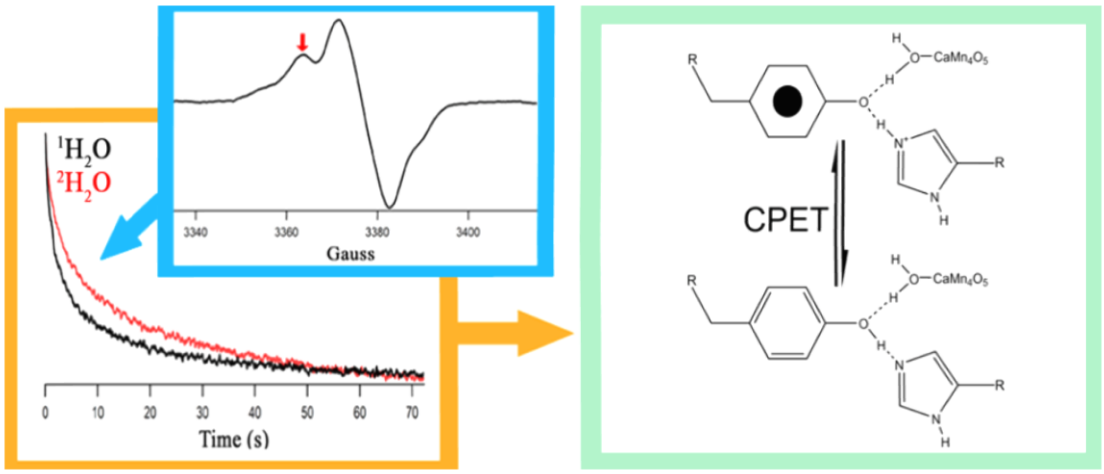

Abstract: In photosynthetic oxygen evolution, redox active tyrosine Z (Y_Z) plays an essential role in proton coupled electron transfer (PCET) reactions. Four sequential photooxidation reactions are necessary to produce oxygen at a Mn_4CaO_5 cluster. The sequentially oxidized states of this oxygen-evolving cluster (OEC) are called the S_n states, where n refers to the number of oxidizing equivalents stored. The neutral radical, $Y_Z^{\bullet}$, is generated and then acts as an electron transfer intermediate during each S state transition. In the X-ray structure, Y_Z, Tyr 161 of the D1 subunit, is involved in an extensive hydrogen-bonding network, which includes calcium-bound water. Oxidation of the Mn_4CaO_5 cluster may activate these calcium-bound water molecules and alter Y_Z PCET through changes in the hydrogen-bonding network. We compared the S_0 and S_2 states, which differ in Mn oxidation state, and found a significant difference in the $Y_Z^{\bullet}$ decay rate ($t_{1/2} = 3.3 \pm 0.3$ s in S_0; $t_{1/2} = 2.1 \pm 0.3$ s in S_2) and in the kinetic isotope effect (KIE) on the reaction (1.3 ± 0.3 in S_0; 2.1 ± 0.3 in S_2). Although the Y_Z site is known to be solvent accessible, the recombination rate and KIE were pH independent in both S states. To define the origin of these effects, we measured the YZ• recombination rate in the presence of ammonia, which inhibits oxygen evolution and disrupts the hydrogen

bond network. We report that ammonia dramatically slows the $Y_Z^{\bullet}$ recombination rate in the S_2 state, but has a smaller effect in the S_0 state. In contrast, ammonia had no significant effect on $Y_D^{\bullet}$, the stable tyrosyl radical in PSII. Therefore, the alterations in $Y_Z^{\bullet}$ decay, observed with S state advancement, are attributed to alterations in OEC hydrogen-bonding and consequent differences in the YZ midpoint potential/pK_a. These changes may be caused by activation of metal bound water molecules, which hydrogen bond to YZ. These observations document the importance of redox control in proton coupled electron transfer react

3.2 Introduction

Photosynthetic oxygen evolution occurs at a Mn_4CaO_5 cluster in the thylakoid membrane associated reaction center, photosystem II.(1) Each reaction center contains the transmembrane subunits D1, D2, CP43, and CP47, which bind the redox-active cofactors and antenna pigments, chlorophyll (chl) and carotenoids (Figure 3.1A). A photoinduced charge separation is generated between the dimeric chl donor, P_{680}, and a bound plastoquinone, Q_A. Q_A^- reduces a second quinone, Q_B, and P_{680}^+ oxidizes a tyrosine residue, Y_Z, Y161-D1

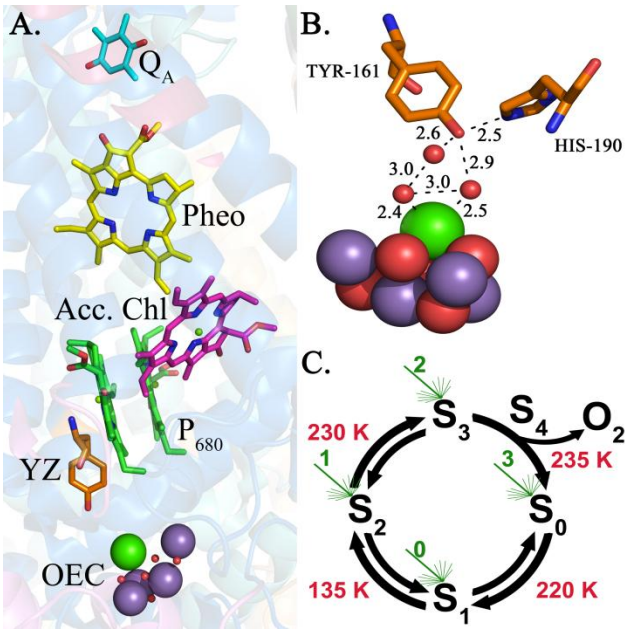

Figure 3.1. (A) Redox active cofactors involved in the charge recombination of Q_A^- with $Y_Z^\bullet$. The phytyl chains of the cofactors have been removed for clarity.(1) (B) Local environment of Y_Z with predicted hydrogen bonds shown as black dashes and distance shown in Angstroms (The Pymol Molecular Graphics System, Version 1.3, Schrödinger, LLC). (C) S state cycle showing the reported half inhibition temperatures(2) in red, and the number of laser flashes required to achieve that state in green.

polypeptide. The radical, $Y_Z^\bullet$, is a powerful oxidant.(3, 4) Under physiological conditions, $Y_Z^\bullet$ oxidizes the Mn_4CaO_5 cluster, where water oxidation occurs (Figure 3.1B).(1) Four sequential photooxidations lead to the release of molecular oxygen, and the yield of O_2 fluctuates with period four.(5) The sequentially oxidized states of the Mn_4CaO_5 cluster are the S_n states, where *n* refers the number of oxidizing equivalents stored (Figure 3.1C). Y_Z acts as an electron transfer intermediate between P_{680}^+ and the Mn_4CaO_5 cluster on each S state transition and is required for oxygen evolution.(6) A single short laser flash advances the OEC from one S state to the next. For example, a short flash given to the so-called S_1 state (generated by dark adaptation), generates the S_2 state. This S_1 to S_2 transition corresponds to the oxidation of a Mn(III) to Mn(IV).(7)

During the S state cycle, water oxidation occurs on the microsecond to millisecond time scale, oxygen is produced during the S_3 to S_0 transition.(5, 8)

Tyrosyl radicals play an important role in proton coupled electron transfer (PCET) in many biological systems.(9) The tyrosine side chain can participate in PCET reactions when the pH is below the pKa of the phenolic oxygen (~10). Oxidation of tyrosine under these conditions leads to production of a neutral tyrosyl radical, due to the dramatic decrease in pK_a of the phenolic oxygen in the radical state.(10) Results from PSII, RNR, and model systems indicate that solvent accessibility and hydrogen-bonding can control the lifetime and midpoint potential of tyrosyl radicals.(11-15) These studies also suggest that conformational changes of the redox active tyrosine are coupled with the oxidation reactions.(16, 17)

In PSII, YZ plays a critical role in the water splitting reactions. Mutations at this tyrosine, Y161-D1, inactivate water oxidation.(18, 19) In the absence of Y_Z, Q_A^- decays by recombination with P_{680}^+ on the microsecond time scale.(19) Interestingly, PSII contains a second tyrosyl radical, $Y_D^\bullet$ (Y160-D2), which has different redox chemistry, when compared to Y_Z in the D1 subunit.(20, 21) Y_D forms a much more stable radical (minutes-hours)(22) and has a lower midpoint potential, compared to Y_Z.(23) While Y_D does not play a direct role in oxygen evolution, this redox-active tyrosine may play a role in assembly of the Mn_4CaO_5 cluster.(24) The 1.9 Å structure suggests that hydrogen-bonding distinguishes the Y_D and Y_Z pockets,(1) and our previous EPR study concluded that PCET distinguishes the two redox active tyrosines.(14)

In the X-ray structure of PSII, Y_Z is 5 Å from the Mn_4CaO_5 cluster and is predicted to participate in a hydrogen bond network, which includes two water molecules

and the side chain of His190 in the D1 subunit (Figure 3.1B).(1) This extensive hydrogen bond network may play a role in catalysis.(1, 14, 25) One of the hydrogen bonded water molecules is directly bound to calcium while the other is in the second coordination sphere of calcium (Figure 3.1B).(1) Changes in OEC oxidation state are likely to alter the acidity of these metal bound water molecules. This change in acidity can then modulate the strength of the hydrogen-bonding network to Y_Z, providing a control mechanism over the pK_a and midpoint potential of Y_Z. This is potentially important question, because Y_Z must deprotonate and reprotonate on each S state transition in order to have the high midpoint potential that is necessary to oxidize water (see discussion in ref (26)).

In this study, we use electron paramagnetic resonance EPR spectroscopy to investigate the effect of OEC oxidation on $Y_Z^{\bullet}$ PCET reactions. The term, PCET, is used to refer to any reaction that involves transfer of a proton and an electron, regardless of the detailed mechanism.(27) The mechanism of PCET reactions will be sensitive to changes in distance, angle and strength of hydrogen bonds to Y_Z/ $Y_Z^{\bullet}$. In principle, EPR is a sensitive method with which to measure the kinetics of light induced paramagnetic species, such as $Y_Z^{\bullet}$. However, in the presence of the OEC, $Y_Z^{\bullet}$ is reduced rapidly by the Mn_4CaO_5 cluster; this fast decay rate complicates its facile detection by EPR spectroscopy. Another complication is that $Y_D^{\bullet}$ and $Y_Z^{\bullet}$ give rise to overlapping g=2.0 signals with similar hyperfine splittings, with Y_D forming the more stable radical.

To monitor $Y_Z^{\bullet}$ specifically with EPR spectroscopy, we used the approaches described previously, in which high microwave powers and low temperatures were employed.(14, 26) Normally, $Y_Z^{\bullet}$ is reduced on the microsecond to millisecond time

scale by the OEC.(8) The use of low temperature blocks this OEC to Y_Z reaction (Figure 3.1C), leaving Y_Z as the terminal electron donor, which can be oxidized by single flash and will decay on the seconds time scale by recombination with Q_A^-.(14, 26) The use of high microwave powers saturates the $Y_D^\bullet$ EPR signal and allows $Y_Z^\bullet$ kinetics to be monitored independently of $Y_D^\bullet$, which is more distant (20 Å) from the Mn_4CaO_5 cluster.(1)

To investigate the dependence of Y_Z PCET on S state, flash-freeze quench techniques were used to prepare the S_0 state, attributed to $(Mn(III)_3(MnIV)_1$, or the S_2 state, attributed to $Mn(III)_1(Mn(IV)_3$.(28-30) At room temperature, saturating flashes are given to PSII samples, dark adapted in the S_1 state, to generate either the $S_0Y_ZQ_A$ (three flashes) or the $S_2Y_ZQ_A$ state (Figure 3.1C). The samples are then flash frozen to 190 K. At this temperature, the S_0 to S_1, S_2 to S_3, and Q_A^- to Q_B transitions are blocked (Figure 3.1C).(2, 14, 26, 31) After a saturating flash to these samples at 190 K, $Y_Z^\bullet$ is generated and then decays on the seconds time scale by recombination with Q_A^-, which is a single electron donor and is not protonated (reviewed in ref (32)). $Y_Z^\bullet$ reduction occurs by a PCET reaction, and the mechanism of the reaction can be interrogated by pH and solvent isotope alterations. This approach has the advantage of preserving the structural interactions between the OEC and Y_Z, while allowing effects on the rate of $Y_Z^\bullet Q_A^-$ recombination to be assessed by EPR spectroscopy in a facile manner.

Here, the dependence of the $Y_Z^\bullet Q_A^-$ recombination rate on solvent isotope and pL in two different OEC oxidation states, S_0 and S_2, is reported. These two states were chosen because their half inhibition temperatures are similar, with a high activation barrier. In addition, ammonia, a substrate analog and PSII inhibitor(25, 33-35) was used

as a probe of Y_Z hydrogen-bonding interactions with the OEC. Through vibrational spectroscopy, it has been shown recently that ammonia alters the OEC hydrogen-bonding network during the S_1 to S_2 transition.(25) The results presented here are consistent with a change in Y_Z PCET mechanism when the S_0 and the S_2 states are compared. Also, we report a dramatic, S state dependent effect of ammonia on $Y_Z^{\bullet}Q_A^-$ recombination, which is consistent with alterations in $Y_Z^{\bullet}$/water hydrogen-bonding.

3.3 Materials and Methods

PSII Samples. PSII was isolated from market spinach.(36) The average oxygen evolution rate was 800 μmol O_2/mg chl-hr.(37) The samples were solvent exchanged by repeated centrifugation at 100,000 x g in a ^1H_2O or ^2H_2O (99% Cambridge Isotopes, Andover, MA) buffer containing 0.4 M sucrose, 15 mM NaCl, and 50 mM buffer at each of the following pL values: pL 5.0 (succinate), 5.5 (succinate), 6.0 (2-(N-morpholino)ethanesulfonic acid, (MES), 6.5 (MES), 7.0 (4-(2-hydroxyethyl)-1-piperazineethanesulfonic acid, (HEPES), 7.5 (HEPES). Experiments above pL 7.5 were not possible due to inactivation of the OEC and loss of oxygen evolution at these values. The final concentrations were 4 and 2 mg/mL, respectively, for the S_2YZ and S_0YZ samples, and samples were stored at -70 °C. The pL is reported as the uncorrected meter reading, accounting for the solvent isotope dependence of the glass electrode and the compensating change in the pKa of acids and bases in ^2H_2O.(38)

$Y_Z^{\bullet}$ *Experiments.* After a 15 min dark adaptation to trap the S_1 state, samples were homogenized with 500 μM potassium ferricyanide and flashed either one or three times at 1 Hz with a 532 nm flash from a Continuum (Santa Clara, CA) Surelite III Nd:YAG laser at room temperature. The laser intensity was 40 mJ/cm^2, and the beam

was expanded with a cylindrical lens. The 100 mM ferricyanide stock solution was made either in ^1H_2O or ^2H_2O on the same day as the experiment. The ferricyanide was present to oxidize the quinone acceptors after each flash. Samples were immediately submersed in liquid N_2 and transferred into the EPR cavity at 190 K. The samples generated with one flash correspond to a dark state of $S_2Y_ZQ_A$. The samples generated with three flashes correspond to a dark state of $S_0Y_ZQ_A$. In some experiments, the dark state, $S_2Y_ZQ_A$ was generated by 190 K illumination.(14) A field swept spectrum was recorded to select a field position. The 190 K samples were flashed with a 532 nm pulse, generating either $S_0Y_Z^{\bullet}Q_A^-$ or $S_2Y_Z^{\bullet}Q_A^-$ and the decay of the $Y_Z^{\bullet}$ EPR signal was monitored. Transient data, associated with $S_2Y_Z^{\bullet}Q_A^-$ decay, were averaged from 3-8 samples, with 15 transients recorded per sample. Transient data, associated with $S_0Y_Z^{\bullet}Q_A^-$ decay, were averaged from 3-10 samples, with 15 transients recorded per sample. An offset, averaged from 10 s of data before the flash, was subtracted. Flash 1 to 15 yielded similar kinetics. The data from 15 flashes were fit with three exponentials and that fit was used to derive a $t_{½}$ value. This $t_{½}$ value was derived from multiple samples to give an average (mean) and a standard deviation. The EPR analysis was conducted on a Bruker (Billerica, MA) EMX spectrometer equipped with a Bruker ER 4102ST cavity and Bruker ER 4131VT temperature controller. EPR parameters were: magnetic field: 3375 G, microwave frequency: 9.46 GHz, power: 101 mW, modulation amplitude: 5 G, conversion: 20 ms, time constant: 164 ms. High microwave powers were used in order to saturate the $Y_D^{\bullet}$ signal.(14, 26)

To estimate the yield of the S_2 state, two different methods of preparation were compared. In the first approach, one flash was used to generate the S_2 state from a dark-

adapted sample (in S_1). In the second approach, the dark-adapted sample was continuously illuminated with red light at 190 K. The second procedure is expected to generate a ~100% yield of S_2.(31) The kinetic data obtained were similar. Thus, the percentage of centers in the S_2 state is assumed to 100% using either illumination protocol. Data from the two methods were therefore averaged. This prediction concerning the flash induced yield of the S_2 state agrees with a recent report, which was consistent with 0% misses (100% yield) on the first flash.(39)

Three flashes were used to generate the S_0 state from a dark-adapted sample in the S_1 state (Figure 3.1C). The percentage of the S_0 state can be estimated by assuming 0% misses on the first flash (see above) and 14% misses on the second and third flash.(5) The expected distribution after three flashes is 0% S_1, 2% S_2, 24% S_3, and 74% S_0. Thus, the state generated with three flashes is primarily S_0, but has a small contribution from S_3 and S_2. The S_0 and S_2 states were chosen for comparison because the barrier heights for the S_0 to S_1 and S_2 to S_3 transitions were predicted to be similar (Figure 1C).(2)

The S_0 and S_2 states were chosen for comparison because the barrier heights for the S_0 to S_1 and S_2 to S_3 transitions were predicted to be similar (Figure 3.1C). We were not able to measure $Y_Z^{\bullet}Q_A^-$ recombination rates in the S_1 and S_3 states at 190 K because the activation barriers were too low (but see ref (2) for a previous report concerning the S_3 state).

As an additional control, alkaline Tris treatment was used to remove the OEC. (40) The procedure incubated the sample at 1.5 mg/mL in Tris buffer (0.8 M Tris, 2 mM EDTA, pH 8.0) for 30 minutes under room light in a shaker. After the incubation, the sample is pelleted by centrifugation. The sample is then resuspended in SH buffer (400

mM sucrose, 50 mM HEPES, pH 8.0), homogenized and pelleted by centrifugation. Following three resuspensions in SH buffer, the sample is resuspended in SH-Cl buffer (400 mM sucrose, 15 mM NaCl, 50 mM HEPES, pH 7.5). EPR spectra were acquired under the same conditions as the oxygen evolving samples.

$Y_D^{\bullet}$ Experiments. Samples were dark adapted up to 24 hours in order to trap the S_1 state and generate a dark state in which $Y_D^{\bullet}$ had decayed. After this 24 hour dark adaptation, samples were still active and evolved oxygen at a rate of 700 μmol O_2/mg chl-hr. After dark adaptation, samples were homogenized with 500 μM ferricyanide. A control sample was compared to samples in which either 200 mM NaCl or 200 mM NH_4Cl was added. In some experiments, 10 μM 3-(3,4-dichlorophenyl)-1,1-dimethylurea (DCMU) was added from a 1 mM stock solution in ethanol. In these cases, the final concentration of ethanol was 1%. Samples were transferred to a Wilmad Lab Glass (Buena, NJ) WG-808-S-Q flat cell. Experiments were performed at 300 ± 1 K following a single laser flash. Experiments at lower temperatures were not possible due to the extremely long relaxation time of $Y_D^{\bullet}$. The data were fit with a monoexponential function to derive a $t_{1/2}$. The laser intensity was 40 mJ/cm^2, and the beam was expanded with a cylindrical lens. EPR parameters: magnetic field: 3496 G, microwave frequency: 9.85 GHz, power: 2 mW, modulation amplitude: 5 G, conversion: 5.24 s, time constant: 2.62 s, sweep time: 21,400 s.

Field-swept EPR spectra. Following collection of the transient EPR data, EPR spectra were measured by illuminating the sample within the EPR cavity with red filtered light (600 μmol photons/m^2-s, Dolan Jenner Industries, Boxborough, MA) at 190 K. To show that the expected $Y_Z^{\bullet}$ hyperfine splitting is observed, the microwave power and

modulation amplitude were decreased compared to the conditions used for the EPR transients. Because the microwave power is low, this field swept spectrum also has a contribution from $Y_D^{\bullet}$. The spectra shown are the average of three samples with three spectra obtained for each sample. EPR parameters were: frequency: 9.46 GHz, power: 0.64 mW, and modulation amplitude: 2 G (Figure 3.2) or 5 G (Figure 3.4), conversion time: 41 ms, time constant: 164 ms, sweep time: 21 s.

3.4 Results

In Figure 3.2, we present a comparison of the light induced X-band EPR spectra, as detected in the S_2 state (A) and in the S_0 state (B). The data in Figures 3.2A and B were recorded at 190 K under illumination at low microwave power and reflect overlapping $Y_Z^{\bullet}$ and $Y_D^{\bullet}$ contributions. These free radical signals, measured in the S_0 and S_2 states, have similar partially resolved hyperfine splittings, a ~20 G overall linewidth, and the expected g-value of 2.004.(41, 42) A narrow 7-10 G g=2 signal, which overlaps the $Y_D^{\bullet}$/ $Y_Z^{\bullet}$ signals is attributed to low yield chlorophyll and carotenoid radicals. These species are known to be generated by continuous illumination at low temperatures.(31) Under these conditions, Q_A^- exhibits a spin-coupled signal with the Fe^{2+} ion and is not detected.(43)

In Figures 3.2A and B, the red arrow indicates the magnetic field used to obtain the kinetic data. This position allows for unambiguous monitoring of time dependent changes in the $Y_Z^{\bullet}$ EPR signal without contribution from narrow chlorophyll and carotenoid radicals. The use of high microwave power for transient data saturates the $Y_D^{\bullet}$ signal, which decays on a much longer time scale, compared to $Y_Z^{\bullet}$.(26) The kinetic transients in Figures 3.2C and D result from $Y_Z^{\bullet}$ recombination with Q_A^- in ^1H_2O and

^2H_2O buffer at pL 6.5 (black and red respectively). These transients were normalized to their initial amplitude for presentation purposes. As observed, the rate of $Y_Z^{\bullet}Q_A^-$ recombination slows in ^2H_2O both in the S_2 (Figure 3.2C, red) and the S_0 (Figure 3.2D, red) states. Because Q_A^- is not protonated, a significant solvent isotope effect is consistent with a PCET mechanism for $Y_Z^{\bullet}$ decay in both S states.

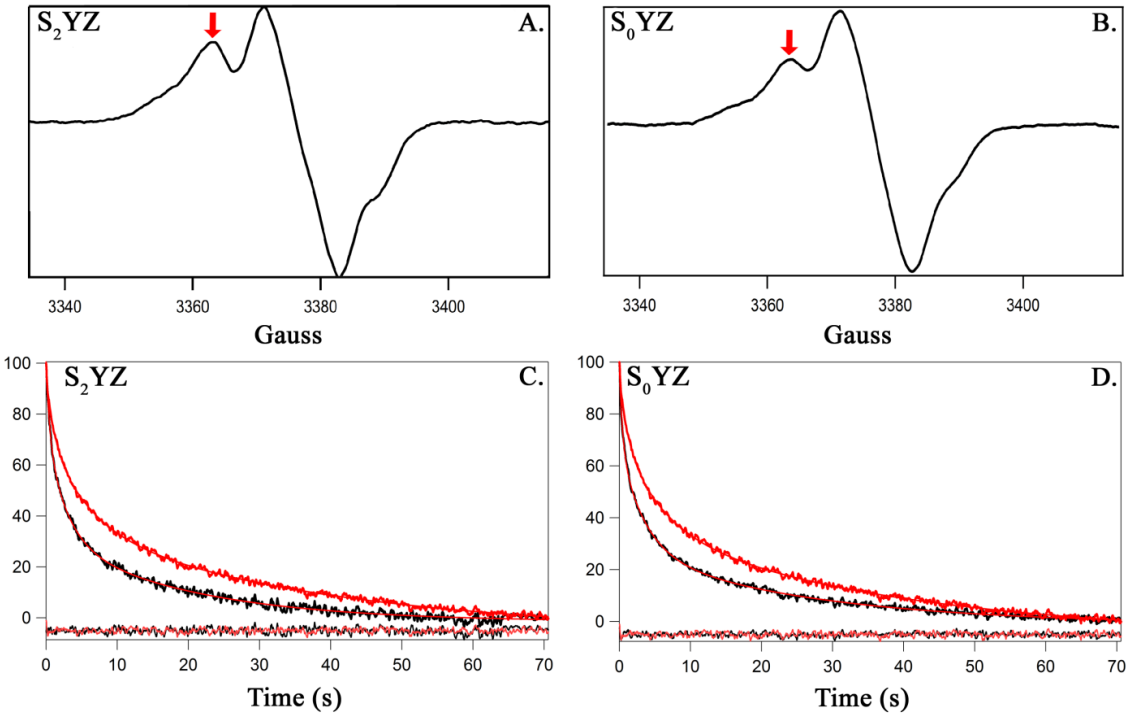

Figure 3.2. Comparison of representative EPR spectra (A and B) and averaged decay transients (C and D) derived for $S_2Y_Z^{\bullet}$ (A and C) and $S_0Y_Z^{\bullet}$ (B and D). Spectra were recorded under illumination at 190 K, pH 6.5, and yield a g-value of 2.004. The red arrows in A and B indicate the magnetic field position, which were used to monitor the kinetics in C and D. The transients in C and D were acquired either in ^1H_2O (black) or ^2H_2O (red), respectively. The transients were normalized for presentation purposes. Triexponential fits to the data and residuals are shown with in red and black.

The data were fit with three exponentials, and the fits were used to derive a $t_{½}$ value as a function of pL in S_2 and S_0 (Figure 3.3A and B, ^1H_2O-black and ^2H_2O-red).

Averaged over pL (where L refers to the lyonium ion), the rates of $Y_Z^{\bullet}Q_A^-$ recombination were slightly different in the S_0 and the S_2 states, with $t_{½}$ values of 3.3 ± 0.7 s and 2.1 ± 0.3 s in ^1H_2O buffer. The average $t_{½}$ value measured in the S_2 state is in agreement with a previous report.(14) As shown in Figure 3.3A and B, there was no significant pH dependence in either S state.

The $t_{½}$ values in ^1H_2O and ^2H_2O were divided to give a solvent or kinetic isotope effect (KIE). In Figures 3.3C and D, the KIE was plotted as a function of pL in the S_2 and S_0 states, respectively. The average KIE was higher in the S_2 state, when compared to the S_0 state (S_0, 1.3 ± 0.3 and S_2, 2.1 ± 0.3). The KIE was pL independent (from pL 5.0 to

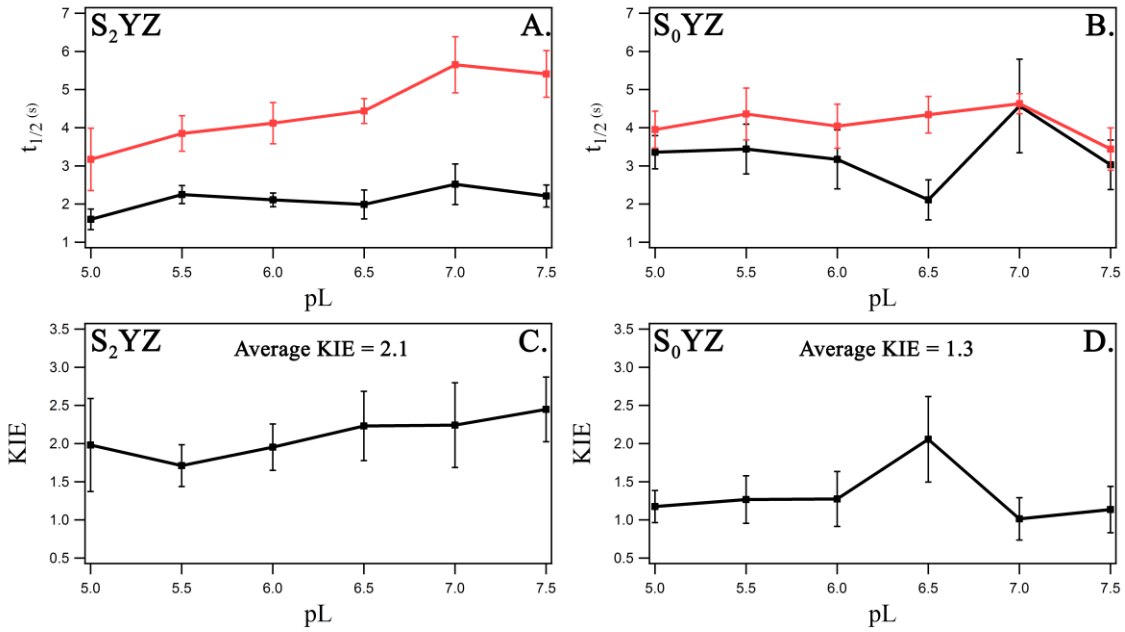

Figure 3.3. pL and solvent isotope dependence of $Y_Z^{\bullet}$ decay at 190 K, as assessed by the half-time for the overall reaction. (A) pL dependence in the S_2 state. The black line shows data acquired in ^1H_2O and the red line shows data acquired in ^2H_2O. (B) pL dependence in the S_0 state. The black line shows data acquired in ^1H_2O, and the red line shows data acquired in ^2H_2O. (C) pL dependence of the kinetic isotope effect (KIE) in the S_2 state. (D) pL dependence of the kinetic isotope effect (KIE) in

the S_0 state. The KIE values were derived by dividing the ^2H_2O $t_{½}$ values by the ^1H_2O $t_{½}$ values.

7.5) in both S states. The lack of pH dependence for the KIE was reported previously for the S_2 state, generated by continuous illumination.(14) In the PSII X-ray structure, the Y_Z pocket is exposed and readily accessible to water.(1) Thus, the lack of pL dependence cannot be attributed to lack of solvent accessibility.

In these studies, we report the effect of pL and deuterium isotope on the overall halftime of the $Y_Z^{\bullet}Q_A^-$ reaction, as a measure of k_{obs}. The individual rate constants and amplitudes derived from the three exponential fits are summarized in the Appendix B. The use of the overall $t_{1/2}$ as a measure of the reaction rate has the advantage that it is independent of assumed mechanism and that this value can be derived from the triexponential fits to the data with high precision. As an alternative, the pL and isotope dependence of the individual rate constants and amplitudes were also evaluated (Appendix B, Figures. B.1-4). Given the standard deviations, no significant pL dependence was observed either in the derived rate constants or amplitudes using this approach (Appendix B, Tables and Figures), consistent with our analysis of the $t_{1/2}$ values. The effect of ^2H_2O was difficult to evaluate because of the decrease in precision using this alternative approach.

To test the effect of changes in OEC hydrogen-bonding, PSII was treated with either 200 mM NH_4Cl or 200 mM NaCl (as a control for the ionic strength and chloride concentration change) at pH 7.5. Ammonia is known to bind to the OEC in the S_2 state.(25, 35) In Figure 3.4A, representative EPR spectra, recorded under illumination, are shown for samples prepared in the S_2 or S_0 state. These spectra yield the expected signal with a g-value of 2.004 and an overall linewidth of 20 G. Small changes in

lineshape are attributed to changes in the yield of narrow signals from chlorophyll or carotenoid radicals, generated under continuous illumination.

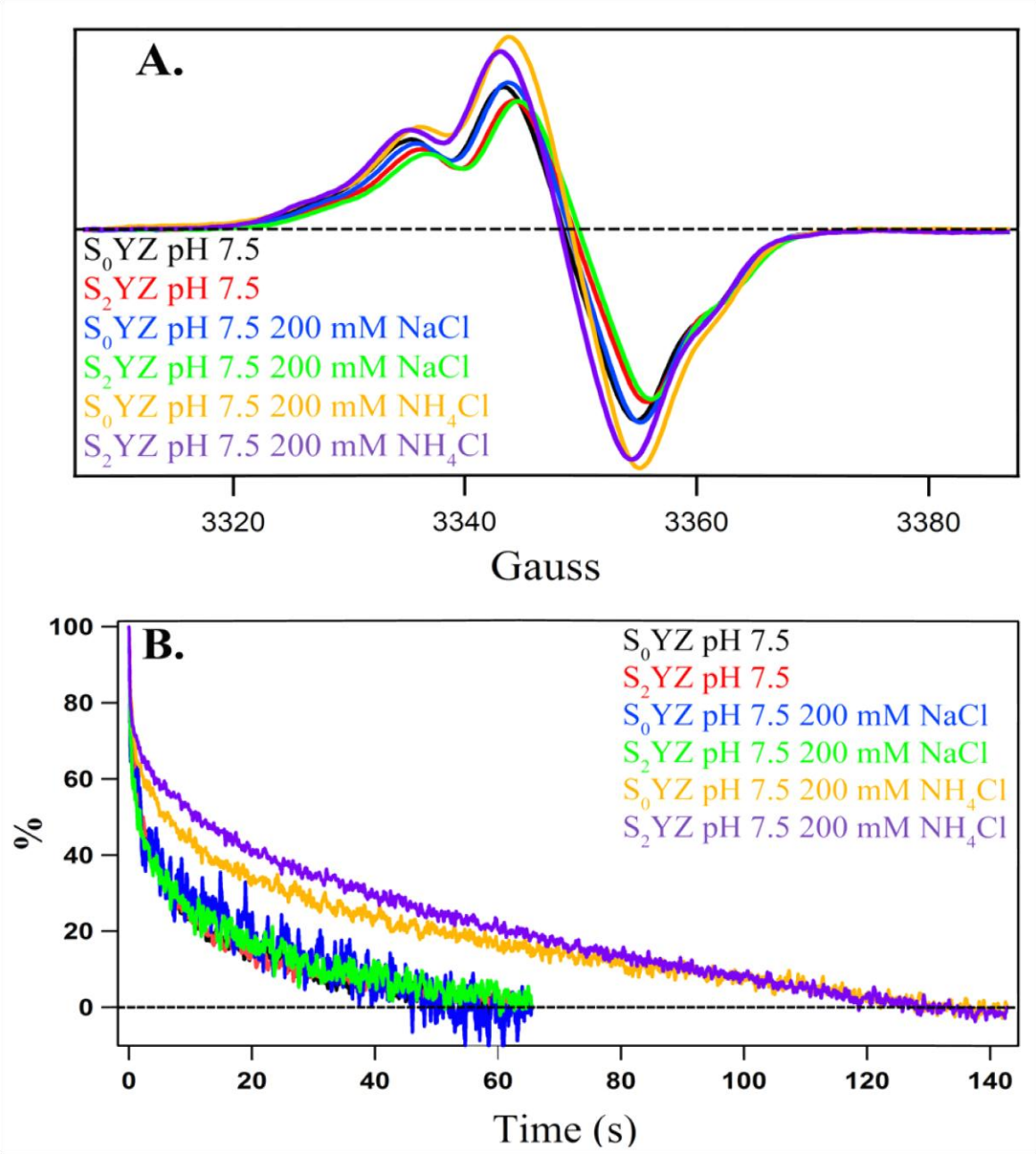

Figure 3.4. EPR spectra and transients, showing the effect of ammonia on $Y_Z^{\bullet}$ decay at 190 K and pH 7.5. (A) Representative EPR spectra for $S_0Y_Z^{\bullet}$ (black), $S_2YZ\bullet$ (red), $S_0Y_Z^{\bullet}$ + 200 mM NaCl (blue), $S_2Y_Z^{\bullet}$ + 200 mM NaCl (green), $S_0Y_Z^{\bullet}$ + 200 mM NH_4Cl (orange), and $S_2Y_Z^{\bullet}$ + 200 mM NH_4Cl (purple). Spectra in (A) were recorded under illumination and yield a g-value of 2.004. The red arrow in (A) indicates the magnetic field position, used to monitor the kinetics in (B). The transients in (B)

reflect $S_0Y_Z^{\bullet}$ (black), $S_2YZ\bullet$ (red), $S_0Y_Z^{\bullet}$ + 200 mM NaCl (blue), $S_2Y_Z^{\bullet}$ + 200 mM NaCl (green), $S_0Y_Z^{\bullet}$ + 200 mM NH_4Cl (orange), and $S_2Y_Z^{\bullet}$ + 200 mM NH_4Cl (purple). The transients were baseline corrected and normalized for presentation purposes.

In Figure 3.4B, the decay of the $Y_Z^{\bullet}Q_A^-$ state was monitored at constant field, as described above, either in 200 mM NaCl (green and blue) or in 200 mM NH_4Cl (orange and purple). In both the S_2 (purple) and S_0 (orange) states, the addition of ammonia resulted in a significant decrease in the rate of decay. There was no detectable change induced by the addition of 200 mM NaCl (compare black and red with blue and green, Figure 3.4). The $t_{½}$ values were derived from the transient data (Figure 3.4B). The values in the S_2 state were 1.4 $\pm$ 0.8 s in the control 200 mM NaCl sample and 15.3 $\pm$ 4.4 s in the 200 mM NH_4Cl sample. The values in the S_0 state were 1.9 $\pm$ 1.4 s in the control 200 mM NaCl sample and 8.2 $\pm$ 1.9 s in the 200 mM NH_4Cl sample. As controls for irreversible inactivation of the OEC by ammonia, we examined the rate of radical decay in Tris-washed PSII(40), in which the Mn_4CaO_5 cluster is purposely removed. In this preparation, radical decay was much faster ($t_{½}$ = 0.7 s) and was on the time scale consistent with oxygen evolving samples (Figure B.6). We conclude that the ammonia-induced slowing of $Y_Z^{\bullet}$ decay is not due to irreversible removal of the Mn_4CaO_5 cluster.

As shown in Figure 4, ammonia decreased the rate of decay of the $S_2Y_Z^{\bullet}Q_A^-$ state by a factor of ~11, and caused a ~4 fold decrease in the rate of $S_0Y_Z^{\bullet}Q_A^-$ decay. This value for the $S_0Y_Z^{\bullet}Q_A^-$ is an upper limit, because this sample is expected to have a small contribution from the S_2 and S_3 states (see Materials and Methods).

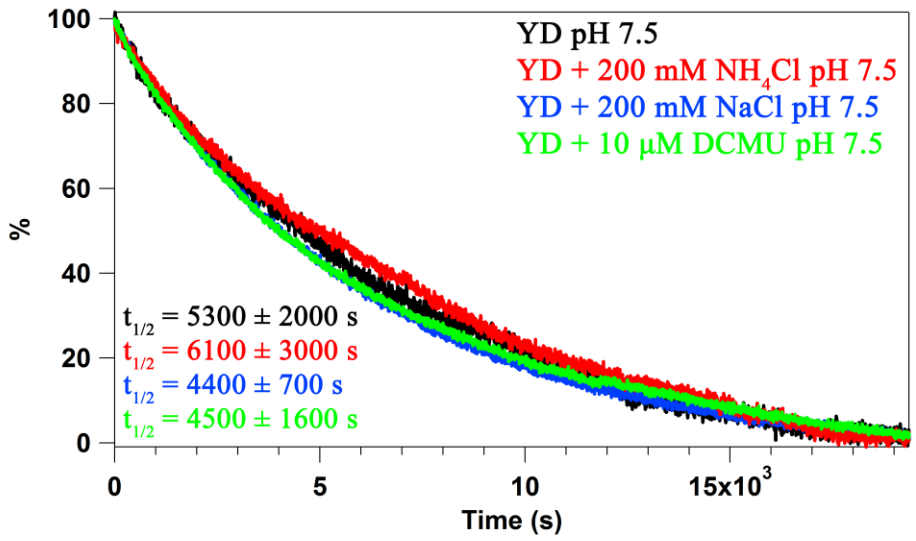

Figure 3.5. EPR transients, showing the effect of 200 mM NaCl or NH_4Cl on $Y_D^{\bullet}$ decay at 300 K and pH 7.5. The transients were recorded from oxygen evolving PSII and correspond to $Y_D^{\bullet}$ (black), $Y_D^{\bullet}$ + 200 mM NH_4Cl (red), $Y_D^{\bullet}$ + 200 mM NaCl (blue), and Y_D + 10 µM DCMU (green). The transients were baseline corrected and normalized for presentation purposes.

As an additional control, we investigated the effect of ammonia on $Y_D^{\bullet}Q_A^-$ recombination. In Figure 3.5, the decay of $Y_D^{\bullet}$ at 300 K is shown in a control (black), 200 mM NaCl (blue), 200 mM NH_4Cl (red), and 10 µM DCMU (green) at pH 7.5. The $t_{½}$ values were 5300 ± 2000 s, 6200 ± 3000 s, 4400 ± 700 s, 4500 ± 1600 s respectively. As expected, the rate of recombination was insensitive to the addition of DCMU,(44) an inhibitor that binds at the Q_B site. This result verifies that $Y_D^{\bullet}Q_A^-$ recombination is monitored in Figure 5. Given the standard deviation, there was no significant effect of ammonia on $Y_D^{\bullet}Q_A^-$ recombination.

Previous EPR measurements have investigated the pH dependence of $Y_D^{\bullet}Q_A^-$ decay.(38, 45) In Figure 3.6, we plot the $t_{½}$ value, derived from those $Y_D^{\bullet}$ data, and compare to the pL dependence of $S_0Y_Z^{\bullet}Q_A^-$ and $S_2Y_Z^{\bullet}Q_A^-$ recombination. As shown, the $Y_D^{\bullet}Q_A^-$ recombination rate is three orders of magnitude slower, when compared to $Y_Z^{\bullet}Q_A^-$

recombination at high pH values. However, the $Y_D^{\bullet}$ rates exhibit more than a 1000 fold stimulation as the pH decreases, while the $Y_Z^{\bullet}$ data do not show a significant pH effect in either S state.

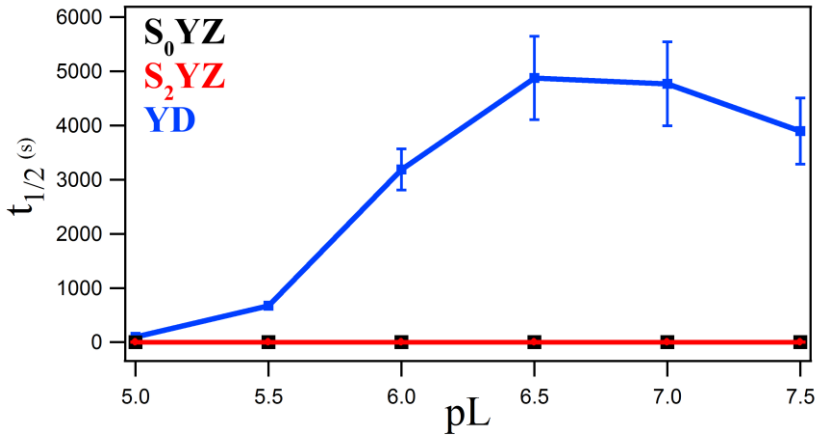

Figure 3.6. Comparison of the pL dependence for $Y_D^{\bullet}$, $S_2Y_Z^{\bullet}$, and $S_0Y_Z^{\bullet}$ decay. Both $Y_Z^{\bullet}$ and $Y_D^{\bullet}$ decay by recombination with Q_A^-. These $Y_D^{\bullet}$ data were acquired in OEC-depleted PSII (14, 38)

Figure 3.7 provides a comparison of the hydrogen-bonding environment of Y_D and Y_Z.(1) As shown, Y_Z participates in an extensive hydrogen-bonding network, but Y_D does not. In our experiments, addition of ammonia, which decreases hydrogen-bonding in the S_2 state,(25) increased the $Y_Z^{\bullet}$ lifetime by a factor of eleven at pL 7.5. Thus, when ammonia displaces bound water, the kinetic behavior of the $Y_Z^{\bullet}$ radical is observed to be more similar to that of the long-lived $Y_D^{\bullet}$ radical.

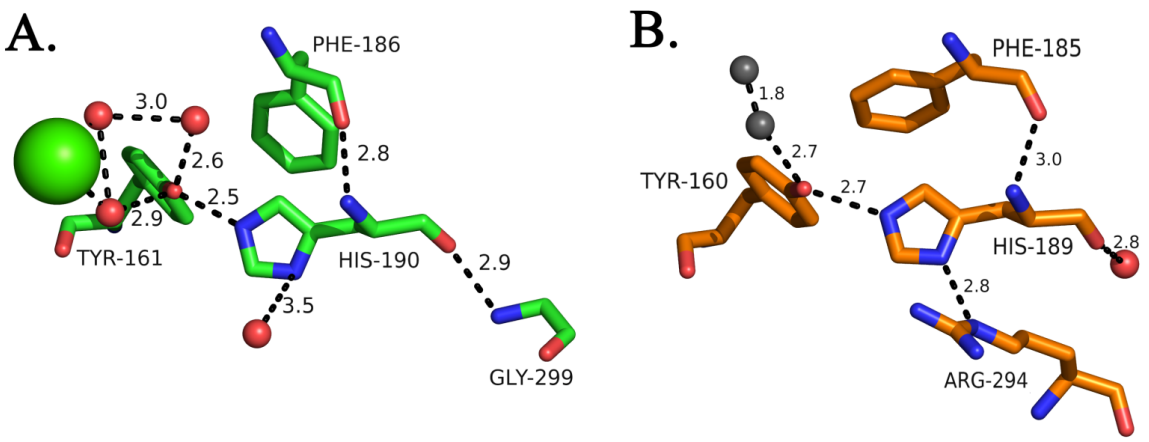

Figure 3.7. A comparison of the local hydrogen-bonding environment for Y_Z (A) and Y_D (B).(1) Amino acid residues predicted to hydrogen bond with Y_Z and Y_D are shown in green (A) and orange (B), respectively. Assigned, bound water molecules are shown in red (A and B), and the calcium ion is in green (A). An assigned water molecule, which is predicted to have partial occupancy, is shown in gray (B). Predicted hydrogen bonds are depicted with black dashed lines and with distances in Angstroms (The Pymol Molecular Graphics System, Version 1.3, Schrödinger LLC).

3.5 Discussion

Summary of results. In this paper, we report that Mn_4CaO_5 redox reactions and the addition of ammonia alter the rate of $Y_Z^{\bullet}$ reduction and the average solvent isotope effect on the reduction reaction. We compared two different OEC oxidation states, the S_0 (three flashes) and the S_2 state (1 flash or continuous illumination at 190 K). These states are known to differ in Mn oxidation state, with S_0 assigned to a $Mn(III)_3Mn(IV)_1$ state and S_2 assigned to a $Mn(III)_1Mn(IV)_3$ oxidation state.(28, 30, 46) Mn oxidation reactions are likely to change hydrogen-bonding interactions among the bound water molecules in the OEC.(46, 47) We found that the rate of $Y_Z^{\bullet}Q_A^{-}$ recombination and the average KIE were altered, when the S_0 and S_2 states were compared. However, the halftimes and KIE values were pL independent in both the S_0 and S_2 states, given the standard deviations of the measurements. This is in contrast to the pronounced pH dependence, previously

reported for $Y_D^{\bullet}Q_A^-$ recombination. The addition of ammonia dramatically slowed the rate of $Y_Z^{\bullet}$ decay, but had no significant effect on $Y_D^{\bullet}$. We attribute this effect to substitution of ammonia into the OEC hydrogen-bonding network, surrounding Y_Z, and the subsequent, expected decrease in hydrogen bond strength.(25) Taken together, these data suggest that hydrogen-bonding changes are linked with the S state cycle. Such hydrogen-bonding changes would alter the midpoint potential and/or pK_a, and, thereby, could change the rate of $Y_Z^{\bullet}$ recombination.

Overview of PCET reactions and Y_Z. Figure 8 shows a general scheme for PCET reactions involving Y_Z and $Y_Z^{\bullet}$. In this paper, we focus on the recombination reactions, shown in the blue brackets, in which an electron and proton are transferred orthogonally to the tyrosyl radical.

Tyrosine-based PCET reactions may occur by three different mechanisms.(12, 48-57) When the proton and electron are transferred together through a single transition state, the reaction is CPET (Figure 3.9). Many tyrosine-based model compounds exhibit a CPET mechanism.(12, 48, 49, 53, 56, 57) Experimental and theoretical approaches have concluded that intermolecular and intramolecular hydrogen bonds facilitate CPET reactions.(12, 48, 49, 53, 54, 56-58) For tyrosine redox reactions, CPET reactions avoid the formation of high-energy intermediates, such as a tyrosine cation radical, but occur at the expense of a high reorganization energy.(12, 48, 49, 53) Alternatively, the electron can be transferred before the proton (ETPT) or the proton can be transferred before the

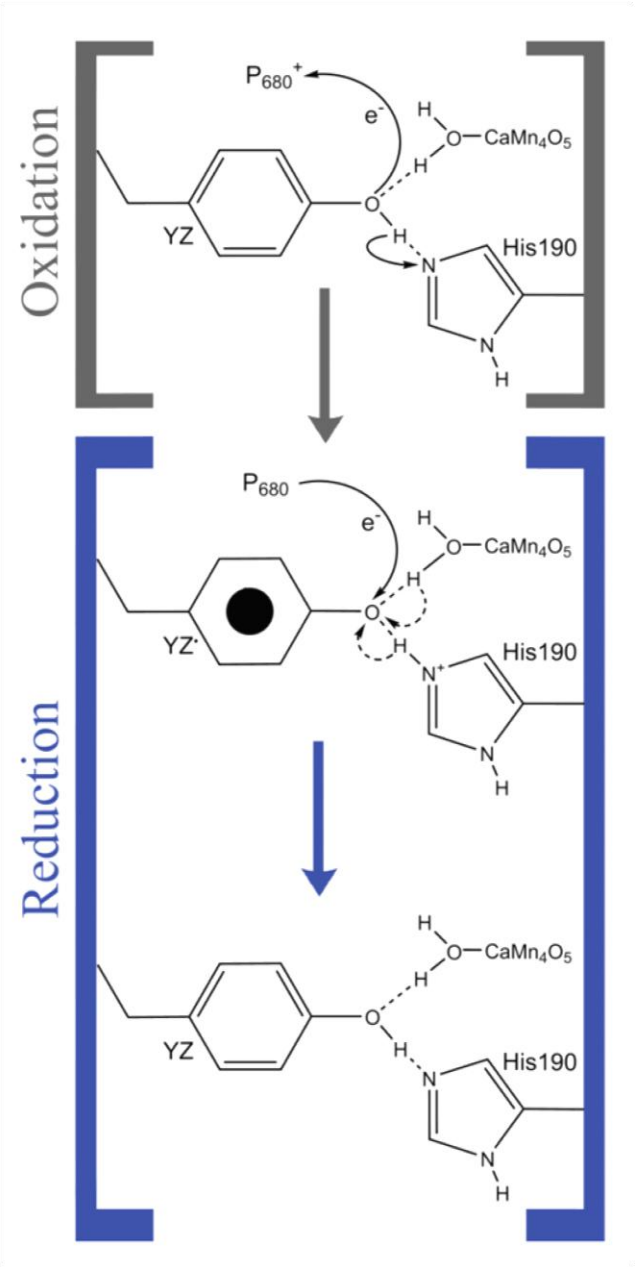

Figure 3.8. Oxidation (top) and reduction (bottom) reactions for Y_Z, which is depicted as hydrogen bonded to a calcium-bound water and to the side chain of His190-D1. In the top panel, P_{680} oxidizes Y_Z generating a neutral radical. In the bottom panel, the reduction of Y_Z and calcium bound water and His190-D1 compete to donate a proton. In this paper, we are monitoring the reduction (bottom) reaction.

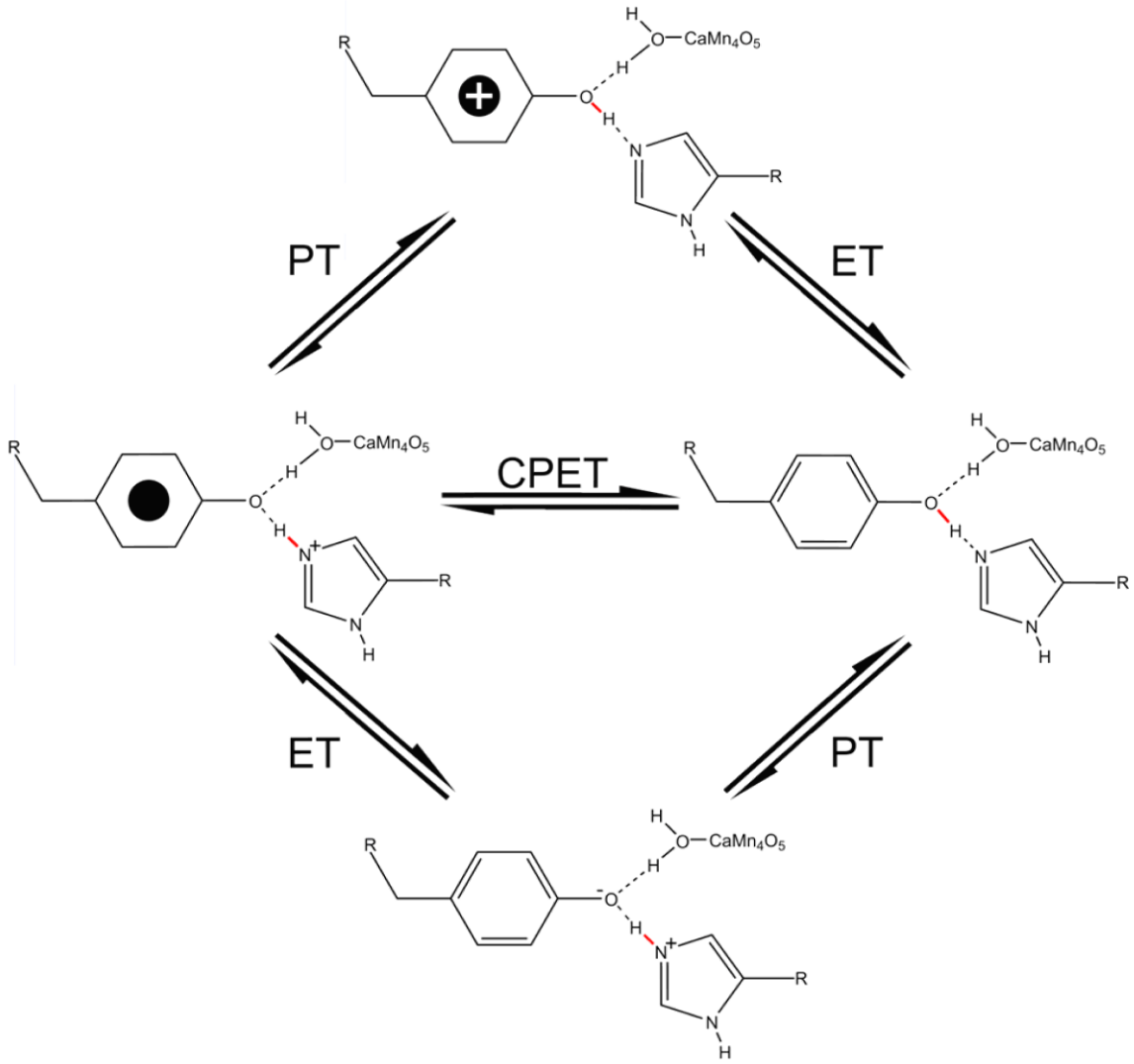

Figure 3.9. Reaction diagram illustrating the stepwise and concerted pathways for PCET reactions of tyrosine with histidine acting as a proton donor. The top pathway begins with a proton transfer to create the tyrosyl cation radical followed by an electron transfer to form tyrosine. The bottom pathway starts with and electron transfer that creates tyrosinate followed by a proton transfer to form tyrosine. The middle pathway concertedly transfers an electron and a proton in a single step to transition from a neutral tyrosyl radical to tyrosine.

electron (PTET). In PTET, the intermediate in the two-step reaction is a tyrosine cation radical. In ETPT, the intermediate in the two-step reaction is the tyrosinate singlet state.

Summary of Previous Results: Oxidation of Y_Z. Previous studies have focused on PCET during the oxidation reaction (Figure 3.8, top) in which Y_Z is both an electron and a proton donor. Electron transfer from Y_Z to P_{680}^+ follows the rapid, picosecond time scale, light-induced production of the $P_{680}^+Q_A^-$ state and, then occurs predominantly on the nanosecond time regime.(59-61) This process is complete before the beginning of data acquisition under our conditions. In oxygen-evolving centers, the rate of Y_Z to P_{680}^+ electron transfer exhibited no significant isotope effect in most studies ((59-62) and references therein).

Electron transfer to $Y_Z^\bullet$. In this paper, we are studying the recombination reaction in which $Y_Z^\bullet$ accepts an electron and a proton (Figure 3.8, bottom). The detailed mechanism of electron transfer during recombination is not known, but can be imagined to involve a direct one-step recombination or a multistep mechanism.(63, 64) Dutton's ruler, an empirical relationship that estimates the rate of electron transfer (65), can be used to estimate the direct transfer mechanism. In the equation below, the exponential decay of tunneling rate is k_{et} (in s^{-1}), with edge-to-edge distance R (in Å) and a parabolic dependence of log rate on ΔG and λ (in eV).(65)

The Y_Z midpoint potential has been reported as 1 V (19), the P_{680} potential as 1.26 V (63), and the Q_A potential as ~0 V (66). A reorganization energy of 0.7 V is often assumed (65). For the 34.1 Å distance between Q_A to Y_Z, predicted by the X-ray structure (1), a rate of 10^{-6} s^{-1} is predicted using these measurements and assumptions. This rate is many orders of magnitude slower than our observed recombination times (~1 s^{-1}). Thus, a direct one step mechanism is not favored.

A multi-step recombination mechanism may occur via the $P_{680}^{+}Q_A^{-}$ couple. A simple mechanism of electron transfer in the back reaction can be written with two elementary steps:

Step 1:

Step 2:

where k_{in} is the intrinsic rate of charge recombination through $P_{680}^{+}Q_A^{-}$ (which occurs on the microsecond time scale).(67-69)

For this pre-equilibrium mechanism, the velocity of the reaction can be written,

which can be rearranged to give:

—

As shown in the derivation above, for this two-step, pre-equilibrium recombination mechanism, the measured rate constant, k_{obs}, is the product of the $P_{680}^{+}Q_A^{-}$ recombination rate constant, k_{in}, and the equilibrium constant governing redox reactions between Y_Z and P_{680}^{+}. The k_{in} recombination rate has been reported as ~7 x 10^2 s^{-1} (67) or 5 x 10^3 s^{-1} (69) and is pH and solvent isotope independent (67, 69). The value of k_1 has been reported as ~ 10^7 s^{-1} (59). Using our experimentally measured value of k_{obs} (~0.2-0.3 s^{-1}), the pre-equilibrium two-step mechanism predicts the value of k_2 to be ~10^4 s^{-1}. Estimating the distance between Y_Z and P_{680} in the crystal structure(1) as 13.5 Å and using the potentials and reorganization energies given above. Dutton's ruler predicts that

an electron transfer (ET only) rate constant over this distance will be ~10^3 s^{-1}. An adjustment of the reorganization energy to 0.6 V gives a predicted rate of 10^4 s^{-1}. This analysis suggests that the two-step mechanism is a reasonable kinetic scheme for the YZ• recombination reaction. However, more complex mechanism, involving thermal relaxation events among $Y_Z^{\bullet}$ and P_{680}^{+} substates cannot be excluded. The use of the overall $t_{1/2}$ in our analyses has the advantage that it is independent of assumed mechanism.

The PSII X-ray structure predicts multiple proton donors to $Y_Z^{\bullet}$. The recent PSII X-ray structure(1) suggests that activated, calcium bound water and protonated histidine side chain compete for proton donation to Y_Z (Figures 3.1B and 3.7A). It should be noted that it is not known which S state is represented in the X-ray structure.(1) As depicted in Figures 3.1B and 3.7A, Y_Z is involved a network of strong hydrogen bonds and is 2.5 Å from His190-D1, 2.6 Å from a bound water, and 2.8 Å from a calcium bound water molecule. Calcium acts as a Lewis acid and will decrease the pKa of the water and increase its acidity by ~1000 fold.(70) As the oxidation of the Mn_4CaO_5 cluster increases, calcium will become a stronger Lewis acid. Chemical complementation suggested a role for His190-D1 in proton transfer to $Y_Z^{\bullet}$;(71) evidence for another proton donor was obtained from EPR studies of a His190-D1 mutant.(72) Water, especially activated water, and protonated His 190-D1 side chain are both expected to be facile proton donors.(70, 73-75)

pH independence of the $Y_Z^{\bullet}Q_A^{-}$ recombination rate. The pH independence of the $Y_Z^{\bullet}Q_A^{-}$ recombination rate, reported here, is an interesting observation. pH independence for recombination in the S_0 state was reported previously, by monitoring the production

of a coupled Y_Z-metal signal at liquid helium temperature.(76) In that work, lack of pH dependence was attributed to a lack of solvent exchange and a hydrophobic Y_Z environment. However, the more recent PSII X-ray structure shows that the Y_Z environment is hydrophilic. Also, we observe a significant KIE in both S_0 and S_2 states, demonstrating that solvent isotope exchange does occur. To explain the lack of pH dependence on recombination in the S_2 state, we recently proposed that the network of strong hydrogen bonds, predicted in the X-ray structure, facilitates a coupled proton transfer reaction (CPET). CPET reactions can proceed by a pH independent mechanism.(12, 51, 76) Alternatively, if the two-step preequilibrium model is the correct mechanism, the lack of pH independence could be attributed to compensating pH effects on the forward, k_1, and back reaction, k_2. However, compensation may not explain the solvent isotope dependence, because k_1 and k_{in} have both been reported to be independent of solvent isotope effects, as described above.(59-61, 67, 69)

Y_Z and Y_D have different PCET mechanisms. Comparison of Y_Z to Y_D aids in the interpretation of these results (Figure 3.7). Previous work used EPR spectroscopy to investigate the mechanism of $Y_D^{\bullet}$ PCET.(38, 45) The reaction followed was recombination of $Y_D^{\bullet}$ with Q_A^-. Through analysis of the pH and solvent isotope dependence, the $Y_D^{\bullet}$ reaction was deduced to be PTET at low pL and to be CPET at high pL values, for example pL 8.(38) The PTET reaction showed a dramatic increase in rate as the pH decreased, consistent with titration of the $Y_D^{\bullet}$ radical and its proton donor. The PTET reaction was not associated with a significant KIE. However, a significant KIE (2.4) was observed at pL 8.0. A proton inventory on the CPET reaction at pL 8.0 was consistent with multiple proton transfer reactions through two different pathways. One

pathway was suggested to involve water and the other pathway was suggested to involve His189-D2 (Figure 3.7B).(45) The 1.9 Å X-ray crystal structure supports this interpretation.(1)

Unlike $Y_D^{\bullet}$ PCET, $Y_Z^{\bullet}$ PCET does not show pH dependence. When comparing the environment surrounding Y_Z and Y_D (Figure 3.7), the hydrogen-bonding environment is dissimilar. One difference between the environments of Y_Z and Y_D is the presence of Arg294 in the D2 polypeptide, which is 2.8 Å from His189-D2. Y_D has potential pi-cation interactions with this arginine (at 6.4 Å from YD) and with Arg-272-D2 in the CP47 subunit (at 7.8 Å). The corresponding arginines are not found in the Y_Z environment. Studies of biomimetic PSII-inspired peptides, which conduct a tyrosine based PCET reaction involving a pi-pi stacked histidine, concluded that pi-cation interactions with arginine lower the potential of redox active.(13, 77) This effect may account for the lower reported midpoint potential of Y_D (23); when compared to Y_Z.(19) An additional impact of the Arg294/His189 interaction will be to decrease the pK_a of His189-D2, making it a better proton donor, compared to His190-D1.

A second difference between Y_D and Y_Z is the distance between the potential proton donating histidine and the redox active tyrosine. His190-D1 is 2.5 Å from Y_Z; the analogous His189-D2 is 2.7 Å from Y_D. However, the potential impact of this small change in hydrogen bond length to histidine is not clear. A recent study on a series of ruthenium bound tyrosine complexes with varying hydrogen bond distances from 2.54-2.75 Å was conducted.(57) This study concluded that all of these compounds proceed through a CPET mechanism with a varying KIE. Interestingly, the compound with a hydrogen bond donor-acceptor distance of 2.54 Å exhibited more rapid PCET and was 2-

3 orders of magnitude faster when compared to a compound with a donor-acceptor distance of 2.75 Å.(57) However, the 2.54 and 2.75 Å compounds were found to have KIE values of 1.4 and 4.0 respectively, while Y_Z and Y_D have similar KIE's on the CPET reaction (at high pL for Y_D). Also, it should be noted that a kinetic study of phenol-amines did not report this exquisite distance dependence.(15)

Another difference between the environments of Y_Z and Y_D is that Y_Z is involved in a network of strong hydrogen bonds involving multiple bound water molecules (Figure 3.7A). Y_D does not participate in this network and is hydrogen bonded just to His 189-D2 and a single bound water molecule with partial occupancy. Y_Z is 2.6 Å from the closest bound water molecule, whereas Y_D is 2.7 Å from the water molecule with partial occupancy.(1) The effects of ammonia on $Y_Z^{\bullet}$ kinetics, but not on $Y_D^{\bullet}$ kinetics, suggest that this hydrogen-bonding network plays a role in control of $Y_Z^{\bullet}$ kinetics (Fig 10).

$Y_Z^{\bullet}$ PCET and the S state transitions. In this paper, we report that the KIE and halftime for Y_Z recombination are distinct in two different S states, corresponding to two different oxidation states of the Mn cluster. We attribute this to oxidation-induced changes in hydrogen-bonding network of the OEC. For example, oxidation of the Mn may decrease the pK_a of metal bound water, making calcium bound water a more effective proton donor in the higher S state. Theoretical studies have suggested that OEC oxidation may control pathways for water transfer by changes in electrostatic interactions.(29, 47)

As discussed above, three different pathways (Figure 3.9) can be imagined for non-synchronous transfer of a proton and electron to $Y_Z^{\bullet}$. This reaction corresponds to k_1 and k_2 in the two-step, pre-equilibrium mechanism (see step 1). This square scheme

(Figure 3.9) is introduced here to account for the kinetic isotope dependence observed in our experiments.

In PTET (Figure 3.9, top), the k_2 reaction is written:

The overall rate in PTET is the product of the preequilibrium constant for formation of the tyrosyl cation radical and deprotonation of a histidine side chain (estimated as 10^{-8}) and the intrinsic k_{et}. Using the estimated value of 10^4 s for k_2, as estimated above, the PTET scheme predicts that the intrinsic ET rate, k_{et}, would have to be very rapid, on the order of 10^{12} s^{-1}. Lower values of the pK_a, consistent with activated water serving as the proton donor (estimated as $pK_a = 2$ (75)) still give an estimated k_{et} of 10^8 s^{-1}. These ET rate constants are greater than expected for an uphill electron transfer reaction over 13 Å. Moreover, in PTET, pH dependence is expected due to titration of the proton acceptor, $Y_Z^{\bullet}$, and the proton donor(s) in a solvent accessible environment. Such a pronounced pH dependence was observed for the Y_D PCET reaction at low pH values for example(38, 45), which also involves water and an imidazole side chain (His189-D2) as proton donors. Therefore, a PTET mechanism for k_2 is not favored.

In ETPT, the k_2 reaction, estimated as 10^4 s^{-1}, also consists of two steps and can be written:

The ETPT reaction will be pH independent and exhibit only a small isotope effect if electron transfer is the rate limiting step.(12, 49, 50) (12, 49, 50) Rate-limiting ET is

expected in this scenario, because proton transfer from a protonated histidine to tyrosinate will be significantly downhill in free energy. For example, using pK_a values of 6 and 10, respectively, for His190-D1 (or another proton donor) and tyrosine, the intrinsic k_{et} rate would indeed be predicted to be slow (1 s^{-1}). In fact, this value is much slower than the estimate for pure ET from Dutton's ruler for this reaction (see above). However, the KIE values measured for the S_2 (2.1) and S_0 (1.3) states are significant and may not be consistent with ETPT. Therefore, an ETPT mechanism is not favored, especially for the S_2 state reaction.

In CPET, a significant KIE (>1.6) is expected, and the reaction may be pH independent.(12, 49, 51) Therefore, a CPET mechanism can account for the pH independence and solvent isotope effects on $Y_Z^{\bullet}$ decay kinetics in both S states. Adiabatic Marcus theory can be used to explain CPET reactions and that these reactions have smaller rate constants than a pure ET reaction, due to a larger activation barrier for these reactions.(50) If the k_2 reaction operates by a CPET mechanism, however, a question remains concerning the forward reaction, governed by k_1 (see our previous discussion in ref (14)). This nanosecond time-scale reaction was reported to have no solvent isotope effect in some studies, although there are some discrepancies in the literature.(59-62, 67, 69) One possible answer may be that complex protein dynamics accompanies this reaction. In that case, the mechanism for $Y_Z^{\bullet}$ formation and decay would be more complex than the two-step mechanism, and may involve, for example, additional elementary relaxation events in the P_{680}^{+} and the $Y_Z^{\bullet}$ states. Resolving this question will require further experimentation.

Ammonia alters $Y_Z^{\bullet}$ decay kinetics by replacing water in the OEC hydrogen-bonding network. To explain the S state dependence of Y_Z PCET, we propose that the hydrogen-bonding environment of Y_Z is altered by changes in Mn oxidation state and activation of calcium bound water. Supporting the interpretation that hydrogen-bonding is important, we found that the effects of ammonia distinguished the S_0 and S_2 states. Ammonia is an inhibitor of photosynthetic oxygen evolution and has been proposed to act as a substrate-based inhibitor.(34, 78) Magnetic resonance studies have concluded that ammonia binds directly to Mn ions in the Mn_4CaO_5 cluster.(79) FT-IR studies have shown that ammonia displaces bound water molecules in the OEC and disrupts a hydrogen-bonding network.(25) Such a change in hydrogen bond strength is expected.(80, 81) Ammonia binding to the OEC has been monitored previously by Mn EPR spectroscopy, in which a modified g=2 multiline signal from the S_2 state was detected.(35, 82) These studies concluded that ammonia binds to the OEC in the S_2 and S_3 states, but not in the S_0 and S_1 states.(35) Recent FT-IR studies of the S_1 to S_2 transition have shown that ammonia induces a change in OEC peptide carbonyl frequencies, consistent with a change in hydrogen-bonding in the S_2 state.(25) Through comparison with the amtB ammonia transporter,(83) it was proposed that ammonia displaces water molecules in an extended hydrogen-bonding network, which involves peptide carbonyl groups.(25)

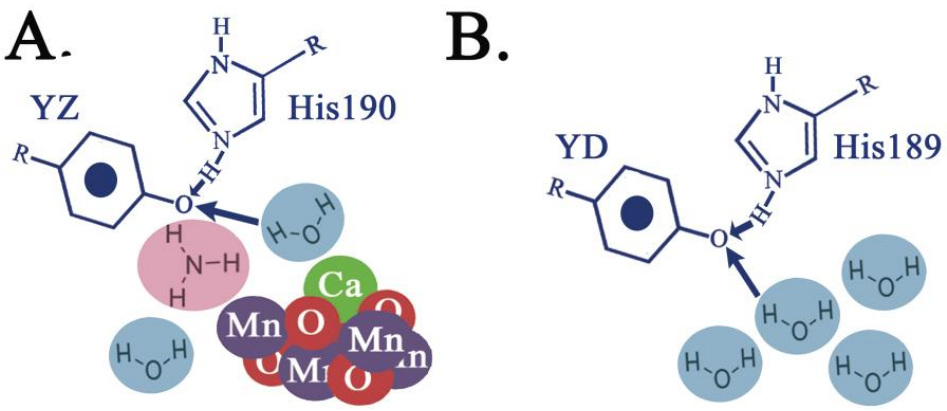

Figure 3.10. Proton donation to Y_Z (A) and Y_D (B) in ammonia treated PSII. A two pathway model for proton donation to Y_D was suggested by a proton inventory study.(45)

In these EPR studies, we used ammonia as a probe of Y_Z hydrogen-bonding interactions. Ammonia had differential effects on the S_2 and S_0 states, and the observed effect of ammonia on the recombination reaction was dramatic. Ammonia is expected to form weaker hydrogen bonds.(80, 81) Therefore, the observed slowing of the reaction rate is attributed to a decrease in $Y_Z/Y_Z^{\bullet}$ hydrogen-bonding, when water is displaced by ammonia in the OEC hydrogen-bonding network (Figure 10). We observed no significant ammonia effect on the rate of $Y_D^{\bullet}Q_A^{-}$ recombination. $Y_D^{\bullet}$ and Q_A^{-} are not predicted to interact with water molecules in the hydrogen-bonding network (Figure 10).

The addition of ammonia increased the lifetime of $Y_Z^{\bullet}$, making its kinetic behavior more similar to the slow kinetic behavior of $Y_D^{\bullet}$. Ammonia may induce a change in Y_Z midpoint potential, with the direct effect from changes in hydrogen-bonding (~3-5 kcal/mole) estimated as ~0.1-0.2V. Interestingly, the midpoint potential of Y_D has been reported to be 250 mV lower when compared to Y_Z(19, 23) and Y_D is shown to be less extensively hydrogen bonded in the X-ray structure.(1) The slowing of the Y_Z recombination rate in the presence of ammonia is reminiscent of the effects reported

when the OEC is removed by treatment with alkaline Tris. Under those conditions, the midpoint potential $Y_Z^{\bullet}$ decreased by ~100 mV, and its lifetime increased.(68) These previous reports support the interpretation that a decrease in midpoint potential can decrease the rate of PSII tyrosyl radical decay. It should be noted that ammonia addition is not leading to loss of Mn, because, in a control experiment in which we purposely removed the OEC, the rate of $Y_Z^{\bullet}$ decay dramatically increased. By contrast, our data show that ammonia slows the rate of $Y_Z^{\bullet}$ decay in both S states and has a reversible effect on oxygen evolution.

Implications. Using $Y_Z^{\bullet}$ kinetics as a probe, our experiments provide evidence that the hydrogen-bonding environment of Y_Z is altered when the S_0 and S_2 states are compared. This hydrogen-bonding change is attributed to the accumulation of positive charge, which is expected to activate calcium-bound water molecules and alter the strength of the hydrogen-bonding network with His190-D1. Such hydrogen-bonding changes could potentially play a crucial role in controlling the acid/base chemistry during proton transfer reactions. For example, charge accumulation on the Mn_4CaO_5 has been predicted to control the movement of water to the active site.(46, 47) Comparing the S_0 and S_2 states, our kinetic results are consistent with a change in Y_Z midpoint potential or pK_a, which is mediated by the Mn oxidation reaction. This dynamic interplay between water, Y_Z, and the Mn_4CaO_5 may regulate the unique and complex chemistry of photosynthetic water oxidation.

Acknowledgments: The authors thank Brandon Polander for helpful conversations. This work was supported by a grant from the National Institutes of Health, GM43273 (B.A.B.).

3.6 References

1. Umena Y., Kawakami K., Shen J.-R., & Kamiya N. (2011) Crystal structure of oxygen-evolving photosystem II at a resolution of 1.9 Å. *Nature* 473(7345):55-60.

2. Styring S. & Rutherford A. W. (1988) Deactivation kinetics and temperature dependence of the S-state transitions in the oxygen-evolving system of photosystem II measured by EPR spectroscopy. *Biochimica et Biophysica Acta* 933:378-387.

3. MacDonald G. M., Steenhuis J. J., & Barry B. A. (1995) A difference infrared spectroscopic study of chlorophyll oxidation in hydroxylamine treated photosystem II. *Journal of Biological Chemistry* 270:8420-8428.

4. Hoganson C. W. & Tommos C. (2004) The function and characteristics of tyrosyl radical cofactors. *Biochimica et Biophysica Acta - Bioenergetics* 1655(0):116-122.

5. Joliot P. & Kok B. (1975) Oxygen evolution in photosynthesis. *Bioenergetics of Photosynthesis*, ed Govindjee (Academic Press, New York), pp 388-412.

6. Gerken S., Brettel K., Schlodder E., & Witt H. T. (1988) Optical characterization of the immediate donor to Chlorophyll a_{II}^{+} in O_2-evolving photosystem II complexes. *FEBS Letters* 237:69-75.

7. Haumann M., Grabolle M., Neisius T., & Dau H. (2002) The first room-temperature X-ray absorption spectra of higher oxidation states of the tetra-manganese complex of photosystem II. *FEBS Letters* 512:116-120.

8. Dekker J. P., Plijter J. J., Ouwehand L., & Gorkom H. J. V. (1984) Kinetics of manganese redox transitions in the oxygen-evolving apparatus of photosynthesis. *Biochimica et Biophysica Acta* 767:176-179.

9. Dempsey J. L., Winkler J. R., & Gray H. B. (2010) Proton-Coupled Electron Flow in Protein Redox Machines. *Chemical Reviews* 110(12):7024-7039.

10. Dixon W. T. & Murphy D. (1976) Determination of the acidity constants of some phenol radical cations by means of electron spin resonance. *Journal of the Chemical Society London, Faraday Trans. II* 72:1221-1229.

11. Stubbe J., Nocera D. G., Yee C. S., & Chang M. C. Y. (2003) Radical initiation in the class I ribonucleotide reductase: Long-range proton-coupled electron transfer? *Chemical Reviews* 103(6):2167-2201.

12. Bonin J., Costentin C., Louault C., Robert M., Routier M., & Savéant J.-M. (2010) Intrinsic reactivity and driving force dependence in concerted proton–electron transfers to water illustrated by phenol oxidation. *Proceedings of the National Academy of Sciences* 107(8):3367-3372.

13. Sibert R. S., Josowicz M., & Barry B. A. (2010) Control of Proton and Electron Transfer in de Novo Designed, Biomimetic β Hairpins. *ACS Chemical Biology* 5(12):1157-1168.

14. Keough J. M., Jenson D. L., Zuniga A. N., & Barry B. A. (2011) Proton Coupled Electron Transfer and Redox-Active Tyrosine Z in the Photosynthetic Oxygen-Evolving Complex. *Journal of the American Chemical Society* 133(29):11084-11087.

15. Markle T. F., Rhile I. J., & Mayer J. M. (2011) Kinetic Effects of Increased Proton Transfer Distance on Proton-Coupled Oxidations of Phenol-Amines. *Journal of the American Chemical Society* 133(43):17341-17352.

16. Barry B. A. (2011) Proton coupled electron transfer and redox active tyrosines in Photosystem II. *Journal of Photochemistry and Photobiology B: Biology* 104(1–2):60-71.

17. Barry B. A., Chen J., Keough J., Jenson D., Offenbacher A., & Pagba C. (2012) Proton-Coupled Electron Transfer and Redox-Active Tyrosines: Structure and

Function of the Tyrosyl Radicals in Ribonucleotide Reductase and Photosystem II. *The Journal of Physical Chemistry Letters* 3(4):543-554.

18. Debus R. J., Barry B. A., Sithole I., Babcock G. T., & McIntosh L. (1988) Directed mutagenesis indicates that the donor to P680+ in photosystem II is Tyr-161 of the D1 polypeptide. *Biochemistry* 27:9071-9074.

19. Metz J. G., Nixon P. J., Rögner M., Brudvig G. W., & Diner B. A. (1989) Directed alteration of the D1 polypeptide of photosystem II: evidence that tyrosine-161 is the redox component, Z, connecting the oxygen-evolving complex to the primary electron donor, P_{680}. *Biochemistry* 28:6960-6969.

20. Barry B. A. & Babcock G. T. (1987) Tyrosine radicals are involved in the photosynthetic oxygen-evolving system. *Proceedings of the National Academy of Sciences* 84:7099-7103.

21. Debus R. J., Barry B. A., Babcock G. T., & McIntosh L. (1988) Site-specific mutagenesis identifies a tyrosine radical involved in the photosynthetic oxygen-evolving complex. *Proceedings of the National Academy of Sciences* 85:427-430.

22. Kim S., Liang J., & Barry B. A. (1997) Chemical complementation identifies a proton acceptor for redox-active tyrosine D in photosystem II. *Proceedings of the National Academy of Sciences* 94:14406-14412.

23. Boussac A. & Etienne A. L. (1984) Midpoint potential of signal II (slow) in tris-washed photosyste II particles. *Biochimica et Biophysica Acta* 766:576-581.

24. Ananyev G. M., Sakiyan I., Diner B. A., & Dismukes G. C. (2002) A functional role for tyrosine-D in assembly of the inorganic core of the water complex of photosystem II and the kinetics of water oxidation. *Biochemistry* 41:974-980.

25. Polander B. C. & Barry B. A. (2012) A hydrogen-bonding network plays a catalytic role in photosynthetic oxygen evolution. *Proceedings of the National Academy of Sciences* 109:6112-6117.

26. Ioannidis N. Z., G; Petrouleas, V (2008) The EPR spectrum of tyrosine-Z* and its decay kinetics in O_2-evolving photosystem II. *Biochemistry* 47:6292-6300.

27. Huynh M. H. V. & Meyer T. J. (2007) Proton-Coupled Electron Transfer. *Chemical Reviews* 107(11):5004-5064.

28. Grundmeier A. & Dau H. (2012) Structural models of the manganese complex of photosystem II and mechanistic implications. *Biochimica et Biophysica Acta - Bioenergetics* 1817(1):88-105.

29. Yamaguchi K., Isobe H., Yamanaka S., Saito T., Kanda K., Shoji M., Umena Y., Kawakami K., Shen J. R., Kamiya N., & Okumura M. (2012) Full geometry optimizations of the mixed-valence CaMn4O4X(H2O)4 (X=OH or O) cluster in OEC of PS II: Degree of symmetry breaking of the labile Mn-X-Mn bond revealed by several hybrid DFT calculations. *International Journal of Quantum Chemistry*.

30. Gatt P., Stranger R., & Pace R. J. (2011) Application of computational chemistry to understanding the structure and mechanism of the Mn catalytic site in photosystem II – A review. *Journal of Photochemistry and Photobiology B: Biology* 104(1–2):80-93.

31. De Paula J. C., Innes J. B., & Brudvig G. W. (1985) Electron transfer in photosystem II at cryogenic temperatures. *Biochemistry* 24(27):8114-8120.

32. Nelson N. & Yocum C. F. (2006) Structure and function of photosystems I and II. *Annual Review of Plant Biology* 57:521-565.

33. Velthuys B. R. (1975) Binding of the inhibitor NH3 to the oxygen-evolving apparatus of spinach chloroplasts. *Biochimica et Biophysica Acta - Bioenergetics* 396(3):392-401.

34. Sandusky P. O. & Yocum C. F. (1983) The mechanism of amine inhibition of the photosynthetic oxygen evolving complex. Amines displace functional chloride from a ligand site on manganese. *Federation of European Biochemical Societies, Letters* 162:339-343.

35. Boussac A., Rutherford A. W., & Styring S. (1990) Interaction of ammonia with the water splitting enzyme of photosystem II. *Biochemistry* 29(1):24-32.

36. Berthold D. A., Babcock G. T., & Yocum C. F. (1981) A highly resolved, oxygen-evolving Photosystem II preparation from spinach thylakoid membranes. *FEBS Letters* 134:231-234.

37. Barry B. A. (1995) Tyrosyl radicals in photosystem II. *Methods in Enzymology* 258:303-319.

38. Jenson D. L., Evans A., & Barry B. A. (2007) Proton-coupled electron transfer and tyrosine D of photosystem II. *The Journal of Physical Chemistry B* 111(43):12599-12604.

39. Han G., Mamedov F., & Styring S. (2012) Misses during Water Oxidation in Photosystem II Are S State-dependent. *Journal of Biological Chemistry* 287(16):13422-13429.

40. Yamomoto Y., Doi M., Tamura N., & Nishimura N. (1981) Release of polypeptides from highly active O_2-evolving photosystem-2 preparation by Tris treatment. *Federation of European Biochemical Societies, Letters* 133:265-268.

41. Barry B. A., El-Deeb M. K., Sandusky P. O., & Babcock G. T. (1990) Tyrosine radicals in photosystem II and related model compounds. *The Journal of Biological Chemistry* 265:20139-20143.

42. Ayala I., Range K., York D., & Barry B. A. (2002) Spectroscopic properties of tyrosyl radicals in dipeptides. *Journal of the American Chemical Society* 124:5496-5505.

43. Rutherford A. W. & Zimmerman J. L. (1984) A new EPR signal attributed to the primary plastosemiquinone acceptor in photosystem II. *Biochimica et Biophysica Acta* 767:168-175.

44. Metz J. G., Pakrasi H. B., Seibert M., & Arntzen C. J. (1986) Evidence for a dual function of the herbicide-binding D1 protein in photosytem II. *Federation of European Biochemical Societies, Letters* 205:269-274.

45. Jenson D. L. & Barry B. A. (2009) Proton-Coupled Electron Transfer in Photosystem II: Proton Inventory of a Redox Active Tyrosine. *Journal of the American Chemical Society* 131(30):10567-10573.

46. Yamanaka S., Saito T., Kanda K., Isobe H., Umena Y., Kawakami K., Shen J. R., Kamiya N., Okumura M., & Nakamura H. (2012) Structure and reactivity of the mixed-valence CaMn4O5 (H2O) 4 and CaMn4O4 (OH)(H2O) 4 clusters at oxygen evolution complex of photosystem II. Hybrid DFT (UB3LYP and UBHandHLYP) calculations. *International Journal of Quantum Chemistry*.

47. Siegbahn P. E. M. (2011) Recent theoretical studies of water oxidation in photosystem II. *Journal of Photochemistry and Photobiology B: Biology* 104(1–2):94-99.

48. Sjödin M., Styring S., Åkermark B., Sun L., & Hammarström L. (2000) Proton-Coupled Electron Transfer from Tyrosine in a Tyrosine−Ruthenium−tris-Bipyridine Complex: Comparison with TyrosineZ Oxidation in Photosystem II. *Journal of the American Chemical Society* 122(16):3932-3936.

49. Mayer J. M. & Rhile I. J. (2004) Thermodynamics and kinetics of proton-coupled electron transfer: stepwise vs. concerted pathways. *Biochimica et Biophysica Acta - Bioenergetics* 1655:51-58.

50. Rhile I. J., Markle T. F., Nagao H., DiPasquale A. G., Lam O. P., Lockwood M. A., Rotter K., & Mayer J. M. (2006) Concerted Proton Electron Transfer in the Oxidation of Hydrogen-Bonded Phenols. *Journal of the American Chemical Society* 128(18):6075-6088.

51. Sjödin M., Irebo T., Utas J. E., Lind J., Merényi G., Åkermark B., & Hammarström L. (2006) Kinetic Effects of Hydrogen Bonds on Proton-Coupled Electron Transfer from Phenols. *Journal of the American Chemical Society* 128(40):13076-13083.

52. Costentin C., Robert M., & Savéant J.-M. (2007) Concerted Proton−Electron Transfer Reactions in Water. Are the Driving Force and Rate Constant Depending on pH When Water Acts as Proton Donor or Acceptor? *Journal of the American Chemical Society* 129(18):5870-5879.

53. Irebo T., Reece S. Y., Sjodin M., Nocera D. G., & Hammarstrom L. (2007) Proton-Coupled Electron Transfer of Tyrosine Oxidation: Buffer Dependence and Parallel Mechanisms. *Journal of the American Chemical Society* 129(50):15462-15464.

54. m L. (2008) The Rate Ladder of Proton-Coupled Tyrosine Oxidation in Water: A Systematic Dependence on Hydrogen Bonds and Protonation State. *Journal of the American Chemical Society* 130(29):9194-9195.

55. din M., Johansson O., & Ha m L. (2009) The Kinetic Effect of Internal Hydrogen Bonds on Proton-Coupled

Electron Transfer from Phenols: A Theoretical Analysis with Modeling of Experimental Data. *Journal of Physical Chemistry B* 113(50):16214-16225.

56. Bonin J. & Robert M. (2011) Photoinduced Proton-Coupled Electron Transfers in Biorelevant Phenolic Systems. *Photochemistry and Photobiology* 87(6):1190-1203.

57. - m L. (2011) Proton-Coupled Electron Transfer from Tyrosine: A Strong Rate Dependence on Intramolecular Proton Transfer Distance. *Journal of the American Chemical Society* 133(34):13224-13227.

58. Hammes-Schiffer S. & Soudackov A. V. (2008) Proton-Coupled Electron Transfer in Solution, Proteins, and Electrochemistry. *Journal of Physical Chemistry B* 112(45):14108-14123.

59. Haumann M., Bogershausen O., Cherepanov D., Ahlbrink R., & Junge W. (1997) Photosynthetic oxygen evolution: H/D isotope effects and the coupling between electron and proton transfer during redox reactions at the oxidizing side of Photosystem II. *Photosynthesis Research* 51:193-208.

60. Karge M., Irrgang K.-D., & Renger G. (1997) Analysis of the reaction coordinate of photosynthetic water oxidation by kinetic measurements of 355 nm absorption changes at different temperatures in photosystem II preparations suspended in either H_2O or D_2O. *Biochemistry* 36:8904-8913.

61. Schilstra M. J., Rappaport F., Nugent J. H. A., Barnett C. J., & Klug D. R. (1998) Proton/Hydrogen Transfer Affects the S-State-Dependent Microsecond Phases of P_{680}^+ Reduction during Water Splitting. *Biochemistry* 37(11):3974-3981.

62. Ahlbrink R., Haumann M., Cherepanov D., Bogershausen O., Mulkidjanian A., & Junge W. (1998) Function of tyrosine Z in water oxidation by photosystem II: Electrostatical potential instead of hydrogen abstractor. *Biochemistry* 37:1131-1142.

63. Rappaport F., Guergova-Kuras M., Nixon P. J., Diner B. A., & Lavergne J. (2002) Kinetics and pathways of charge recombination in photosystem II. *Biochemistry* 41:8518-8527.

64. Cser K. & Vass I. (2007) Radiative and non-radiative charge recombination pathways in Photosystem II studied by thermoluminescence and chlorophyll fluorescence in the cyanobacterium Synechocystis 6803. *Biochimica et Biophysica Acta - Bioenergetics* 1767(3):233-243.

65. Page C., Moser C., Chen X., & Dutton P. (1999) Natural engineering principles of electron tunnelling in biological oxidation-reduction. *Nature* 402:47-52.

66. Krieger A., Rutherford A. W., & Johnson G. N. (1995) On the determination of redox midpoint potential of the primary quinone electron acceptor, QA, in Photosystem II. *Biochimica et Biophysica Acta - Bioenergetics* 1229(2):193-201.

67. Diner B. A., Force D. A., Randall D. W., & Britt R. D. (1998) Hydrogen bonding, solvent exchange, and coupled proton and electron transfer in the oxidation and reduction of redox-active tyrosine Y_Z in Mn-depleted core complexes of photosystem II. *Biochemistry* 37:17931-17943.

68. Yerkes C. T., Babcock G. T., & Crofts A. R. (1983) A Tris-induced change in the midpoint potential of Z, the donor to photosystem II, as determined by the kinetics of the back reaction. *FEBS Letters* 158:359-363.

69. Conjeaud H. & Mathis P. (1980) The effect of pH on the reduction kinetics of P-680 in Tris-treated chloroplasts. *Biochimica et Biophysica Acta* 590:353-359.

70. Breslow R. (2006) Artificial Enzymes. *Artificial Enzymes*, (Wiley-VCH Verlag GmbH & Co. KGaA), pp 1-35.

71. Hays A.-M. A., Vassiliev I. R., Golbeck J. H., & Debus R. J. (1998) Role of D1-His190 in proton-coupled electron transfer reactions in photosystem II: a chemical complementation study. *Biochemistry* 37:11352-11365.

72. Pujols-Ayala I. & Barry B. A. (2002) His 190-D1 and Glu 189-D1 provide structural stabilization in photosystem II. *Biochemistry* 41:11456-11465.

73. Bonin J., Costentin C., Robert M., & Saveant J.-M. (2011) Pyridine as proton acceptor in the concerted proton electron transfer oxidation of phenol. *Organic & Biomolecular Chemistry* 9(11):4064-4069.

74. .-M. (2011) Water (in Water) as an Intrinsically Efficient Proton Acceptor in Concerted Proton Electron Transfers. *Journal of the American Chemical Society* 133(17):6668-6674.

75. Lesnichin S. B., Shenderovich I. G., Muljati T., Silverman D., & Limbach H.-H. (2011) Intrinsic Proton-Donating Power of Zinc-Bound Water in a Carbonic Anhydrase Active Site Model Estimated by NMR. *Journal of the American Chemical Society* 133(29):11331-11338.

76. Zhang C. (2006) Interaction between tyrosineZ and substrate water in active photosystem II. *Biochimica et Biophysica Acta - Bioenergetics* 1757(7):781-786.

77. Sibert R.; Josowicz M. P., F.; Veglia, G.; Range, K.; Barry, B.A. (2007) Proton-Coupled Electron Transfer in a Biomimetic Peptide as a Model of Enzyme Regulatory Mechanisms. *Journal of the American Chemical Society* 129(14):8.

78. Sandusky P. O. & Yocum C. F. (1984) The chloride requirement for photosynthetic oxygen evolution. Analysis of the effects of chloride and other anions on amine inhibition of the oxygen evolving complex. *Biochimica et Biophysica Acta* 766:603-611.

79. Britt R. D., Zimmermann J.-L., Sauer K., & Klein M. P. (1989) Ammonia binds to the catalytic Mn of the oxygen-evolving complex of photosystem II: Evidence by electron spin-echo envelope modulation spectroscopy. *Journal of the American Chemical Society* 111:3522-3532.

80. Fersht A. R., Shi J.-P., Knill-Jones J., Lowe D. M., Wilkinson A. J., Blow D. M., Brick P., Carter P., Waye M. M. Y., & Winter G. (1985) Hydrogen bonding and biological specificity analysed by protein engineering. *Nature* 314(6008):235-238.

81. Dixon D. A., Dobbs K. D., & Valentini J. J. (1994) Amide-Water and Amide-Amide Hydrogen Bond Strengths. *Journal of Physical Chemistry* 98(51):13435-13439.

82. Beck W. F., Paula J. C. d., & Brudvig G. W. (1986) Ammonia binds to the manganese site of the O_2-evolving complex of photosystem II in the S_2 state. *Journal of the American Chemical Society* 108:4018-4022.

83. Khademi S., O'Connell J., III, Remis J., Robles-Colmenares Y., Miercke L. J. W., & Stroud R. M. (2004) Mechanism of Ammonia Transport by Amt/MEP/Rh: Structure of AmtB at 1.35 Å. *Science* 305(5690):1587-1594.

CHAPTER 4

GLOBAL INCORPORATION OF THE NON-NATURAL AMINO ACID 3-FLUORO-L-TYROSINE INTO CYANOBACTERIAL PHOTOSYSTEM II

by

James M. Keough, Ashley N. Zuniga, Zhanjun Guo, and Bridgette A. Barry*

School of Chemistry and Biochemistry and the Petit Institute for Bioengineering and Bioscience, Georgia Institute of Technology, Atlanta, GA 30332

4.1 Introduction

Photosynthetic oxygen evolution occurs within the protein complex photosystem II (PSII). Proton coupled electron transfer (PCET) reactions act to store energy in an oxygen-evolving complex (OEC) composed by a Mn_4CaO_5 cluster. A key intermediary in this PCET process is tyrosine Z (Y_Z), Tyr161 of the D1 polypeptide. Y_Z is oxidized by a dimer of chlorophyll molecules known as P_{680}, which produces a neutral tyrosyl radical ($Y_Z^{\bullet}$). The photooxidation of tyrosine causes deprotonation because the pKa of the radical is -2.(1)

Previously we have shown that PCET reactions of Y_Z in the S_0 and S_2 states are pH independent with significant kinetic isotope effects (KIE). These results were unexpected due to the nature of PCET reactions. The Nernst equation predicts that if there is a change in the protonation state of a molecule during PCET then the rate will show pH dependence. This pH dependence has been shown previously for the decay of $Y_D^{\bullet}Q_A^{-}$.(2)

The pKa of tyrosine is ~10 and that of histidine is ~6.(1, 3) The pH range (5.0-7.5) previously studied is expected to titrate the histidine within this PCET pair, yet no pH dependence has been seen. The pKa of Y_Z is too high to titrate with pH adjustments, because the alkaline conditions would remove the Mn_4CaO_5 cluster. Removing the OEC drastically affects the kinetics of the reaction and is not comparable to *in vivo* applications. In order to assess the nature of these PCET reactions involving Y_Z, we propose lowering the pKa and increasing the midpoint potential by substituting non-natural amino acid derivatives of fluoro-L-tyrosine (FY). FY variants can alter the midpoint potential by up to 300 mV and have pKa varying from 8.4 down to 6.3.(4)

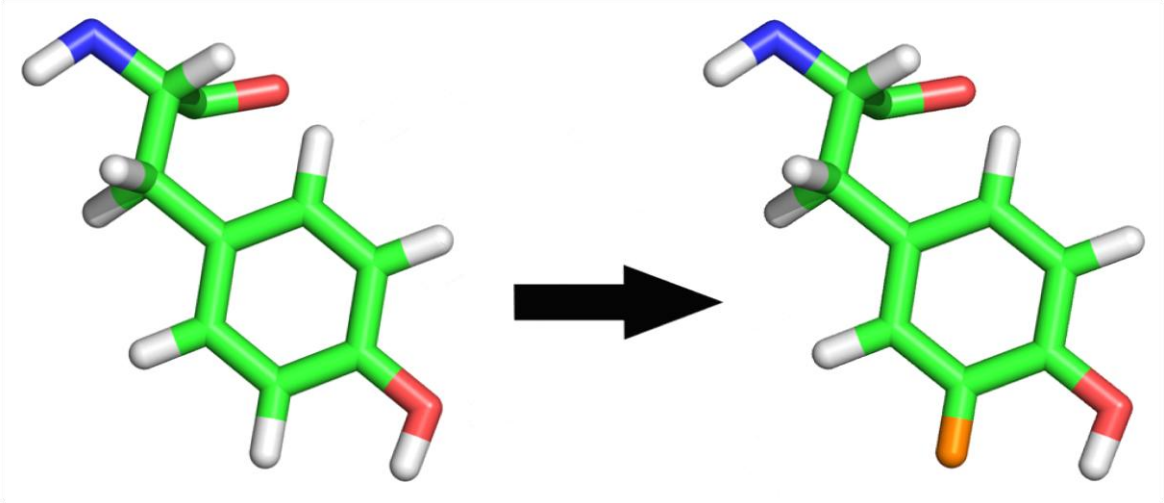

Figure 4.1. Change upon incorporation of 3FY. Tyrosine is shown on the left and 3FY is shown on the right. Green, red, blue, white, and orange represent carbon, oxygen, nitrogen, hydrogen, and fluorine respectively.

The global incorporation of fluorinated tyrosines into PSII presents an intriguing and challenging possibility. The allure of fluorinated tyrosine is created by the control that can be exhibited on the midpoint potential and the pKa of the tyrosine by changing the extent and position of the fluorination. Fluorination can alter the midpoint potential by 300 mV and the pKa by up to 5 units.(4) By lowering the pKa of Y_Z, titration should occur within a pH range that will leave the enzyme in an oxygen evolving state. The challenge presented is that fluorinated tyrosine is toxic to most organisms. Some proteins are more easily manipulated to allow site specific incorporation of fluorinated amino acid than others. Mutation of aminoacyl-tRNA synthetase and intein chemistry has allowed for the incorporation of fluorotyrosines into ribonucleotide reductase.(4) Unfortunately, these techniques do not work for all proteins.

Previously, researchers incorporated 3-fluoro-L-tyrosine (3FY) into photosystem II (PSII).(5) They incorporated 3FY into *Synechocystis* by growing the cyanobacteria in 10 L minimal media until they reached a cellular optical density of 730 nm of ~0.5 abs

units. They then added 1 L of 0.5 mM 3FY, 0.5 mM phenylalanine, and 0.25 mM tryptophan bringing the final concentration to 45 μM amino acids. Addition of amino acids to the media induced apoptosis, so the cells were harvested and the proteins were purified. They did not report oxygen evolution for the cells or for the purified PSII. A procedure to remove the Mn_4CaO_5 cluster was performed using hydroxylamine. The PSII was characterized by optical studies and EPR. Undoubtedly, they were able to incorporate 3FY into PSII utilizing this technique. However, the extent of incorporation is questionable. Instead of using mass spectrometry to quantify the percent incorporation, they opted to use EPR simulations. From simulations they estimated the extent of incorporation to be 75%. From this 75% incorporation, they received similar kinetic results to previously published Mn-depleted studies.(5, 6) The applicability of these results to the native system is questionable due to the removal of the Mn cluster. The more interesting experiments would be to study 3FY within oxygen-evolving PSII.

In this study a strain of *Synechocystis sp.* PCC 6803 with a hexa-histidine tag located on the 3' terminus of the CP47 subunit is utilized as a host for the incorporation of 3FY into PSII. *Synechocystis sp.* PCC 6803 is a very sensitive organism. Slight alterations in the media can cause extreme reactions. This sensitivity makes the incorporation of amino acids very difficult. In order to incorporate amino acids into *Synechocystis,* we start by growing them on a very low concentration (10 μM) to build a tolerance and slowly increase until the desired concentration (250 μM) is reached. *Synechocystis* is highly adaptable, so adjusting the concentration slowly allows time for the cells to evolve.

4.2 Materials and Methods

Synechocystis sp. PCC 6803 cultures were maintained on solid media containing BG-11,(7) 250 µM 3FY (Synquest Laboratories), phenylalanine, and tryptophan buffered with 5 mM TES-NaOH, pH 8.0, and 6 mM $Na2S_2O_3$.(8) Liquid cultures were grown in BG-11, 5 mM TES-NaOH, pH 8.0, and 10 µg/mL kanamycin, and were bubbled with sterile air. Liquid cultures began growing in 50 mL of media and are grown for 7-10 days. These cells were then transferred to 15 L of sterile BG-11 media and allowed to grow for one month. To prepare 15 L of BG-11 media, it is autoclaved in a concentrated form in order to accommodate the sterile addition of amino acids. Due to the low solubility of aromatic amino acids, stock solutions are prepared at 1 mM concentration. To make 15 L of media, 3.75 L of amino acids must be added to 11.25 L of BG-11 that contains enough nutrients for 15 L.

After being grown for a month, the cells were harvested with an Amicon DC-10 hollow fiber concentrator to concentrate the cells to ~ 1 L. The use of the concentrator is necessary with this cell line for multiple reasons. Firstly, the yield is low, so large volumes are employed by growing six 15 L (90 L) carboys. This volume would take days to centrifuge concentrate. Secondly, when these cells are stressed they tend to float more. Stress can cause cyanobacteria to float by either upregulating their gas vacuoles or storing more lipids, either scenario makes centrifugation difficult. Once the cells were concentrated down to ~1 L, they were centrifuged at 30,000 x g for 10 minutes. Once pelleted, the cells were resuspended in freeze buffer (25% glycerol, 20 mM $CaCl_2$, 20 mM $MgCl_2$, 20 mM MES, pH 6.0), pelleted again, and frozen at -70 °C.

To purify thylakoid membranes from cells, the pellets were resuspended in 1 L of break buffer (0.8 M sucrose, 50 mM MES, pH 6.0) and pelleted by centrifugation for 10 min at 30,000 x g. The cells were resuspended in approximately 300 mL of break buffer and incubated for 60 min on ice in the dark. They were then pelleted by centrifugation for 10 min at 30,000 x g. After incubating, the cells were resuspended in ~50 mL of break buffer to which was added 0.5 mg of DNase I, 1.5 mg of N-tosyl-L-phenylalanine chloromethyl ketone, 5 mg of phenylmethanesulfonylfluoride, 0.25 mg of pepstatin A, and 1.25 g of bovine serum albumin. The cells were added to a chilled bead beater that was two-thirds full with 0.l mm diameter glass beads (Bio-spec Products). The chamber was then filled with break buffer, and the outside jacket was filled with an ice/water slurry. The cells were broken in the dark for 7 cycles of 30-s blending and 15-min rest. The lysate was separated from the beads by decanting the fluid off the top. The beads were washed four times with 200 mL of break buffer in each wash. This solution was then centrifuged for 30 min at 7,500 x g. $CaCl_2$, was added to the supernatant to give a final concentration of 40 mM. Thylakoid membranes were then pelleted by a at 24,000 x g for 30 min. The thylakoid membrane pellet was resuspended in freeze buffer (25% glycerol, 20 mM MES pH 6.0,20 mM CaCl, 20 mM MgC12), an aliquot was taken for oxygen assays, and the membranes were pelleted again by centrifugation at 44,000 x g for 30 min. These pellets were stored at -70 °C.

The pellets from the thylakoid membrane preparation contain all of the photosynthetic proteins. In order to separate PSII, thylakoid membrane pellets were thawed and resuspended in minimal his-tag buffer (25% glycerol, 5 mM $CaCl_2$, 10 mM $MgCl_2$, 50 mM MES-NaOH, pH 6.0) to 0.6 mg/mL chl, 1% lauryl maltoside, and 0.01

mg/ml phenylmethanesulfonylfluoride while shaking on ice. The sample was shaken for 10 min and then centrifuged at 100,000 x g for 60 min. After centrifuging, the supernatant was gently loaded on to a His-Pur cobalt resin (Fisher Scientific). The sample was allowed to flow through the column until there was just enough liquid to keep the top of the column hydrated. His-tag wash buffer (25% glycerol, 0.04% lauryl maltoside, 5 mM $CaCl_2$, 10 mM $MgCl_2$, 50 mM MES-NaOH, pH 6.0) was then run slowly through the column until baseline absorbance at 280 nm was achieved. Once the absorbance was zero, his-tag elution buffer (25% glycerol, 100 mM histidine, 0.04% lauryl maltoside, 5 mM $CaCl_2$, 10 mM $MgCl_2$, 50 mM MES-NaOH, pH 6.0) was run through the column. The fractions containing PSII were collected and concentrated with an Amicon 100MWCO concentrator. The sample were washed three times with equal volumes of his-tag resuspension buffer (25% glycerol, 20 mM $CaCl_2$, 50 mM MES-NaOH, pH 6.0) and an aliquot was taken for oxygen assays.

EPR analysis was conducted on a Bruker (Billerica, MA) EMX spectrometer equipped with a Bruker ER 4102ST cavity and Bruker ER 4131VT temperature controller. EPR spectra were measured in the dark at 190 K. Microwave power and modulation amplitude were set low, to show that the expected $Y_Z^{\bullet}$ hyperfine splitting. Because the microwave power is low, this field swept spectrum also has a contribution from $Y_D^{\bullet}$. EPR parameters were: frequency: 9.39 GHz, power: 0.64 mW, and modulation amplitude: 2 G (Figure 4.3), conversion time: 41 ms, time constant: 164 ms, sweep time: 21 s.

4.3 Results

To begin incorporating 3FY, we developed a cell line that was tolerant to tyrosine in the media. We then used this strain to begin incorporating 3FY through various methods. Each attempt we made with this cell line was unsuccessful.

It was concluded that tyrosine tolerant cells were not helpful when trying to incorporate 3FY. This information led to the conclusion that to incorporate 3FY, the cells need to be tolerant to 3FY. We began directing the evolution of cells by adding 10 μM 3FY, phenylalanine, and tryptophan to the solid media of a hexa-histidine tagged strain of *Synechocystis sp.* PCC 6803. At 10 μM amino acids there was no change in the way that the cells grew. We increased the concentration every couple weeks until we reached 50 μM amino acids. Once the concentration reached 50 μM amino acids, the majority of the cells died with only a few colonies surviving. We continued to select the colonies that were thriving on the 50 μM 3FY media and started growing these cells in liquid cultures that contained 250 μM 3FY media. We continued to increase the concentration of amino acids in the solid media to equimolar to the liquid cultures. We transferred the 3FY tolerant cells to solid media containing 250 μM 3FY, 250 μM phenylalanine, and 250 μM tryptophan, and the cells grew well. In Figure 4.1, we show pictures of 3FY tolerant cells growing on solid (A) and in 15 L liquid media (B) with 250 μM 3FY media.

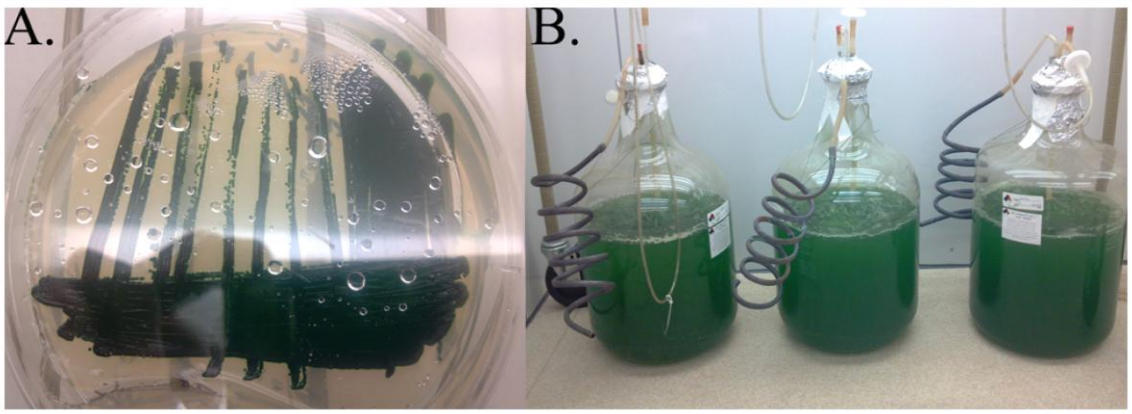

Figure 4.2 A) 3FY tolerant strain of *Synechocystis sp.* PCC 6803 cells growing on a 1.5% agar plate containing BG-11 media with sodium thiosulfate and 250 µM 3FY, tryptophan, and phenylalanine. B) Three 15 L carboys growing 3FY tolerant cells in BG-11 media with 250 µM 3FY, tryptophan, and phenylalanine.

Once the cells have grown for ~1 month in 15 L of media, they were harvested. Figure 4.2 shows the supernatant taken off the cells grown in BG-11 media (A) and (B) BG-11 with 250 µM 3FY media during concentration. It is easy to see the difference in the cyanobacteria's response to stress. In both the lighter (A) and the darker (B) carboy the unknown pigment exhibits the same absorption spectrum (Figure 4.2C). In Figure 4.2C, an absorption spectrum is shown from 200 to 750 nm of the compound that is excreted during growth. The concentration of this orange compound is extremely high in the cells grown on 3FY media. Each step of the purification process releases more of this compound. Modifying the purification procedure to accommodate this compound is necessary, because the compound binds to the Co-NTA column. To effectively run a his-tag purification on the 3FY labeled PSII the orange pigment should be removed from solution. Running an anion exchange column to separate the photosynthetic proteins from the orange chromophore prior to running a his-tag column should increase the efficacy of the his-tag column.

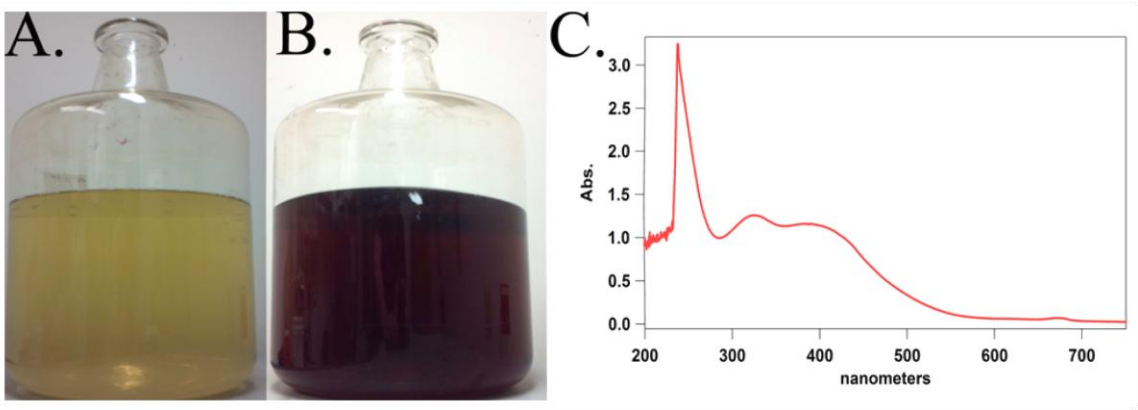

Figure 4.3 Color difference in the supernatant between cells grown in BG-11 media (A) and BG-11 media with 250 µM 3FY, tryptophan, and phenylalanine. (C) Absorption spectrum of the orange compound that is produced by the 3FY tolerant cyanobacteria.

Cells that have been harvested to date show very similar oxygen evolution rates within the error of the experiments. Control cells were grown in either BG-11 or BG-11 with 250 µM tyrosine, phenylalanine, and tryptophan and 3FY cells grown in BG-11 with 250 µM 3FY, phenylalanine, and tryptophan evolved oxygen at a rate of 480 µmol O_2/hr•mg chl and 450 µmol O_2/hr•mg chl respectively. Oxygen evolution rates after the thylakoid membranes were purified have been within error of the rates in the cells with rates of 490 µmol O_2/hr•mg chl and 450 µmol O_2/hr•mg chl respectively for control and 3FY which is expected.

The yield from these cells and thylakoid membrane preparations has been extremely low. We have run one his-tag purification for the control and 3FY cells. The control cells were purified with low oxygen evolution activity. For purified cyanobacterial PSII, rates should be above 2000 µmol O_2/hr•mg chl, but instead rates were 570 µmol O_2/hr•mg chl. The 3FY his-tag purification led to oxygen evolution rates of 900 µmol O_2/hr•mg chl, but the yield was extremely low (200 µg chl). These rates might be adequate for 3FY-incorporated PSII. Performing this preparation multiple times

will allow us to know what to expect since no one has purified oxygen-evolving 3FY-PSII previously. The low yield was caused by the chromophore produced by the cells (Figure 4.2B). This compound binds to the his-tag column, so it competes for space on the column and possibly has a higher affinity for the cobalt than the his-tag PSII.

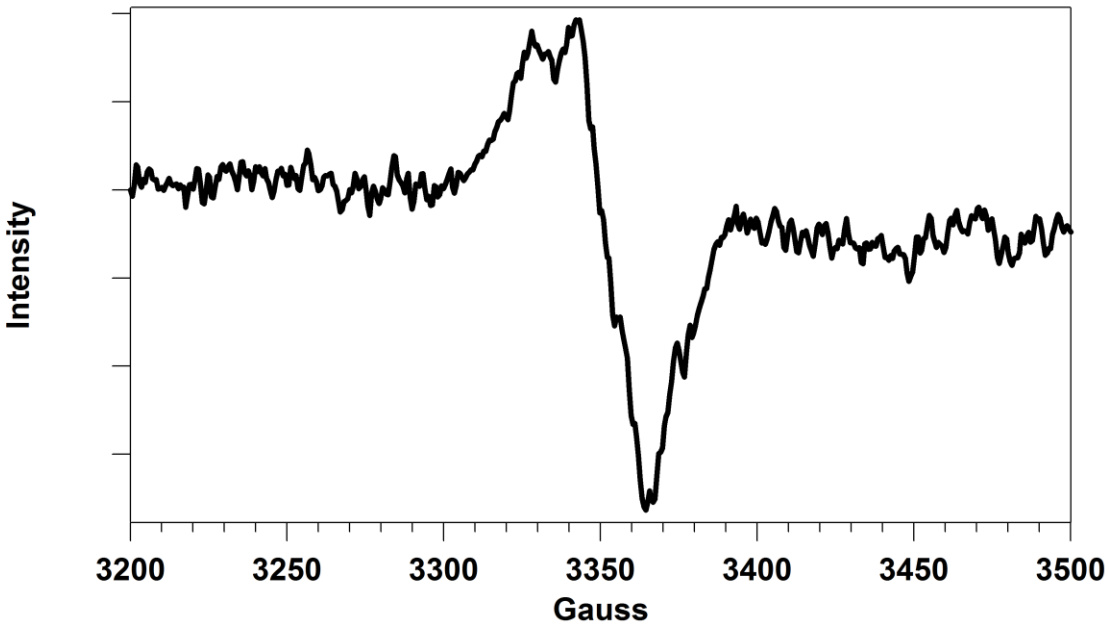

Figure 4.4. Dark field sweep EPR spectrum of PSII from *Synechocystis sp.* PCC 6803 HT3A cell line at pH 6.0 and 190 K.

In Figure 4.3, an EPR field sweep spectrum of cyanobacterial PSII is shown. This is a characteristic dark field sweep signal from cyanobacterial PSII with the expected *g*-value of 2.004. This field sweep data is derived from samples with low oxygen evolution rates that dropped after being frozen to 370 μmol O_2/hr•mg chl. This made the analysis of transient kinetics difficult due to inactivation of the Mn_4CaO_5 cluster.

4.4 Discussion

The successful construction of a 3FY-tolerant strain of *Synechocystis sp.* PCC 6803 is a large step forward. The creation of this strain has led to many other challenges, such as the low yield of PSII and the large quantity of chromophore that is produced under stress by the cyanobacteria. These hurdles will easily be overcome with time and sound experimental practices. We will continue to increase the yield from these cells, by changing growth conditions and optimizing the purification while trying to reduce the cyanobacteria's response to stress.

Currently, different growth protocols are being attempted to minimize the stress cells undergo during incorporation of 3FY. When previous researchers incorporated 3FY into PSII, they used a much lower concentration (45 μM) than the growth protocol that was employed here (250 μM). Previous studies from our lab have shown that incorporation above 95% is seen with 250 μM concentrations of the desired amino acid. Reducing the concentration of 3FY could lead to higher yields of PSII and reduce production of the orange chromophore.

Future experiments include EPR at both cryogenic and room temperature. In these two different conditions we will perform similar experiments that we have employed for spinach thylakoid membranes. The global incorporation of 3FY will create samples that will be useful for analyzing both Y_Z and Y_D. In addition to EPR, fourier transform infrared (FTIR) spectroscopy offers a unique insight into proteins and is capable of probing the electrostatic environment in PSII.(9) FTIR spectroscopy can be performed at room temperature and cryogenic temperature, which will make for a facile comparison between EPR and FTIR results. Characterizing $Y_Z^{\bullet}$ and $Y_D^{\bullet}$ in each of the

available S states with 3FY incorporated PSII will continue to shed light on the critical PCET processes that catalyze water oxidation.

4.5 References

1. Dixon W. T. & Murphy D. (1976) Determination of the acidity constants of some phenol radical cations by means of electron spin resonance. *Journal of the Chemical Society London, Faraday Trans. II* 72:1221-1229.

2. Jenson D. L., Evans A., & Barry B. A. (2007) Proton-coupled electron transfer and tyrosine D of photosystem II. *The Journal of Physical Chemistry B* 111(43):12599-12604.

3. Mesu J. G., Visser T., Soulimani F., & Weckhuysen B. M. (2005) Infrared and Raman spectroscopic study of pH-induced structural changes of L-histidine in aqueous environment. *Vibrational Spectroscopy* 39(1):114-125.

4. Seyedsayamdost M. R., Reece S. Y., Nocera D. G., & Stubbe J. (2006) Mono-, Di-, Tri-, and Tetra-Substituted Fluorotyrosines: New Probes for Enzymes That Use Tyrosyl Radicals in Catalysis. *Journal of the American Chemical Society* 128(5):1569-1579.

5. Rappaport F., Boussac A., Force D. A., Peloquin J., Brynda M., Sugiura M., Un S., Britt R. D., & Diner B. A. (2009) Probing the Coupling between Proton and Electron Transfer in Photosystem II Core Complexes Containing a 3-Fluorotyrosine. *Journal of the American Chemical Society* 131(12):4425-4433.

6. Diner B. A., Force D. A., Randall D. W., & Britt R. D. (1998) Hydrogen bonding, solvent exchange, and coupled proton and electron transfer in the oxidation and reduction of redox-active tyrosine Y_Z in Mn-depleted core complexes of photosystem II. *Biochemistry* 37:17931-17943.

7. Breton J., Chitnis P. R., & Pantelidou M. (2005) Evidence for Hydrogen Bond Formation to the PsaB Chlorophyll of P700 in Photosystem I Mutants of Synechocystis sp. PCC 6803. *Biochemistry* 44(14):5402-5408.

8. Rippka R., Deruelles J., Waterbury J. B., Herdman M., & Stanier R. Y. (1979) Generic Assignments, Strain Histories and Properties of Pure Cultures of Cyanobacteria. *Journal of General Microbiology* 111(1):1-61.

9. Polander B. C. & Barry B. A. (2012) A hydrogen-bonding network plays a catalytic role in photosynthetic oxygen evolution. *Proceedings of the National Academy of Sciences* 109:6112-6117.

CHAPTER 5

5.1 Summary

Innovation begins by understanding fundamental processes. Photosynthesis is the most fundamental energy conversion process known. Photosynthesis is driven by the conversion of light energy into chemical energy. This conversion is facilitated by proton coupled electron transfer (PCET) reactions that limit the amount of high energy intermediates accumulated within the protein matrix. An *ab initio* understanding of PCET reactions within Photosystem II (PSII) might enable innovation that will unlock the greatest sources of energy this planet knows.

Within this thesis, we provide useful techniques that are employed to study the nature of PCET reactions involving redox active tyrosines within PSII. First, we expanded a recently developed electron paramagnetic resonance (EPR) spectroscopy technique that exploits the power saturation difference between tyrosine Z (Y_Z) and tyrosine D (Y_D) to study the pH dependence and the kinetic isotope effects.(1) We then utilized cryogenic temperatures to lock the oxygen evolving complex (OEC) in specific oxidation states.(2) Once the oxidation state of the OEC is locked we utilize time-resolved EPR to monitor kinetics of the recombination of Q_A^- with Y_Z.(3)

We began our focus on the reduction of $Y_Z^\bullet$ set in the S_2 state, throughout the pL range of 5.0-7.5 (where oxygen is evolved) in both ^1H_2O and ^2H_2O. These experiments showed that the rate of recombination for $S_2Y_Z^\bullet Q_A^-$ is pL independent and that Y_Z is solvent exposed due to a significant KIE (~2). These results agreed well with some previously published results.(1, 4) However, the pL independence was unexpected when

compared to experiments with Y_D.(5, 6) PCET reactions that transfer a proton are expected to yield a rate that is pH dependent.(7) However, hydrogen-bonding facilitates pH independent reactions by decreasing the reorganization energy.(8) We proposed that the hydrogen-bonding network around $Y_Z^{\bullet}$ and the calcium ion facilitate a pH independent CPET reaction.(3)

In order to compare Y_Z PCET in different S states we examined the next S state that had similar temperature transition properties, which is the S_0 state. We compared two unique OEC oxidation states, the S_0 and the S_2. These states are known to differ in oxidation state, with S_0 state assigned to a $Mn(III)_3Mn(IV)_1$ state, while the S_2 state is assigned a $Mn(III)_1Mn(IV)_3$ oxidation state.(9-11) Oxidation state changes likely manipulate the hydrogen-bonding interactions among water molecules around the OEC.(9, 12) We found that the rate of $Y_Z^{\bullet}Q_A^{-}$ recombination and the average KIE were altered, when the S_0 and S_2 states are compared. However, the rates and KIE values are pL independent in both the S_0 and S_2 states. This pL independence is dissimilar to the previously reported $Y_D^{\bullet}Q_A^{-}$ recombination rates.(5, 6) We showed that the addition of ammonia is a useful probe for the hydrogen-bonding network and that ammonia dramatically slowed the rate of $Y_Z^{\bullet}$ decay, but had no significant effect on $Y_D^{\bullet}$. We attribute this to substitution of ammonia into the OEC hydrogen-bonding network, surrounding Y_Z, and the subsequently expected decrease in hydrogen bond strength.(13)

To continue studying PCET reactions within oxygen evolving it is necessary to manipulate the system without losing functionality. The incorporation of non-natural amino acids provides the type of alterations that can lead to new understandings of biological and chemical processes. We have successfully evolved a 3-fluoro-L-tyrosine

(3FY)-tolerant strain of cyanobacteria. The incorporation of 3FY into oxygen evolving PSII should prove an excellent probe for PCET reactions due to calculated the changes in chemistry.(14)

This work lays a foundation for many experiments to follow. EPR analysis of the S_1 and S_3 transitions should be explored at lower temperatures (77-100 K). While transitioning to lower temperatures Arrhenius plots of the S_0 and S_2 states could be constructed. Arrhenius plots would allow for activation and reorganization energies to be calculated. The S_3 state is possibly the most interesting of these S states, because it is the gateway to water oxidation (see Appendix C for preliminary data on S_3Y_Z). Another intriguing aspect of the S_3 state is that ammonia binding has been shown to be dependent on the timing of flash protocol that is employed.(15) If 2 flashes are administered quickly (1 Hz) then only one molecule of ammonia binds to the OEC, whereas if two flashes are given slowly (0.03 Hz) then two molecules will bind to the OEC.(15) (16, 17) This differential binding of ammonia in the S_3 state could prove useful in examining the hydrogen bond network that facilitates water oxidation.

An excellent complimentary technique to these EPR studies would be fourier transform infrared (FTIR) spectroscopy, because EPR focuses on electrons while FTIR is able to detect molecular vibrations that can indicate changes in conformation, protonation state, and solvent polarization.(18-23) The information from FTIR studies can provide a more complete understanding of these PCET reactions. 3FY should prove to be an excellent probe for FTIR experiments due to expected shifts in the vibrational modes.(24, 25) Utilizing 3FY as a marker, we can construct double difference spectra that highlight only the features contributed from 3FY in light induced PCET reactions.(13, 26, 27)

Water oxidation is driven by complex PCET reactions that have been evolved over billions of years. Here, we shed light on PCET reaction of redox-active tyrosines within PSII set in the S_0 and S_2 states. $Y_Z^{\bullet}$ decay is very sensitive to the oxidation state of the OEC and hydrogen bond disruptors like ammonia while remaining insensitive to pH. PSII is a complex enzyme that hosts two very unique tyrosine residues. We have shown that both Y_Z and Y_D have unique kinetic properties. Ammonia was shown to be a very specific probe of Y_Z while having no effect on Y_D kinetics. This information will help build a fundamental understanding of the processes that are necessary to harness light energy.

5.2 References

1. Ioannidis N. Z., G; Petrouleas, V (2008) The EPR spectrum of tyrosine-Z* and its decay kinetics in O_2-evolving photosystem II. *Biochemistry* 47:6292-6300.

2. Styring S. & Rutherford A. W. (1988) Deactivation kinetics and temperature dependence of the S-state transitions in the oxygen-evolving system of photosystem II measured by EPR spectroscopy. *Biochimica et Biophysica Acta* 933:378-387.

3. Keough J. M., Jenson D. L., Zuniga A. N., & Barry B. A. (2011) Proton Coupled Electron Transfer and Redox-Active Tyrosine Z in the Photosynthetic Oxygen-Evolving Complex. *Journal of the American Chemical Society* 133(29):11084-11087.

4. Umena Y., Kawakami K., Shen J.-R., & Kamiya N. (2011) Crystal structure of oxygen-evolving photosystem II at a resolution of 1.9 Å. *Nature* 473(7345):55-60.

5. Jenson D. L., Evans A., & Barry B. A. (2007) Proton-coupled electron transfer and tyrosine D of photosystem II. *The Journal of Physical Chemistry B* 111(43):12599-12604.

6. Jenson D. L. & Barry B. A. (2009) Proton-Coupled Electron Transfer in Photosystem II: Proton Inventory of a Redox Active Tyrosine. *Journal of the American Chemical Society* 131(30):10567-10573.

7. Weinberg D. R., Gagliardi C. J., Hull J. F., Murphy C. F., Kent C. A., Westlake B. C., Paul A., Ess D. H., McCafferty D. G., & Meyer T. J. (2012) Proton-Coupled Electron Transfer. *Chemical Reviews* 112(7):4016-4093.

8. m L. (2008) The Rate Ladder of Proton-Coupled Tyrosine Oxidation in Water: A Systematic Dependence on Hydrogen Bonds and Protonation State. *Journal of the American Chemical Society* 130(29):9194-9195.

9. Yamaguchi K., Isobe H., Yamanaka S., Saito T., Kanda K., Shoji M., Umena Y., Kawakami K., Shen J. R., Kamiya N., & Okumura M. (2012) Full geometry optimizations of the mixed-valence CaMn4O4X(H2O)4 (X=OH or O) cluster in OEC of PS II: Degree of symmetry breaking of the labile Mn-X-Mn bond revealed by several hybrid DFT calculations. *International Journal of Quantum Chemistry*.

10. Grundmeier A. & Dau H. (2012) Structural models of the manganese complex of photosystem II and mechanistic implications. *Biochimica et Biophysica Acta - Bioenergetics* 1817(1):88-105.

11. Gatt P., Stranger R., & Pace R. J. (2011) Application of computational chemistry to understanding the structure and mechanism of the Mn catalytic site in photosystem II – A review. *Journal of Photochemistry and Photobiology B: Biology* 104(1–2):80-93.

12. Siegbahn P. E. M. (2011) Recent theoretical studies of water oxidation in photosystem II. *Journal of Photochemistry and Photobiology B: Biology* 104(1–2):94-99.

13. Polander B. C. & Barry B. A. (2012) A hydrogen-bonding network plays a catalytic role in photosynthetic oxygen evolution. *Proceedings of the National Academy of Sciences* 109:6112-6117.

14. Seyedsayamdost M. R., Reece S. Y., Nocera D. G., & Stubbe J. (2006) Mono-, Di-, Tri-, and Tetra-Substituted Fluorotyrosines: New Probes for Enzymes That Use Tyrosyl Radicals in Catalysis. *Journal of the American Chemical Society* 128(5):1569-1579.

15. Boussac A., Rutherford A. W., & Styring S. (1990) Interaction of ammonia with the water splitting enzyme of photosystem II. *Biochemistry* 29(1):24-32.

16. Britt R. D., Zimmermann J.-L., Sauer K., & Klein M. P. (1989) Ammonia binds to the catalytic Mn of the oxygen-evolving complex of photosystem II: Evidence by electron spin-echo envelope modulation spectroscopy. *Journal of the American Chemical Society* 111:3522-3532.

17. Beck W. F., Paula J. C. d., & Brudvig G. W. (1986) Ammonia binds to the manganese site of the O_2-evolving complex of photosystem II in the S_2 state. *Journal of the American Chemical Society* 108:4018-4022.

18. Barth A. (2007) Infrared spectroscopy of proteins. *Biochimica et Biophysica Acta - Bioenergetics* 1767(9):1073-1101.

19. Colthup N. B., Daly L. H., & Wiberley S. E. (1975) *Introduction to Infrared and Raman Spectroscopy* (Academic Press, New York) 2nd Ed.

20. Wang J., Zhuang W., Mukamel S., & Hochstrasser R. (2007) Two-dimensional infrared spectrsocopy as a probe of the solvent electrostatic field for a twelve residue peptide. *Journal of Physical Chemistry B* 112(5930-5937).

21. Kim Y. S. & Hochstrasser R. M. (2009) Applications of 2D IR Spectroscopy to Peptides, Proteins, and Hydrogen-Bond Dynamics. *Journal of Physical Chemistry B* 113(24):8231-8251.

22. Myshakina N. S., Ahmed Z., & Asher S. A. (2008) Dependence of amide vibrations on hydrogen bonding. *Journal of Physical Chemistry B* 112(38):11873-11877.

23. Socrates G. (2001) *Infrared and Raman Characteristic Group Frequencies* (John Wiley & Son, West Sussex).

24. Ayala I., Perry J. J. P., Szczepanski J., Tainer J. A., Vala M. T., Nick H. S., & Silverman D. N. (2005) Hydrogen Bonding in Human Manganese Superoxide Dismutase Containing 3-Fluorotyrosine. *Biophysical Journal* 89(6):4171-4179.

25. Reid P. J., Loftus C., & Beeson C. C. (2003) Evaluating the Potential of Fluorinated Tyrosines as Spectroscopic Probes of Local Protein Environments: A UV Resonance Raman Study. *Biochemistry* 42(8):2441-2448.

26. Kimura Y., Mizusawa N., Ishii A., Yamanari T., & Ono T. A. (2003) Changes of low-frequency vibrational modes induced by universal N-15- and C-15-isotope labeling in S-2/S-1 FTIR difference spectrum of oxygen-evolving complex. *Biochemistry* 42(45):13170-13177.

27. Noguchi T. & Sugiura M. (2003) Analysis of flash-induced FTIR difference spectra of the S-state cycle in the photosynthetic water-oxidizing complex by uniform N-15 and C-13 isotope labeling. *Biochemistry* 42(20):6035-6042.

APPENDIX A

CHAPTER 2 SUPPORTING INFORMATION

Field Sweep Spectra

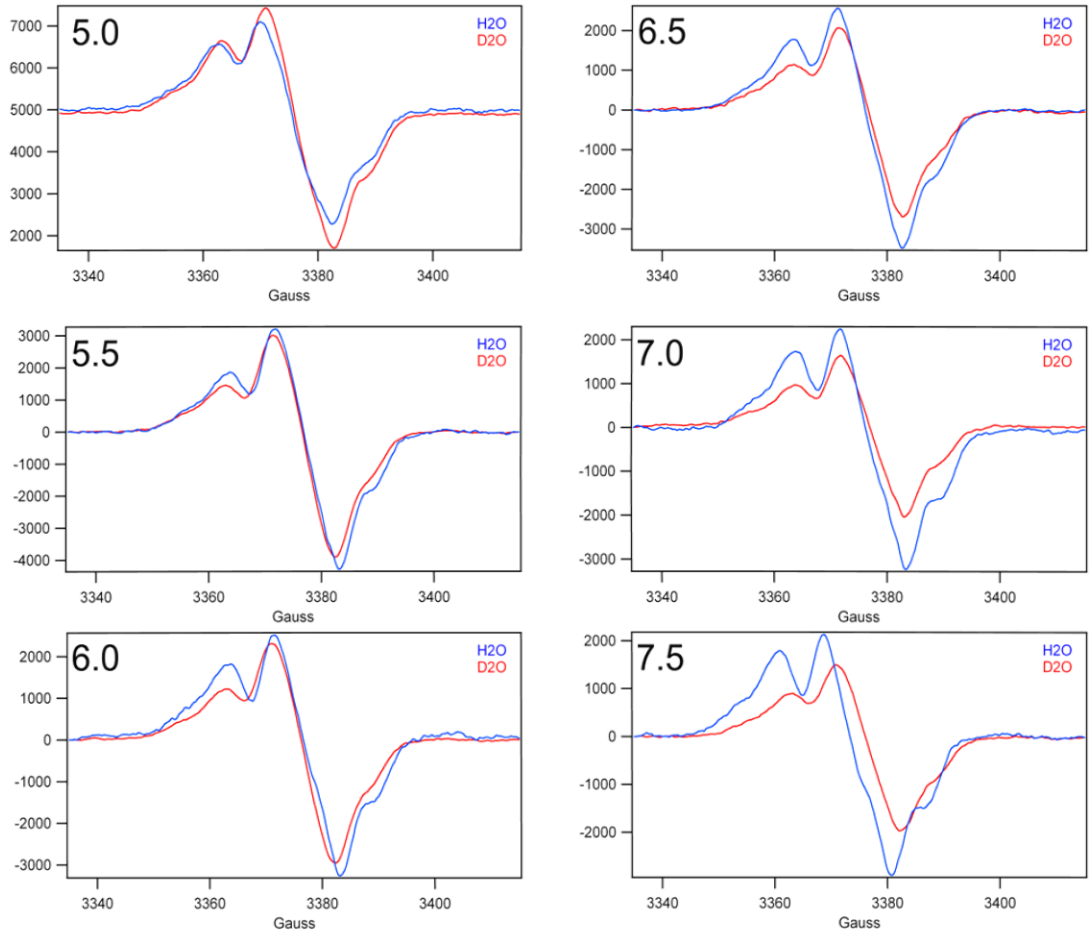

Figure A.1. Field sweep spectra of $Y_Z^{\bullet}$ under illumination at 190 K throughout the pL range 5.0-7.5 in ^1H_2O (blue) and ^2H_2O (red).

Transient EPR spectra

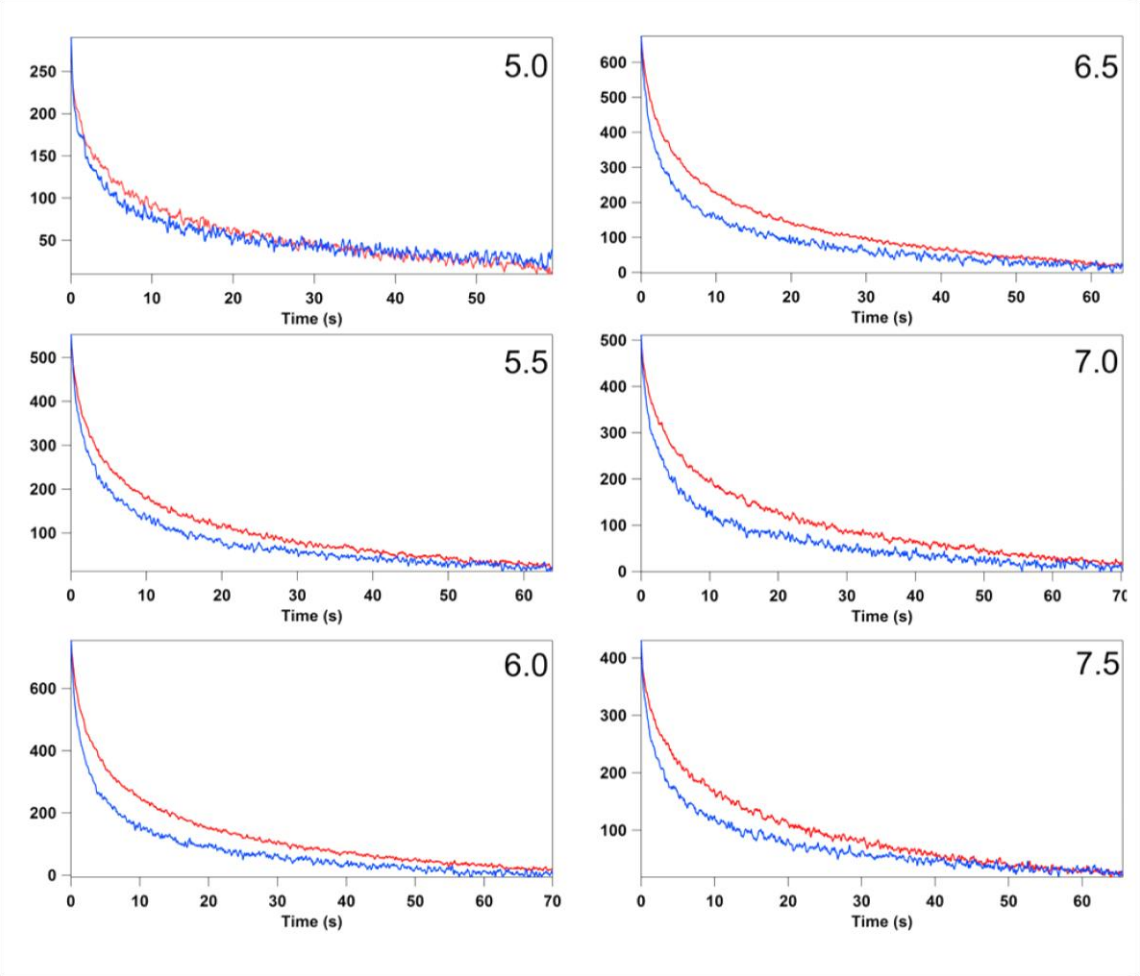

Figure A. 2. EPR transient spectra for the recombination of $Y_Z^{\bullet}$ at 190 K throughout the pL range 0f 5.0-7.5The pL is denoted on the left side within each spectra the transient for $^{1}H_2O$ is blue and $^{2}H_2O$ is red.

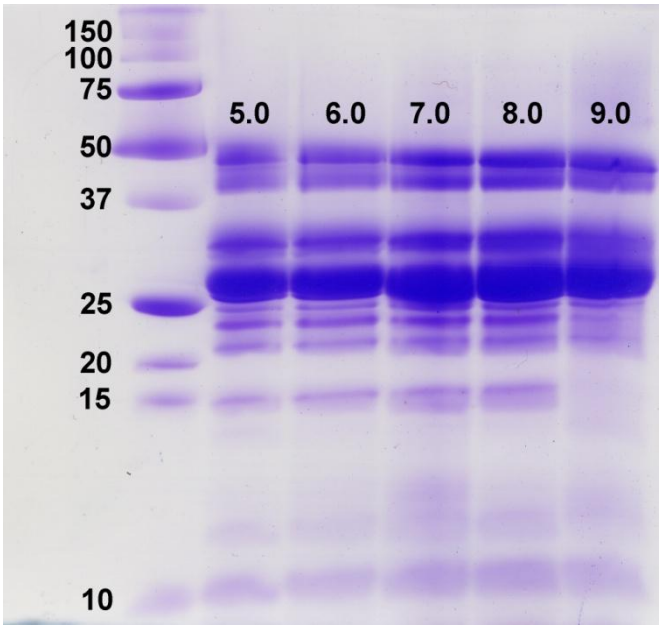

Figure A.3. SDS-urea denaturing polyacrylamide gel electrophoresis of PSII enriched thylakoid membranes. Thylakoids were exchanged into solvents from pH 5.0 – 9.0 as shown in the gel. Each lane was loaded with 6 µg chlorophyll.

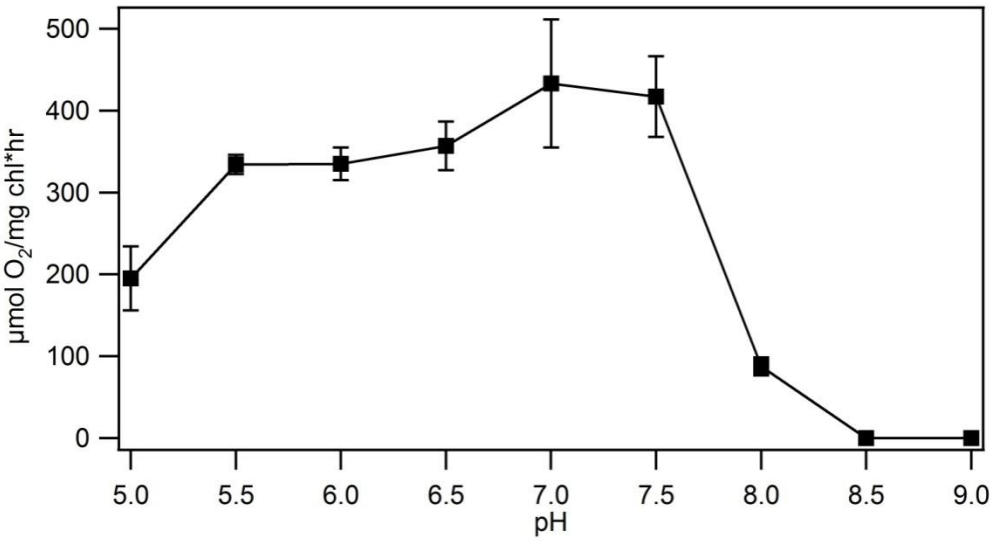

Figure A.4. Rate of oxygen evolution as a function of pH.

APPENDIX B

CHAPTER 3 SUPPORTING INFORMATION

Table B.1. S_0Y_Z: Triexponential fits to transient data throughout the pL range in either $^1H_20$ or ^2H_2O buffers using the equation $f(t) = A_1*e^{(-K1*t)} + A_2*e^{(-K2*t)} + A_3*e^{(-K3*t)} + C$. Percentage contribution of each phase is shown in parenthesis next to the value for the amplitude. Units of rate constants, s^{-1}.

pH	A1	K1	A2	K2	A3	K3	C
5	119 (33)	1.15	128 (36)	0.176	101 (28)	0.023	10 (3)
5.5	193 (33)	1.05	195 (33)	0.181	179 (31)	0.030	-16 (3)
6	165 (36)	0.93	167 (36)	0.171	120 (26)	0.030	12 (3)
6.5	115 (29)	2.24	162 (41)	0.291	116 (29)	0.038	3 (1)
7	115 (26)	1.06	132 (30)	0.146	134 (31)	0.012	-60 (14)
7.5	75 (26)	2.73	108 (38)	0.320	101 (36)	0.040	0 (0)
pD	**A1**	**K1**	**A2**	**K2**	**A3**	**K3**	**C**
5	79 (24)	1.80	122 (37)	0.199	125 (38)	0.026	-5 (2)
5.5	152 (30)	0.68	162 (32)	0.125	179 (35)	0.023	-17 (3)
6	195 (24)	1.05	299 (37)	0.172	300 (37)	0.030	-21 (3)
6.5	144 (23)	0.81	198 (32)	0.160	249 (40)	0.025	-32 (5)
7	201 (33)	0.45	178 (29)	0.075	194 (32)	0.019	-43 (7)
7.5	73 (19)	5.14	117 (31)	0.330	177 (47)	0.036	-10 (3)

Table B.2. S_2YZ: Triexponential fits of transient data throughout the pL range in either $^1H_20$ or ^2H_2O buffers using the equation $f(t) = A_1*e^{(-K1*t)} + A_2*e^{(-K2*t)} + A_3*e^{(-K3*t)} + C$. Percentage contribution of each phase is shown in parenthesis next to the value for the amplitude. Units of rate constants, s^{-1}.

pH	A1	K1	A2	K2	A3	K3	C
5	81 (29)	4.55	113 (40)	0.318	72 (26)	0.035	16 (6)
5.5	174 (35)	1.21	198 (40)	0.187	121 (24)	0.028	-2 (0)
6	157 (31)	1.42	196 (39)	0.249	136 (27)	0.034	-11 (2)
6.5	123 (29)	1.80	172 (41)	0.305	128 (30)	0.040	0 (0)
7	98 (24)	2.03	179 (43)	0.290	138 (33)	0.038	-1 (0)
7.5	116 (30)	1.56	132 (34)	0.263	121 (32)	0.038	14 (4)
pD	**A1**	**K1**	**A2**	**K2**	**A3**	**K3**	**C**
5	74 (25)	2.51	103 (35)	0.231	113 (38)	0.027	-6 (2)
5.5	136 (24)	1.19	211 (37)	0.186	210 (37)	0.027	-13 (2)
6	216 (28)	0.81	252 (32)	0.158	290 (37)	0.029	-17 (3)
6.5	164 (23)	0.93	250 (35)	0.169	274 (38)	0.027	-25 (3)
7	173 (33)	0.44	159 (30)	0.073	173 (32)	0.019	-27 (5)
7.5	74 (18)	1.31	127 (30)	0.221	213 (51)	0.032	-1 (0)

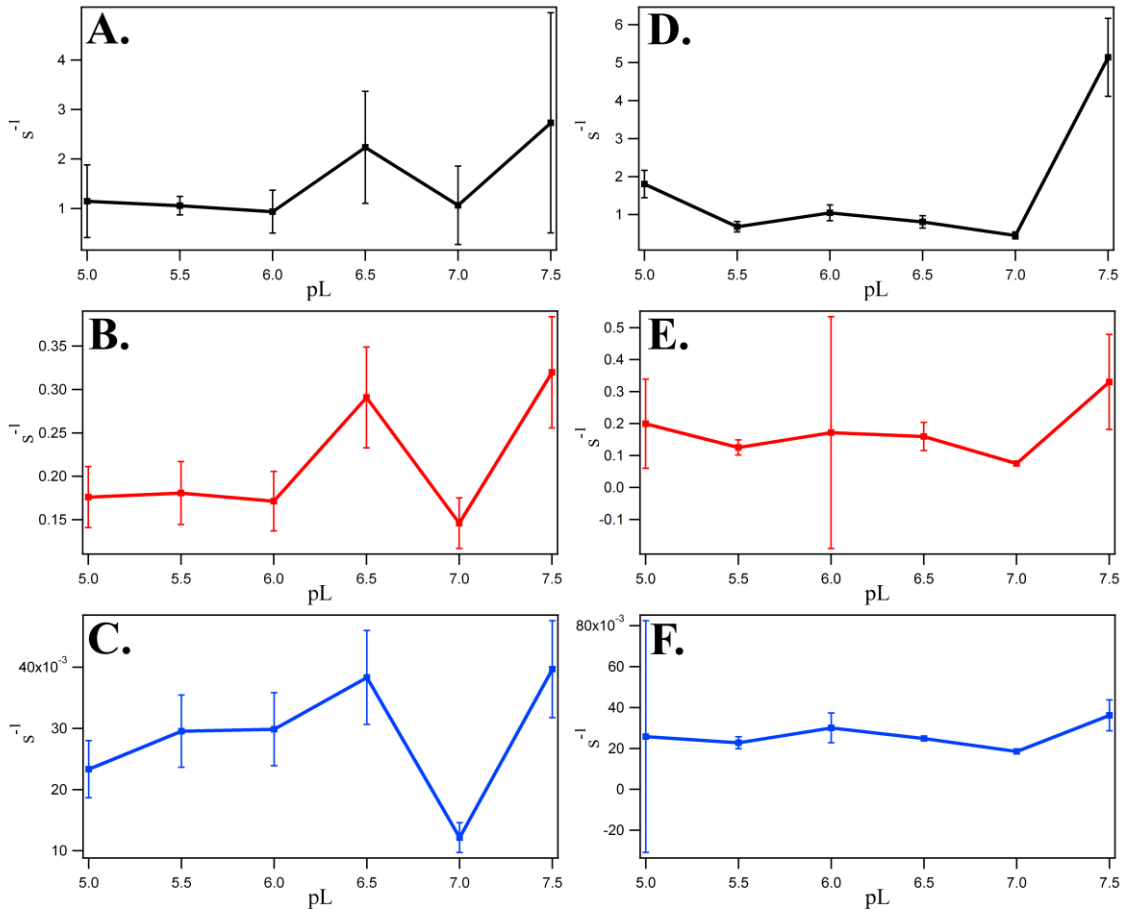

Figure B.1. S_0YZ: Plots of rate constants versus pL in ^1H_2O buffers (A) K_1, (B) K_2, (C) K_3 and ^2H_2O buffers (D) K_1, (E) K_2, (F) K_3. See Table B.1.

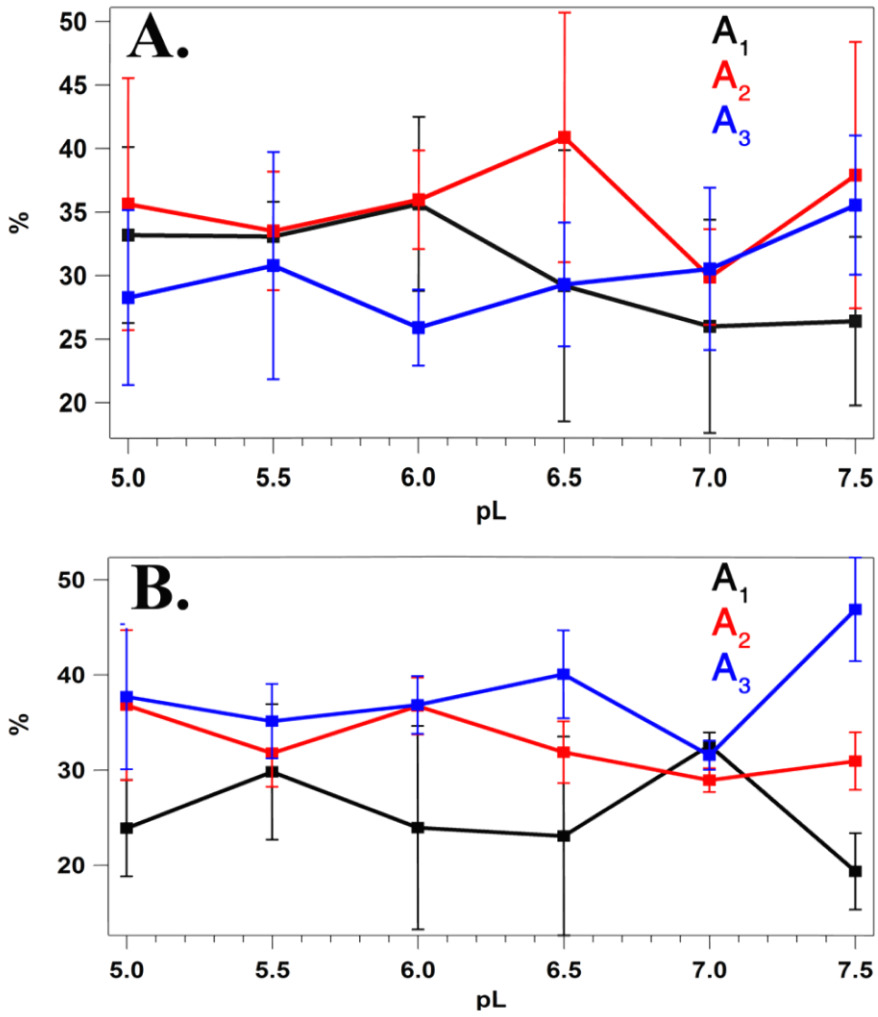

Figure B.2. S_0YZ: Plots of the amplitudes of kinetic phases versus pL in (A) ^1H_2O and (B) ^2H_2O buffers. See Table B.1.

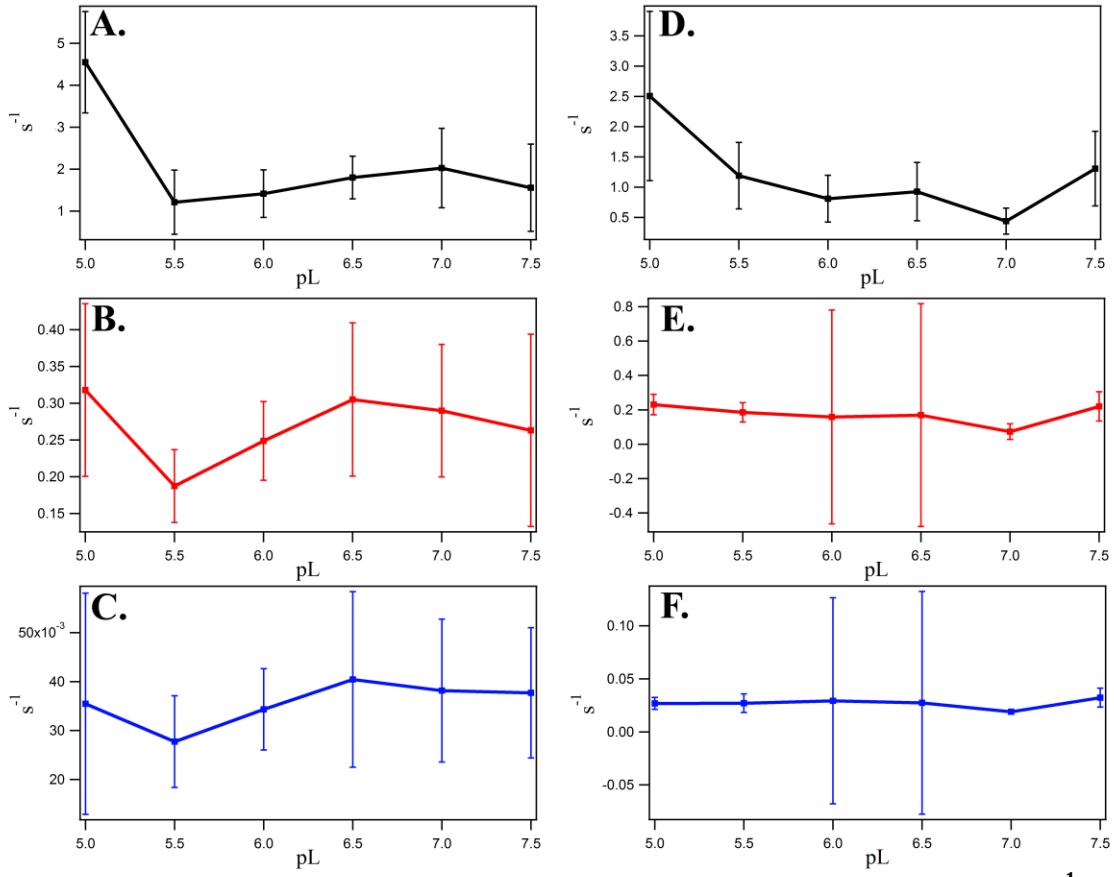

Figure B.3. S_2YZ: Plots of rate constants versus pL for triexponential fits in ^1H_2O buffers (A) K_1, (B) K_2, (C) K_3 and ^2H2O buffers (D) K_1, (E) K_2, (F) K_3. See Table B.2.

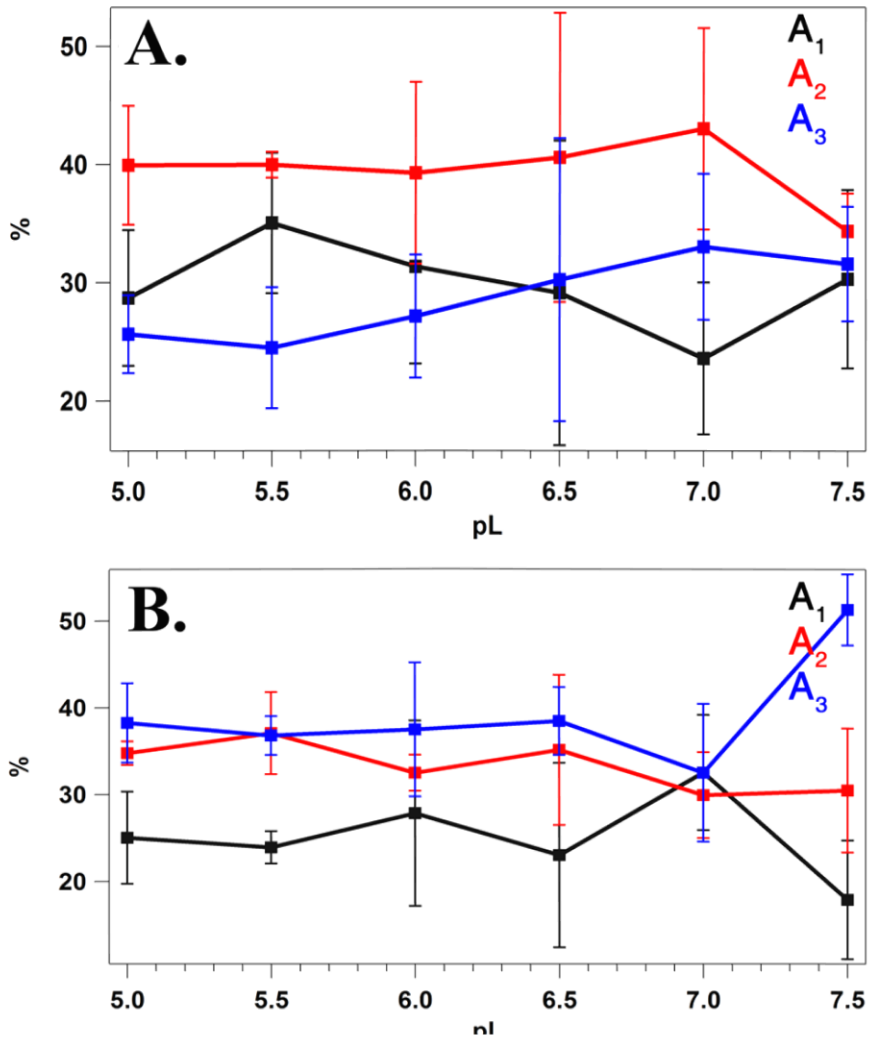

Figure B.4. S_2YZ: Plots of the amplitudes of kinetic phases versus pL in (A) ^1H_2O and (B) ^2H_2O buffers. See Table B.2.

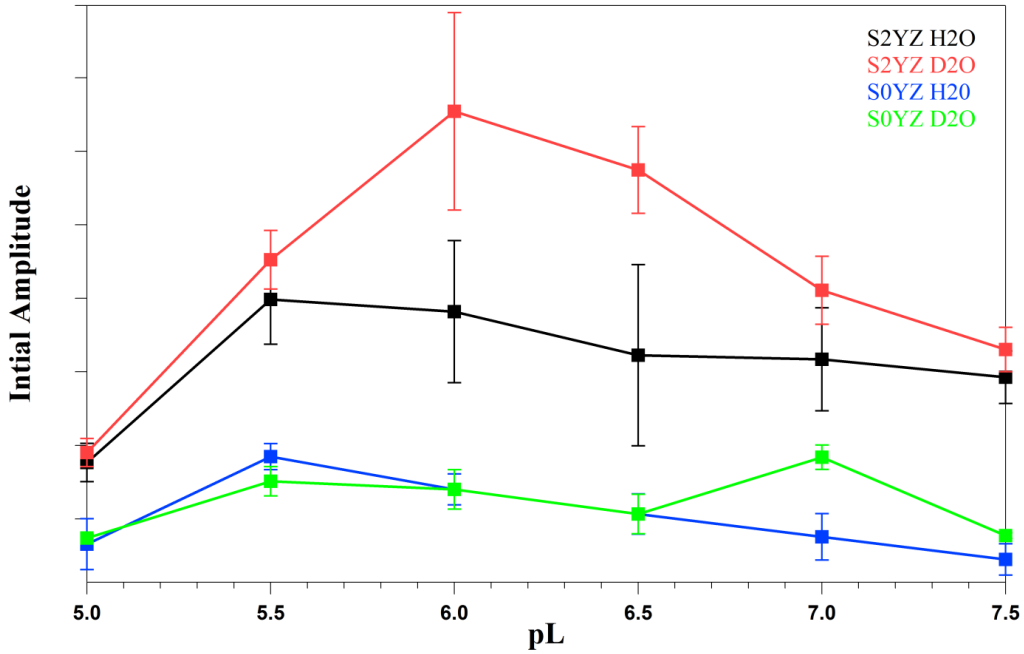

Figure B.5. Plots of the total $Y_Z^{\bullet}$ spectral amplitude, normalized for total chlorophyll concentration, in the S_0 and S_2 states as a function of pL and solvent isotope exchange.

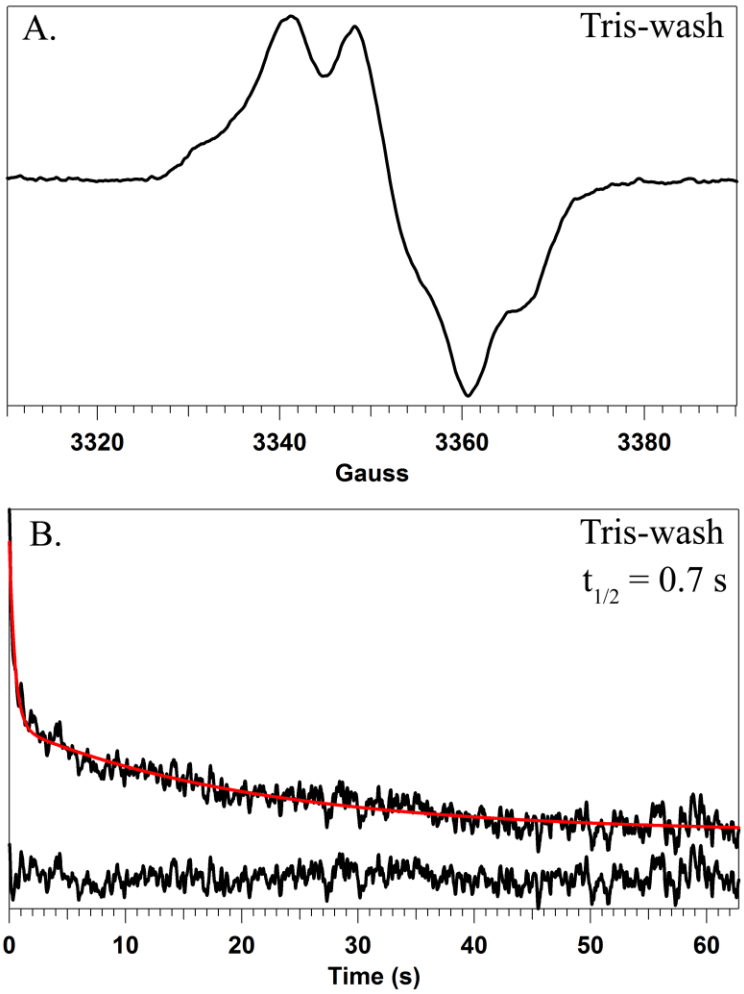

Figure B.6. (A) Representative EPR spectrum of Mn-depleted $Y_D^{\bullet}$ at 190 K and pH 7.0. The spectrum was acquired in the dark. (B) Representative EPR transient reflecting the decay of $Y_Z^{\bullet}$ at pH 7.0 (black) with the fit overlaid (red) and the residual across the bottom (black) at 190K.

APPENDIX C

PROTON COUPLED ELECTRON TRANSFER REACTIONS OF TYROSINE Z SET IN THE S_3 STATE

by

James M. Keough, Ashley N. Zuniga, and Bridgette A. Barry*

School of Chemistry and Biochemistry and the Petit Institute for Bioengineering and Bioscience, Georgia Institute of Technology, Atlanta, GA 30332

Materials and Methods

Sample Preparation. PSII was isolated from market spinach.(1) The average oxygen evolution rate was 800 μmol O_2/mg chl-hr.(2) The samples were solvent exchanged by repeated centrifugation at 100,000 x g in a ^1H_2O or ^2H_2O (99% Cambridge Isotopes, Andover, MA) buffer containing 0.4 M sucrose, 15 mM NaCl, and 50 mM buffer at each of the following pL values: pL 5.0 (succinate), 6.0 (2-(N-morpholino)ethanesulfonic acid, (MES), 6.5 (MES), and 7.0 (4-(2-hydroxyethyl)-1-piperazineethanesulfonic acid, (HEPES). The final concentration was 2 mg/mL, and samples were stored at -70 °C. The pL is reported as the uncorrected meter reading, accounting for the solvent isotope dependence of the glass electrode and the compensating change in the pKa of acids and bases in ^2H_2O.(3)

$S_3Y_Z^\bullet$ Experiments. After a 15 min dark adaptation to trap the S_1 state, samples were homogenized with 500 μM potassium ferricyanide and flashed twice at 1 Hz with a 532 nm flash from a Continuum (Santa Clara, CA) Surelite III Nd:YAG laser at room temperature. The laser intensity was 40 mJ/cm^2, and the beam was expanded with a cylindrical lens. The 100 mM ferricyanide stock solution was made either in ^1H_2O or ^2H_2O on the same day as the experiment. The ferricyanide was present to oxidize the quinone acceptors after each flash. Samples were immediately submersed in liquid N_2 and transferred into the EPR cavity at either 160 or 190 K. A field swept spectrum was recorded to select a field position. Transient data, associated with $S_3Y_Z^\bullet Q_A^-$ decay at 190 K, were averaged from 2-5 samples, with 15 transients recorded per sample. Transient data, associated with $S_3Y_Z^\bullet Q_A^-$ decay at 160 K, was averaged from 4 samples, with 15 transients recorded per sample. An offset, averaged from 10 s of data before the flash,

was subtracted. Flash 1 to 15 yielded similar kinetics. The data from 15 flashes were fit with three exponentials and that fit was used to derive a $t_{½}$ value. This $t_{½}$ value was derived from multiple samples to give an average (mean) and a standard deviation. The EPR analysis was conducted on a Bruker (Billerica, MA) EMX spectrometer equipped with a Bruker ER 4102ST cavity and Bruker ER 4131VT temperature controller. EPR parameters were: magnetic field: 3360 G, microwave frequency: 9.40 GHz, power: 101 mW, modulation amplitude: 5 G, conversion: 20 ms, time constant: 164 ms. High microwave powers were used in order to saturate the $Y_D^{\bullet}$ signal.(4, 5)

Two flashes were used to generate the S_3 state from a dark-adapted sample in the S_1 state. The percentage of the S_3 state can be estimated by assuming 0% misses on the first flash (see above) and 14% misses on the second flash.(6) The expected distribution after two flashes is 0% S_1, 14% S_2, 86% S_3, and 0% S_0. Thus, the state generated with two flashes is primarily S_3, but has a small contribution from S_2.

Field-swept EPR spectra. Following collection of the transient EPR data, EPR spectra were measured by illuminating the sample within the EPR cavity with red filtered light (600 μmol photons/m^2-s, Dolan Jenner Industries, Boxborough, MA) at 190 K. To show that the expected $Y_Z^{\bullet}$ hyperfine splitting is observed, the microwave power and modulation amplitude were decreased compared to the conditions used for the EPR transients. Because the microwave power is low, this field swept spectrum also has a contribution from $Y_D^{\bullet}$. The spectra shown are the average of three samples with three spectra obtained for each sample. EPR parameters were: frequency: 9.46 GHz, power: 0.64 mW, and modulation amplitude: 2 G (Figure 3.2) or 5 G (Figure 3.4), conversion time: 41 ms, time constant: 164 ms, sweep time: 21 s.

Results

In Figure C.1A, we show a representative field sweep spectrum of $S_3Y_Z^{\bullet}$ at pH 6.0 and 190 K. The red arrow in Figure C.1A indicates the magnetic field used to monitor the transient decay depicted in Figure C.1B. Figure C.1B shows kinetic transient data for p^1H 6.0 (black) and p^2H 6.0 (red) at 190 K. The data was fit with three exponentials and the fits were overlaid in red and black for the ^1H_2O and ^2H_2O data respectively.

Figure C.2A plots the $t_{½}$ for the decay of $S_3Y_Z^{\bullet}$ at 190 K as a function of pL. Data acquired in ^1H_2O and ^2H_2O are shown in black and red respectively. $t_{½}$ values were calculated from the fitting parameters to yield values of 1.6, 1.3, and 1.2 s for pH 5.0, 6.0, and 7.0 respectively. Data derived from samples in 2H2O exhibited $t_{½}$ values of 1.9, 2.5, 2.4 s for pD 5.0, 6.0, and 7.0 respectively. These rates are on a similar timescale to rates reported for the S_0 and S_2 states.(4) Figure C.2B plots the KIE as a function of pL for the decay of $S_3Y_Z^{\bullet}$ at 190 K. The KIEs were determined by dividing the $t_{½}$ in ^2H_2O by the $t_{½}$ in ^1H_2O illustrated in Figure C.2A. KIEs were calculated to be 1.2, 2.0, and 2.0 for pL 5.0, 6.0, and 7.0 respectively. The KIEs reported here are on similar magnitudes to KIEs previously reported for the S_0 and S_2 states.

In Figure C.3, we plot of the initial intensity of $S_3Y_Z^{\bullet}$ transients as a function of the number of laser flashes at 190 and 160 K in ^1H_2O and ^2H_2O. Intensities are shown for 14 laser flashes. p^1H data are shown for 5.0 (black), 6.0 (red), and 7.0 (blue) at 190 K. p^2H data are shown for 5.0 (green), 6.0 (orange), and 7.0 (grey) at 190 K. p^1H data is shown for 6.5 (purple at 160 K.

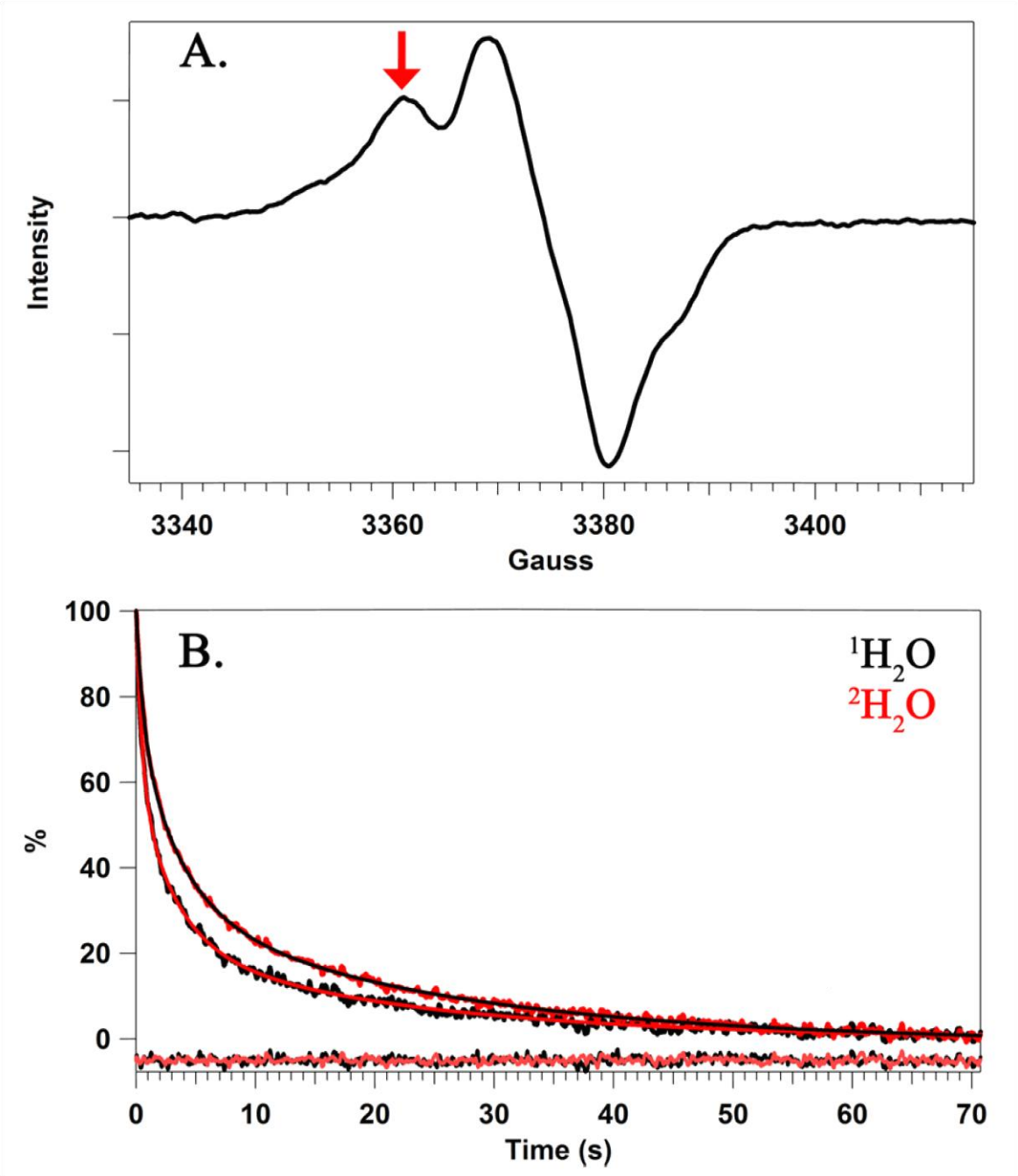

Figure C.1 (A) Representative EPR spectrum of the $S_3Y_Z^{\bullet}$ state at 190 K and pH 6.0. The spectrum was acquired under red-filtered illumination. The red arrow shows the magnetic field used to monitor kinetics. (B) Representative EPR transients reflecting the decay of $Y_Z^{\bullet}$ at p^{1}H 6.0 (black) and p^{2}H 6.0 (red) at 190 K. Transient are overlaid with fits to the data in red (^1H_2O) and black (^2H_2O). Residual for the fits are shown below the data in the same color as the transient data.

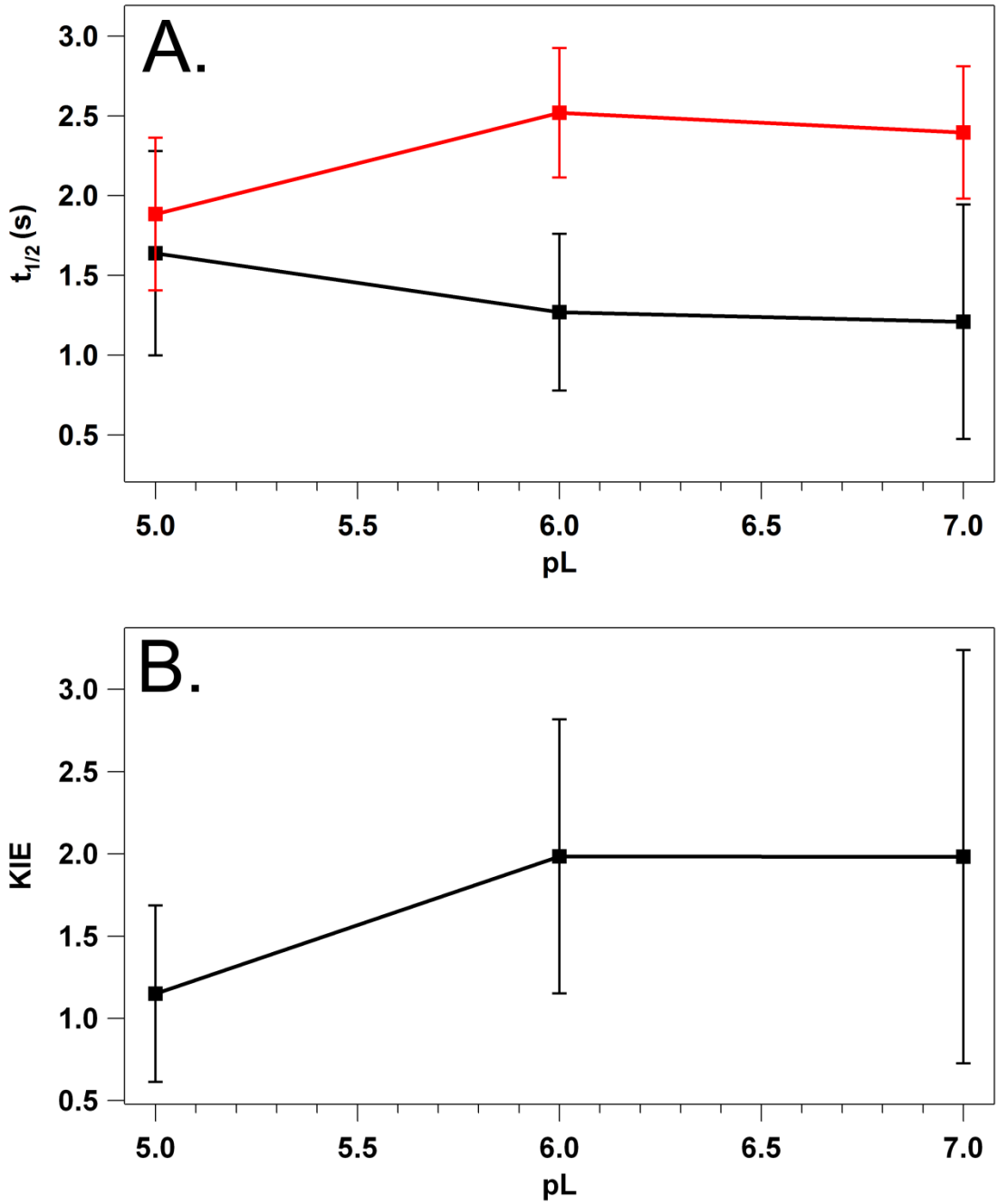

Figure C.2. (A) pL dependence of $Y_Z^{\bullet}$ recombination in the S_3 state at 190 K. Data were acquired either in ^1H_2O (black) or ^2H_2O (red) buffers. (B) pL dependence of the kinetic isotope effect for $S_3Y_Z^{\bullet}$ recombination, derived from the data in (A).

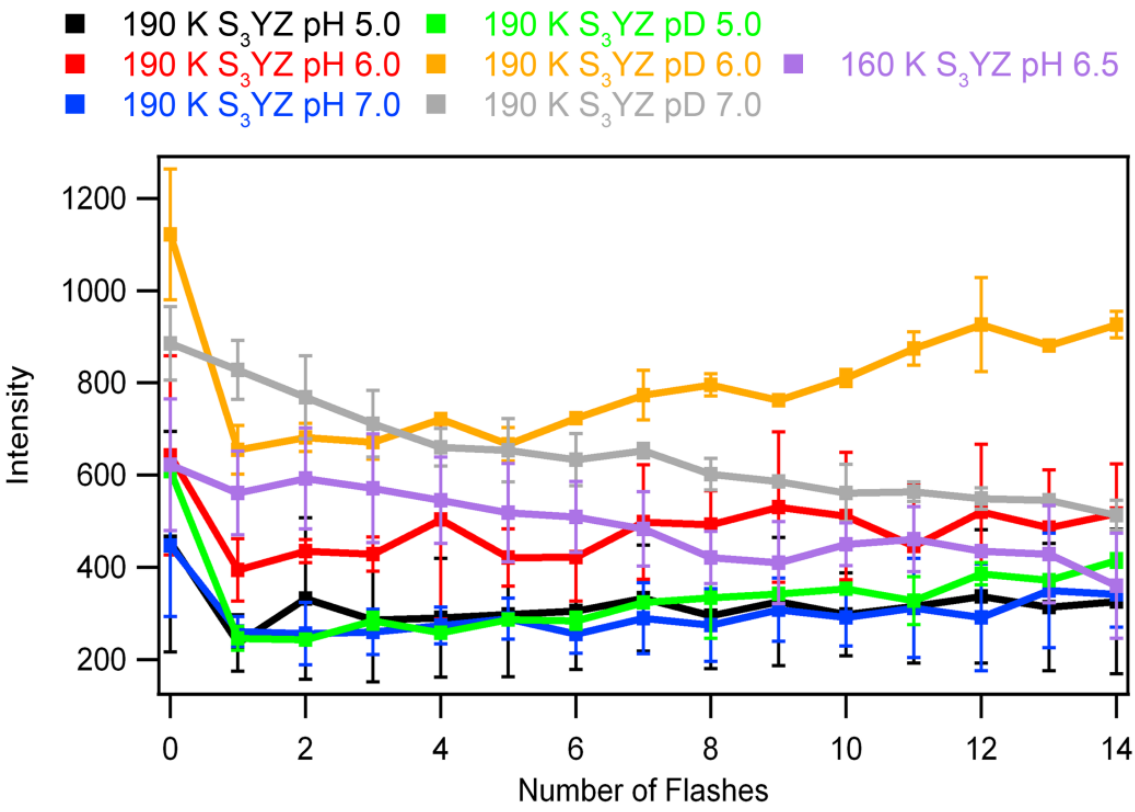

Figure C.3. Plot of the initial intensity of $S_3Y_Z^{\bullet}$ transient as a function of the number of laser flashes at 190 and 160 K. Intensities are shown for 14 laser flashes with standard deviation shown as plus or minus one standard deviation. p^1H data are shown for 5.0 (black), 6.0 (red), and 7.0 (blue) at 190 K. p^2H data are shown for 5.0 (green), 6.0 (orange), and 7.0 (grey) at 190 K. p^1H data is shown for 6.5 (purple at 160 K.

Figure C.4A shows the field sweep spectrum of $S_3Y_Z^{\bullet}$ at pH 6.5 and 160 K. The red arrow in Figure C.4A indicates the magnetic field used to monitor the transient decay depicted in Figure C.4B. Figure C.4B shows kinetic transient data for p^1H 6.4 (black) at 160 K. The data was fit with three exponentials and the fit was overlaid in red. The $t_{½}$ value was derived from the fitting equation for the overall half time for the decay of $S_3Y_Z^{\bullet}$ at 160 K.

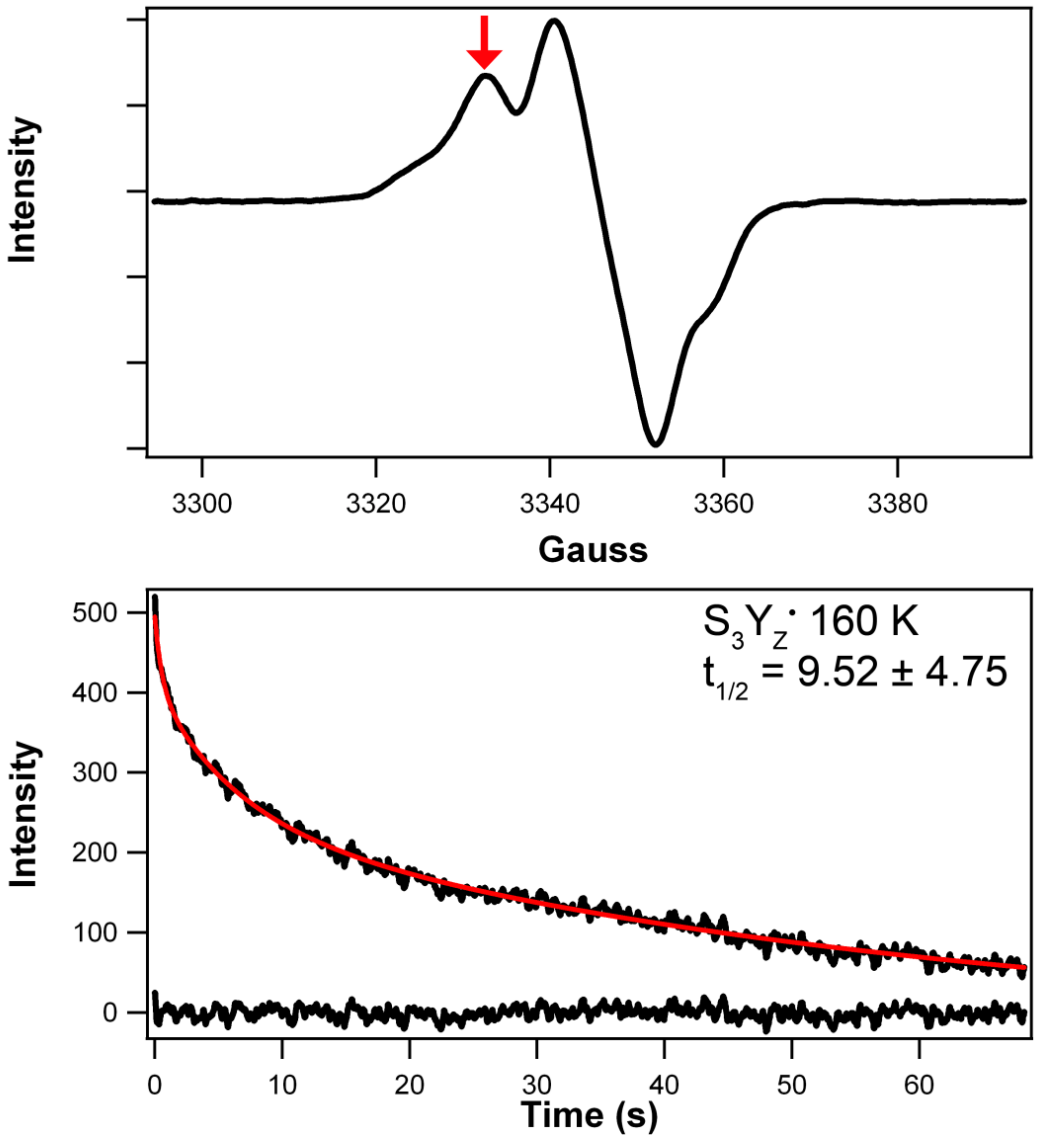

Figure C.4. (A) Representative EPR spectrum of the $S_3Y_Z^{\bullet}$ state at 160 K and pH 6.5. The spectrum was acquired under red-filtered illumination. The red arrow shows the magnetic field used to monitor kinetics. (B) Representative EPR transients reflecting the decay of $Y_Z^{\bullet}$ at pH 6.5 (black) at 160 K. Transient data is overlaid with the fit to the data in red. Residual for the fit is shown below the data in black.

Discussion

Preliminary data presented for the decay of S_3Y_Z at 190 K potentially has an interesting pL dependence that accelerates the rate at low pH (5.0). This type of pL dependence is similar to the data previously acquired for $Y_D^{\bullet}$.(3) However, given the

error at pL 5.0 it is not currently possible to assert this conclusion. Increasing the data set for S_3 state at pL 5.0 should make analysis facile. At pL 6.0 and 7.0 significant KIEs were recorded with an average value of 1.98. The magnitude of this KIE is indicative of a CPET mechanism.

During data acquisition in the S_3 state at 190 K, a trend in the amplitude of the initial intensity of transients was noticed. The amplitude data is shown in Figure C.3. Most notably the trend in amplitude of the data at 190 K S_3Y_Z pD 7.0 (grey data in Figure C.3) caught our attention. The intensity decreased with every laser flash. We were able to reset each of these samples by incubating them in the dark on ice for 30 minutes, which sets the OEC back in the S_1 state. Following this incubation, we administered two laser flashes at 1 Hz and quickly frozen the sample in liquid nitrogen resetting the S_3 state. The samples that were reset into the S_3 state regained 100% of their initial intensity and decreased in amplitude at a similar rate to the previous data acquisition. This caused concern that at 190 K the S_3 to S_0 transition was not fully inhibited.

In order to determine if the S_3 to S_0 transition was inhibited, S_3Y_Z samples were run at 160 K. Figure C.3 shows the amplitude for pH 6.5 samples set in the S_3 state as a function of the number of laser flashes administered. The trend at 160 K is similar to the trend at 190 K. The decrease in amplitude is therefore not attributed to the S_3 to S_0 state transition. This data lends confidence to the data at 190 K and begins the exploration of the S states at lower temperatures.

S_3Y_Z data was analyzed at 160 K to yield a t ½ value of 9.52 ± 4.75 s. The error is this experiment is higher than desired. Data for 160 K was analyzed for five samples, which is on the same order as samples analyzed in the S_0 and S_2 states at 190 K. It could

be that as the temperature is decreased and the length of the transient decay increases that the error will increase.

References

1. Berthold D. A., Babcock G. T., & Yocum C. F. (1981) A highly resolved, oxygen-evolving Photosystem II preparation from spinach thylakoid membranes. *FEBS Letters* 134:231-234.

2. Barry B. A. (1995) Tyrosyl radicals in photosystem II. *Methods in Enzymology* 258:303-319.

3. Jenson D. L., Evans A., & Barry B. A. (2007) Proton-coupled electron transfer and tyrosine D of photosystem II. *The Journal of Physical Chemistry B* 111(43):12599-12604.

4. Keough J. M., Jenson D. L., Zuniga A. N., & Barry B. A. (2011) Proton Coupled Electron Transfer and Redox-Active Tyrosine Z in the Photosynthetic Oxygen-Evolving Complex. *Journal of the American Chemical Society* 133(29):11084-11087.

5. Ioannidis N. Z., G; Petrouleas, V (2008) The EPR spectrum of tyrosine-Z* and its decay kinetics in O_2-evolving photosystem II. *Biochemistry* 47:6292-6300.

6. Joliot P. & Kok B. (1975) Oxygen evolution in photosynthesis. *Bioenergetics of Photosynthesis,* ed Govindjee (Academic Press, New York), pp 388-412.

VITA

James M. Keough

James M. Keough was born in Stone Mountain, Georgia. He attended public schools in West Lafayette, Indiana and Peachtree City, Georgia. He received a B.S. in Chemistry with a concentration on Biochemistry from the Georgia Institute of Technology in 2006. In 2007, he began his doctoral study at the Georgia Institute of Technology by continuing his undergraduate work in Professor Bridgette Barry's laboratory. When he is not working, he enjoys travelling and fishing with his wife and friends.